ABSTRACT

Title of Document: PERFORMANCE AND OIL RETENTION CHARACTERISTICS OF A CO_2 HEAT PUMP WATER HEATER

Nicholas Fernandez, Masters of Science, 2008

Directed By: Dr. Reinhard Radermacher, Mechanical Engineering

A CO_2 heat pump water heater (HPWH) was investigated experimentally and analytically. In the first stage of the study, a baseline performance was measured, investigating the effect of operating parameters on the system performance under typical tank heating scenarios. In the second, the CO_2 HPWH was modeled to investigate the effect of optimizing key components. In the third, the oil retention mass, the increase in pressure drop, and the COP degradation were measured as a function of oil mass fraction. In the fourth, two alternative system configurations were investigated for potential performance enhancement; a two-stage compression cycle with internal heat exchanger and a system with a suction line heat exchanger. Overall, the CO_2 cycle seems uniquely suited for water heating. CO_2 HPWHs have enormous energy savings potential if the cooling from the evaporator can be harnessed during the summer months, and rejected to the environment during the colder months.

PERFORMANCE AND OIL RETENTION CHARACTERISTICS

OF A CO_2 HEAT PUMP WATER HEATER

By

Nicholas Fernandez

Thesis submitted to the Faculty of the Graduate School of the

University of Maryland, College Park in partial fulfillment

of the requirements for the degree of

Master of Science

2008

Advisory Committee:

Professor Reinhard Radermacher, Ph.D., Chairman/Advisor

Associate Professor Yunho Hwang, Ph.D., Committee Member

Associate Professor Kenneth Kiger, Ph.D., Committee Member

Associate Professor Gregory Jackson, Ph.D., Committee Member

Acknowledgements

I would like to thank Dr. Reinhard Radermacher, director of the Center for Environmental Energy Engineering (CEEE), for giving me the opportunity to study here under his guidance. His vision and leadership have been very inspiring and serve as an example of what can be accomplished through organization and a steady focus.

I would like to thank Dr. Yunho Hwang, professor in charge of laboratory research at CEEE. His patience and understanding early in my research helped me to stay on track. Over my graduate career, he has pushed me to achieve more than I thought I was capable of.

I would also like to thank Jan Muehlbauer, the lead engineer of the Heat Pump Lab. Without his advice and guidance in building my test facility, it would not have been nearly as safe or reliable, and I could not have accomplished nearly as much in the time I was here. He was also a great mentor in helping me to understand vapor compression systems and to deal with hardware issues such as faulty sensors and electrical wiring.

I would like to thank my fellow graduate students for providing an enjoyable work environment and much camaraderie. More importantly, however, they provided an intellectual atmosphere to discuss and further my understanding of complex global issues.

Last, but not least, I would like to thank my loving fiancée Aisling. She provided the motivation to stay here at Maryland, following a challenging undergraduate education, and dive into an even more challenging graduate career. She gave me strength and gave my life balance over the course of this project.

Table of Contents

List of Tables

List of Figures

Nomenclature

Acronyms

ASHRAE	American Society of Heating Refrigeration and Air-Conditioning Engineers
AT	Approach Temperature
CEEE	Center for Environmental Energy Engineering, University of Maryland
COP	coefficient of performance
DOE	Department of Energy, United States
EES	Engineering Equation Solver
EHD	electro-hydrodynamic
GWP	global warming potential
HFC	hydro-fluorocarbon
HCFC	hydro-chloro-fluorocarbon
HPWH	heat pump water heater
IHX	internal heat exchanger
LMTD	log-mean temperature difference
MFR	mass flow rate
ODP	ozone depletion potential
OMF	oil mass fraction
OR	oil retention
PDPF	pressure drop penalty factor
SLHX	suction line heat exchanger
UA	heat transfer coefficient (U) times heat transfer area (A)

Abbreviations

“A” Test	initial or full tank heating test
“B” Test	water usage and reheat test
“C” Test	standby loss and reheat test
C_p	specific heat (at constant pressure)
h	specific enthalpy
m	mass
n	number of trials
s	enthalpy
P	pressure

Q	heat
T	temperature
t	time
V	compressor displacement volume
W	work
Wt.%	percentage by weight
Δ	change in
ρ	density
U	uncertainty
η	efficiency
ω	compressor rotational speed

Subscripts

0	initial
c	CO_2
comp	compressor
e	evaporator
f	final
gc	gas cooler
i	inlet
ise	isentropic
LS	oil level sensor
mech	mechanical
n	timestep #
N	total number of timesteps
o	outlet
sat	saturation
R	oil reservoir
vol	volumetric
w	water

1 Background and Literature Review

Water heating has conventionally been performed using electric resistance and gas-fired water heaters. These devices are very inexpensive (on a first cost basis), and for a long time, there was no motivation for any change. However, with growing concerns about global warming and energy supply and security, there has been mounting pressure across the board to reduce energy demand and move toward forms of energy usage that can be accomplished in carbon-constrained world. The most effective societal measure of energy efficiency is a device's primary energy efficiency. It is the amount of energy originally stored in a fuel that is converted to a useful form. Electric water heaters have end-use efficiencies on the order of 90% [26], but in terms of primary energy, that efficiency is typically closer to 30%, since the electricity required to heat the water is created in a power plant, generally with efficiencies on the order of 40%. Gas-fired water heaters use heat from the burning fuel directly, however, not all of the combusted heat can be captured by the water, and consequently, the primary energy efficiencies are typically around 60% [26]. Heat pump water heaters (HPWH's) have the potential to surpass both of these technologies by operating at a coefficient of performance (COP) that is many times higher (typically 3-5 times) than electric resistance water heaters. The COP is defined as the useful heat extracted from the system, divided by the electrical power required to operate it. By using the heat pumping effect, HPWH's can provide heat to the water at primary energy efficiencies of well over 100%. Carbon dioxide (CO_2) appears to be one of the best suited working fluids for use in a HPWH.

CO_2 was originally used as a commercial refrigerant for ships around the turn of the 20th century, but largely faded from any application or interest until Lorentzen [1] studied its properties and proposed a host of new applications for it. CO_2 has recently come into fashion as a natural refrigerant that has the potential to replace hydro-fluorocarbon (HFC) and hydrochlorofluorocarbon (HCFC) refrigerants. CO_2 is non-flammable, non-toxic, has a zero ozone depletion potential, and a negligible global warming potential (GWP) compared to HFC and HCFC refrigerants, which have GWP's thousands of times higher. CO_2 has been proposed for many applications, including automotive air conditioning. Water heating, however, appears to be a particularly strong niche for CO_2. Whereas other applications are limited by the low critical temperature of CO_2 (31°C), during water heating, a counter-flow CO_2-water heat exchanger can extract ample heat from the high pressure, supercritical CO_2. Overcoming this hurdle allows the CO_2 HPWH to take advantage of CO_2's much lower compression ratios, compared to conventional refrigerant cycles. An additional benefit of the cycle is that since the operating pressures are several times higher than conventional refrigerant cycles, pressure drop in the heat exchangers is less of an impedance to performance.

Experimental research into CO_2 HPWH's was performed by Neksa et al. [4] in Norway in 1998. This research sought to measure the COP at different operating conditions and to characterize the optimum high side pressure of the system. Neksa's results were very promising, exhibiting COP's in the range of 3-5. Around the same time, Hwang and Radermacher[3] studied the performance of CO_2 HPWHs for varying

hot water temperatures and compared CO_2 to R22 for water heating applications. Backed by promising early research and motivated by a desire to meet commitments to the Kyoto Protocol, the Japanese government, at the turn of the 21st century, instituted a subsidy for CO_2 HPWHs that now amounts to roughly 5 billion Yen per year [21]. This subsidy accelerated the growth of the fledgling market. Now, stiff competition from nearly a dozen Japanese manufacturers has led to vast improvements in commercial products, which now claim COP's of up to 5.1 at the Japanese intermediate test condition of heating water from 16 to 65˚C at 24˚C ambient temperature [23]. By 2010, 30% of the water heaters in Japan are expected to be CO_2 HPWHs [21].

Meanwhile, research has continued worldwide into HPWHs, with a host of proposed configurations and design modifications. Stene [19] did an experimental study, using a CO_2 HPWH for combined domestic water heating and space heating. The study divided the supercritical heat rejection from the CO_2 into three heat exchangers. On the low temperature side, one heat exchanger pre-heated an inlet water stream. In the intermediate temperature range, a CO_2-air heat exchanger provided space heating, and at the high temperature range, the water was heated the rest of the way. Under this configuration, Stene found that the overall system COP could be improved by 5% over a baseline water-heating-only scenario , and by as much as 25% over a space-heating-only scenario. The research underscores the potential of using a CO_2 HPWH in a combined residential system that can provide most of the thermal needs of the building. This potential is the greatest during the summer months, when the system can be fully utilized for both water heating and space cooling.

Experimental research was done by Kim et al. [18] on the potential performance improvement of a CO_2 HPWH using a suction line heat exchanger (SLHX). Their research indicated that the COP could be improved by as much as 4% by using a SLHX at the specific conditions that were tested. Chaichana et al. [10] investigated the potential of boosting the performance of a CO_2 HPWH by using solar energy. Anderson et al. [28] have demonstrated that by using solar irradiation to heat the evaporator, the COP of an R22 HPWH can be boosted to as high as 5-7 in summertime ambient temperature conditions. Chaichana, however, concluded that the low critical temperature of CO_2 makes it a poor choice for solar boosted HPWH's, because it limits the capacity as the evaporating temperature approaches the critical point.

An important reliability concern with CO_2 HPWHs stems from the fact that CO_2 compressors tend to eject a large amount of compressor oil, along with the CO_2. The purpose of the compressor oil is to keep the compressor's moving parts lubricated. Some oil migration into the system tubing is typical of most vapor compression systems. Discharged compressor oil is carried along with the refrigerant, typically coating the inner annulus of the system tubing in a thin film of oil. This oil film flows along the tubing of the system until it makes it back to the compressor, where it returns to its intended function. With the combination of certain factors, such as low mass flux, vertical upward tubing, and poor miscibility with the refrigerant, oil can have considerable difficulty navigating the system tubing, and a significant volume of oil can collect. If too much oil is present in the system tubing, it can reduce the amount of oil in the compressor to a point that its moving parts are longer properly lubricated.

Previous work at the Center for Environmental Energy Engineering (CEEE) at the University of Maryland has focused on oil retention issues in vapor compression systems. Lee [9] studied the oil retention characteristics of an automotive air conditioning system using CO_2 as the working fluid. Lee found that the oil retention volume in the evaporator increased with the mass fraction of oil (OMF) in the system and decreased with increasing CO_2 mass flow rate. In the gas cooler, Lee reported a very small amount of CO_2 retained, due to a high CO_2 density, low oil viscosity, and low oil surface tension. Lee also studied the effect of the oil on the pressure drop in the heat exchangers, finding that the pressure drop could be increased by up to a factor of 3, based on the presence of an oil film. Cremaschi [14] studied the oil retention characteristics of residential air conditioning systems, using R22, R410A, and R134a as the working fluid. The trends in Cremaschi's data mirrored that of Lee's, however the pressure drop penalty factor he measured was much lower – around 1.5 at high OMFs.

The presence of an oil film has the additional potential to reduce the overall heat transfer coefficient at a given location in a heat exchanger. A partial explanation for this reduced heat transfer coefficient is the increased thermal resistance due to the oil layer. Dang et al. [30] studied the effects of increasing oil mass fraction on the heat transfer and pressure drop in a supercritical CO_2 gas cooler. Dang found that the reduction in heat transfer coefficient was the highest near the pseudocritical temperature, and that at much higher temperatures, more typical of the range found in a HPWH, the reduction in heat transfer coefficient was very minimal. Dang also studied the effect of the OMF on the pressure drop, concluding that the majority of the increase in pressure drop

occurred at low oil mass fractions, and quickly saturated above 1-3%. Dang's research indicated that the effects of the OMF on the heat transfer and pressure drop correlate with the type of flow regime that the oil develops. At low oil mass fractions and low temperatures, the oil flows in small droplets along with the bulk CO_2. At low mass fluxes, the oil flows in a wavy flow regime in a layer along the bottom of horizontal tubing. As mass flux, OMF, and temperature are increased, the flow transitions to a dispersed annular flow, or in other words, to an oil film along the inner tube wall. At high oil mass fractions and high refrigerant mass fluxes, additional oil tends to flow along with the bulk CO_2.

The issue of oil retention can be largely managed through the installation of a suitable oil separator at the compressor discharge. The oil separator collects oil ejected by the compressor and allows it to drain slowly back to the compressor's suction port. This additional component, however, would add cost, weight, and additional complexity to the system.

2 Motivation and Objectives

This project aims to answer the following questions:

- What is the potential COP of the CO_2 cycle for heating water during typical heating of a residential water tank?
- How is the COP affected by operating conditions (ambient temperature, hot water temperature, heating scenario)?
- What are some options for performance enhancement over the baseline cycle?
- How does compressor oil circulation affect the performance of the system?
- In a COP HPWH, is it worthwhile to install an oil separator?

The project was broken down into 4 main stages:

1. Baseline performance evaluation: A CO_2 HPWH measurement facility was constructed in the Heat Pump Laboratory of the University of Maryland. The system's COP and capacity were measured during full tank heating tests at varying ambient temperatures, hot water temperatures, and heating scenarios.

2. Modeling: Based on empirical data from the baseline performance evaluation, a computer model was created to simulate system performance. Key parameters for each of the system components were varied to simulate the use of better or more optimized system components, and to determine the corresponding effect on the COP.

3. Evaluation of Oil Retention: Compressor oil was artificially injected into system components to simulate varying OMF's of oil that could potentially be discharged from a CO_2 compressor. The setup and the procedures used were the same as those used by Lee [9] and Cremaschi [14]. The amount of oil retained, and the effect of this oil on the pressure drop and COP were measured for two different CO_2 mass flow rates.

4. Cycle Enhancement: The baseline cycle was modified to investigate potential performance enhancements using two types of internal heat exchangers. The first modification used two-stage compression with an internal heat exchanger (IHX) between the high and intermediate pressure refrigerant. The second modification used a SLHX to subcool the CO_2 from the gas cooler, while providing additional superheat to the evaporator.

3 Baseline Performance Evaluation

3.1 Description of Performance Measurement Facility

A CO_2 HPWH breadboard was built in the Heat Pump Laboratory of the University of Maryland for the evaluation of the system's baseline performance. The test rig was located inside an environmental chamber capable of strictly controlling the ambient temperature and humidity. A diagram of the system configuration for baseline testing is shown below in Figure 1.

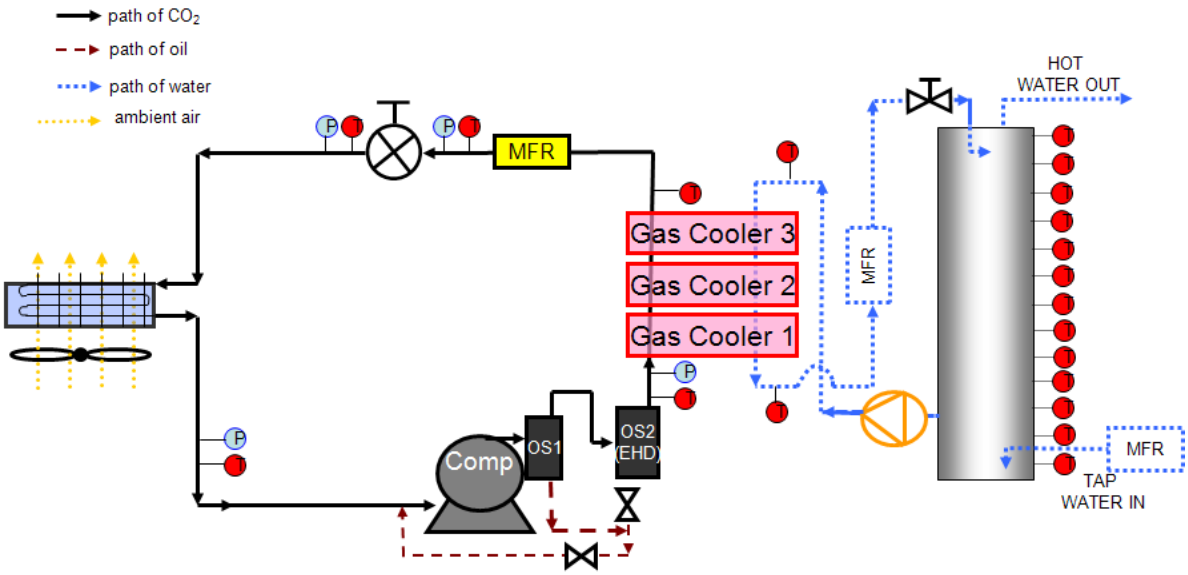

Figure 1: Test facility for baseline performance evaluation

The CO_2 cycle here is a transcritical vapor compression cycle. CO_2 is compressed by the compressor. The compressor is a two-stage rotary piston compressor with a variable speed drive. The inlet state of the CO_2 to the compressor is a subcritical vapor, and the outlet state is a supercritical fluid. Since CO_2 compressors typically discharge a

large amount of compressor oil along with the CO_2, two oil separators were installed at the compressor outlet to filter the oil from the CO_2 and send it back to the compressor. The first oil separator was a centrifugal oil separator. The discharge stream flows radially into a cylindrical chamber within the separator, where the flow forms a vortex that separates the denser oil from the CO_2. The oil collects on the outer wall of the cylinder and drains down to the bottom of the separator. The CO_2 (with any remaining oil) then leaves through the top of the first separator and enters the second oil separator, an electro-hydro-dynamic (EHD) oil separator. This was a prototype oil separator, the design of which is currently under research by the advanced heat transfer group within CEEE. The mechanism for oil separation in the EHD is the creation of a strong electric field inside the oil separator via a high-voltage central electrode within a conducting cylindrical shell. The electrode and the shell are separated by an electrically insulating Teflon layer. Small oil droplets are driven under the electric field to the outer walls of the cylinder, where the oil then drains down and collects with oil from the first stage of separation.

From the outlet of the oil separators, the CO_2 flows into a series of three heat exchangers that collectively make up the "gas cooler." The gas cooler is the analog of the condenser for a transcritical cycle. It is called a gas cooler because the supercritical, high pressure fluid does not condense in the traditional sense, but instead undergoes a cooling process that is more like latent heat removal near the critical point and more like sensible heat removal further away from it. Each heat exchanger contains microchannel passes for the CO_2 that wrap around hollow flat plates for the passage of

the water. The heat exchangers were provided by Modine, a heat exchanger manufacturer based in Wisconsin. Based on the size of the compressor, it was determined that at least three of such heat exchangers would be necessary to provide adequate heat exchange between the CO_2 and water. The CO_2 flows through the gas cooler in counter-flow with the water. This enables the hot water temperature to approach the CO_2 discharge temperature and for the CO_2 stream to be cooled to a temperature approaching the inlet water temperature.

From the outlet of the gas coolers, the CO_2 flows into a Coriolis-type mass flow meter, where the flow rate of CO_2 through the cycle is measured. From that point, the CO_2 is expanded in a manual needle-type expansion valve, and flows into the evaporator. The evaporator is a single-pass louver-finned fin-and-tube heat exchanger with two banks of 9.5 mm diameter stainless steel tubing. Each bank contains 18 tubes, spaced 2.5 cm apart. The length of each tube is 68cm. The evaporator was installed in a wind tunnel inside the environmental chamber with a blower controlled by a variable frequency drive. From the outlet of the evaporator, the CO_2 flows back to the compressor's suction port.

Pressure transducers and in-stream T-type thermocouples measure the temperature and pressure at all points in the cycle relevant to reconstruct the P-h diagram for CO_2.

On the water side of the system, a 113L water tank stores the water that is heated through the gas cooler. When the system is running, water is pumped from the

bottom of the water tank though the gas cooler, through a turbine flow meter, then back into the top of the tank. The pump is a single-speed pump, so the water flow rate was controlled with a needle valve at the end of the water heating loop. T-type thermocouples measure the temperature of water entering and leaving the gas cooler. Water usage can be simulated by introducing tap water to the bottom of the tank, forcing the hot water out of the top of the tank. Another turbine flow meter measures the flow rate of tap water into the system and the flow rate of hot water leaving the system.

Table 1 details all of the instrumentation in the baseline system and its measurement uncertainty.

Table 1: Components and instrumentation for baseline cycle

Instrument	Type	Manufacturer	Model #	Uncertainty
Thermocouples	T	N/A	N/A	+/- 0.5°C
Pressure Transducers	gage	Setra	206/280E	+/- 0.13% f.s.
Pump	Jet pump, water	Dayton	9R756	N/A
Volume flow meter	turbine	Sponsler	MF150	+/-0.25% f.s.
Volume flow meter	turbine	Sponsler	MF100	+/-0.25% f.s.
Mass flow meter	Coriolis	Micro Motion	CMF025	+/-0.1% f.s.

The CO_2 HPHW's performance is reported in terms of two key quantities; the COP and the capacity. The capacity (Q_{gc}) is the amount of heat being exchanged with the water and is equal to

$$Q_{gc} = \dot{m}_{water}\left(h_{water,o} - h_{water,i}\right) = \dot{m}_{CO_2}\left(h_{CO_2,o} - h_{CO_2,i}\right) \quad (1)$$

where h refers to the enthalpy. As Equation 1 indicates, the capacity can be determined either on the water side or the CO_2 side of the system. In this experiment, measurements are taken on both sides of the system and the difference between the two measurements is referred to as the energy balance. A set of measurements is considered to be valid if the energy balance is below 5%, which is roughly the range of error inherent from the propagation of uncertainty from the various measurement devices (see Chapter 3.5). Typically, the water side measurements reveal a slightly lower capacity than the CO_2 side measurements due to heat losses from the gas cooler to the ambient air.

The capacity of the system is based mainly on the size of the compressor and heat exchangers, so its nominal value is unique to this test facility. However, the relative value of the capacity from one test to another is useful in determining how changing conditions affect the capacity in any such system.

The other key performance parameter is the COP. The COP is equal to

$$COP = \frac{Q_{gc}}{W_{comp}} \quad (2)$$

where W_{comp} is the electrical work supplied to the compressor and Q_{gc} is the average of the CO2 side and water side capacity measurements. Heat loss to the ambient air is neglected in this calculation because its magnitude is below the instrumentation error. The COP is a better measure of the inherent energy efficiency of the CO_2 cycle, however the COP can be further improved by installing a more efficient compressor and/or heat exchangers that allow for more complete heat transfer between the two fluids.

All of the system temperatures, pressures, and flow rates were recorded and displayed instantaneously using LabVIEW software. A fluid property calculator called X-Props is used within LabVIEW to automatically calculate the enthalpies at each state point, allowing the COP and capacity to be calculated and displayed in real-time. Figure 2 is a screenshot of the LabVIEW interface. The interface contains alarms that are set off whenever the superheat falls below 3K (since a lack of superheat can damage the compressor) or when the ambient CO_2 concentration in the chamber rises above 1500ppm (indicating an unsafe work environment).

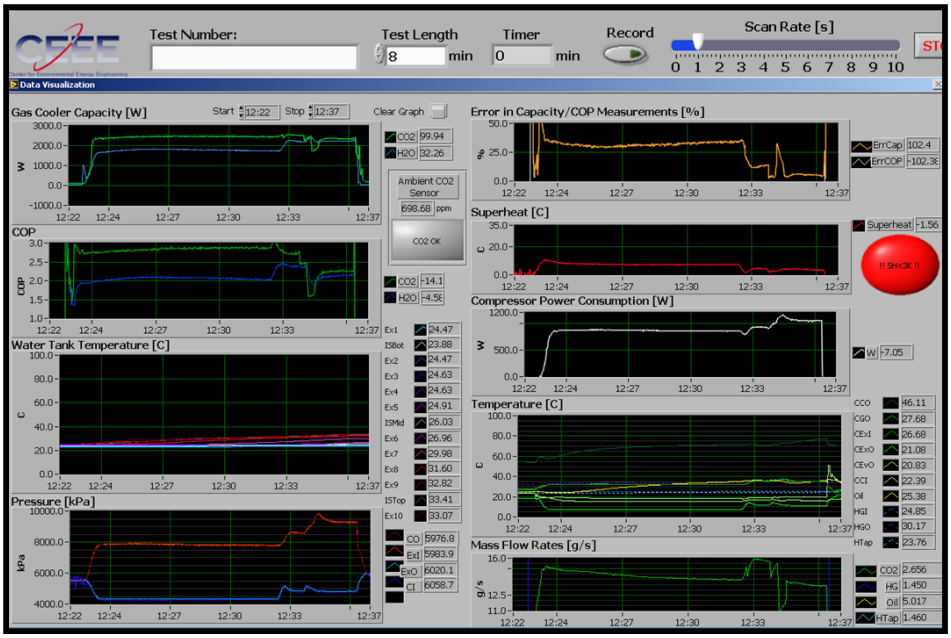

Figure 2: Screeenshot of Labview interface

3.2 Baseline Performance Measurement Procedures

There are a few key environmental operating parameters that can influence the performance of a CO_2 HPWH. These are: ambient temperature, hot water temperature, and the tank water temperature profile over the course of the experiment. Any specific tank water temperature profile is a consequence of both the tap water temperature and the recent heating history. Three possible heating scenarios were identified for the HPWH performance evaluation. Each type of scenario is accompanied by a specific, repeatable tank temperature profile, under constant tap water temperature.

The first scenario is when the entire tank is filled with cold tap water. This would be the case either the first time the water was heated or after heavy water usage (e.g. in a home, after multiple family members consecutively take showers). The second scenario is reheating the tank after normal water usage, which would drain only a

portion of the tank. The third scenario is reheating after standby losses (when the tank loses heat relatively uniformly over time.) In reality, tank temperature profiles represent a mix of these scenarios. For example, a washing machine might draw off some hot water, but the tank might only start to reheat after some additional standby losses. The three prescribed scenarios therefore are only samples, but should be representative of the full scope of operation.

Two organizations provide standards for testing of water heaters in the United States; the Department of Energy (DOE) and the American Society of Heating, Refrigeration, and Air Conditioning Engineers (ASHRAE). The DOE standard is specified in Chapter 10, Part 430, Appendix E of the U.S. Code of Federal Regulations, and is titled "Uniform Test Method for Measuring the Energy Consumption of Water Heaters" [17]. The ASHRAE standard, 118.2-2006 is titled "Method of Testing for Rating Residential Water Heaters" [22]. These rating tests are outside of the scope of this project, but they include helpful guidelines in determining when the water tank is sufficiently heated (cut-out condition) during a test, and when it needs to be reheated (cut-in condition). The two standards are consistent in prescribing a cut-out condition of 57.2°C. The DOE standard prescribes a cut-in condition of 42.2°C. These temperatures are specified as average tank temperatures. In the constructed test facility, average tank temperature is measured by taking the mean temperature from 10 surface thermocouples attached to the body of the water tank every 15cm from top to bottom. With these protocols, the three heating experiments are performed as follows:

- Test A: Efficiency of initial tank heating
    - *The tank is initially filled with cold tap water (15°C+/- 2°)*
    - *The tank is heated from top to bottom until the average tank temperature reaches 57.2°C*
- Test B: Efficiency of tank reheating after water usage
    - *The tank is initially filled with hot water (>55°C).*
    - *Water is drawn from the tank at 75 g/s until the average tank water temperature falls below the 42.2°C cut-in condition*
    - *The tank is reheated back to the cut-out condition of 57.2°C*
- Test C: Efficiency of tank reheating after standby losses
    - *The tank is initially filled with hot water (>55°C).*
    - *The tank sits idle until the average water temperature in the tank falls below the cut-in condition of 42.2°C*
    - *The tank is reheated to an average temperature of 57.2°C*

3.3 Test Matrix

The baseline performance evaluation was designed to provide an appropriate test of all the parameters that affect the COP and capacity. Two separate studies were performed. One was a parametric study of both the ambient temperature and the type of heating scenario. A full factorial study was performed at ambient temperatures of 10°, 15°, 20°, 25° and 30° C for heating scenarios A, B and C, with a 60°C hot water temperature . The second study was a parametric study of hot water temperature. Hot

water temperatures of 55°, 60°, 65° and 70° C were tested at 20°C ambient temperature for heating scenario A. A full description of the test matrix for each study is shown below in Tables 2 and 3.

Table 2: Parametric study: effect of ambient temperature and heating scenario on COP and capacity

Heating Scenarios Studied	Ambient Temperatures Studied	Control Variables	Dependent Variables
A. Initial Tank Heating B. Water Usage and Reheat C. Standby Loss and Reheat	• 10 ˚C • 15 ˚C • 20 ˚C • 25 ˚C • 30 ˚C	• Hot Water Temperature = 60 ˚C • Tap Water Temperature = 15 ˚C (+/- 2 ˚C) • Refrigerant Charge (1.08kg CO_2)	• Overall COP • Average Capacity

Table 3: Parametric study: effect of hot water temperature on COP and Capacity

Hot Water Temperatures Studied	Control Variables	Dependent Variables
• 55 ˚C • 60 ˚C • 65 ˚C • 70 ˚C	• Heating Scenario = Test A • Ambient Temperature = 20 ˚C • Tap Water Temperature = 15 ˚C (+/- 2 ˚C) • Refrigerant Charge (1.08 kg CO_2)	• Overall COP • Average Capacity

In these studies, the overall COP and average capacity are defined as follows:

$$COP_{overall} = \frac{\sum_{n=1}^{N} Q_{gc}}{\sum_{n=1}^{N} W_{comp}} \quad (3)$$

$$Capacity_{average} = \frac{\sum_{n=1}^{N} Q_{gc}}{n} \quad (4)$$

3.4 Control Strategy

Control of the HPWH system is centered around maintaining a constant hot water temperature at the outlet of the gas cooler, since this is a control variable in the first parametric study, and is the varied parameter in the second parametric study. There are two viable control strategies for maintaining a constant hot water temperature under varying environmental conditions. They each involve the simultaneous manipulation of two devices. In commercial HPWH's, the hot water temperature is typically maintained through the opening/closing of an electronic expansion valve, and changing the rotational speed of the variable speed compressor, under a constant water flow rate [23]. Another strategy is to adjust the expansion valve opening and the water flow rate under constant compressor speed. In this experiment, the latter control strategy was chosen.

A superior control strategy would be one that optimizes the COP at each experimental condition. If the COP is not optimized, then the system is not being judged based on its potential at the given environmental conditions. The problem is that for a given hot water temperature, there is a spectrum of possible expansion valve openings and water flow rates (or expansion valve openings and compressor speeds).

Each one will have its own COP, with the optimum point located somewhere along this spectrum.

A useful way to visualize this spectrum is in terms of the approach temperatures in the gas cooler. The approach temperature at the CO_2 inlet side (AT_i) is the difference in temperature between the CO_2 discharge temperature and the hot water temperature. The approach temperature at the CO_2 outlet side (AT_o) is the difference between the CO_2 temperature at the outlet of the gas cooler and the temperature of the water entering the gas cooler from the tank. In practice, the CO_2 discharge temperature can be more or less independently controlled by adjusting the expansion valve. If the water flow rate is then adjusted to hold the water temperature constant, AT_i increases as the increase of the discharge temperature. Increasing AT_i tends to decrease AT_o, increasing the temperature glide of the CO_2, and thus the enthalpy difference in the gas cooler. This increase comes at the expense of the mass flow rate, however, as well as an increase in compressor power. Figure 3 below illustrates the relationship between the approach temperature on each end of the gas cooler and the COP. The axes are the approach temperatures on each side of the gas cooler, and the data points are experimental results under steady state operating conditions for 15°C inlet water temperature at 20°C ambient temperature. One curve is for 55°C hot water and the other curve is for 65°C hot water. The COP at each data point is listed beside the point.

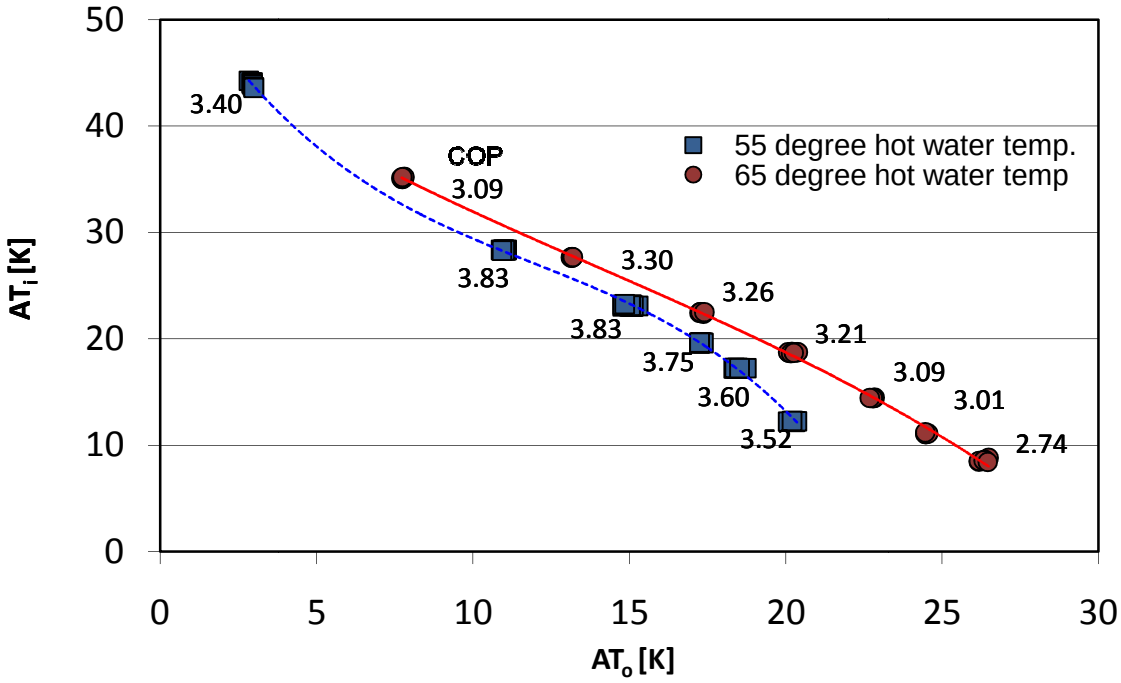

Figure 3: Achieving optimum COP through control of approach temperatures

These curves change at different ambient temperatures and inlet water temperatures, but, from experience in preliminary testing, a good rule of thumb for this system was that the COP tended to decrease below 20K AT_i. If AT_i was above 20K, the COP was generally optimized by opening the expansion valve such that the superheat reached its lowest acceptable value (3K). Thus, the control strategy in all heating tests was to keep the superheat at 3K unless the discharge temperature was less than 20K warmer than the hot water temperature. The 20K rule of thumb is valid for this particular set of components. A model of this system created in Engineering Equation Solver(EES) (and described in detail in Chapter 4) indicated that if the UA value of the gas cooler is increased (or in other words, the gas cooler is made larger or more

efficient), then the approach temperatures at which the optimum COP occurs decrease. In Figure 4 below, the 65°C curve from Figure 3 were reproduced using the model. The overlaid data point is the point of maximum COP. Then the model was run again, this time with a gas cooler twice as large. The curve was shifted down so that the optimum AT_i was about 17K, corresponding to an AT_o of about 5K..

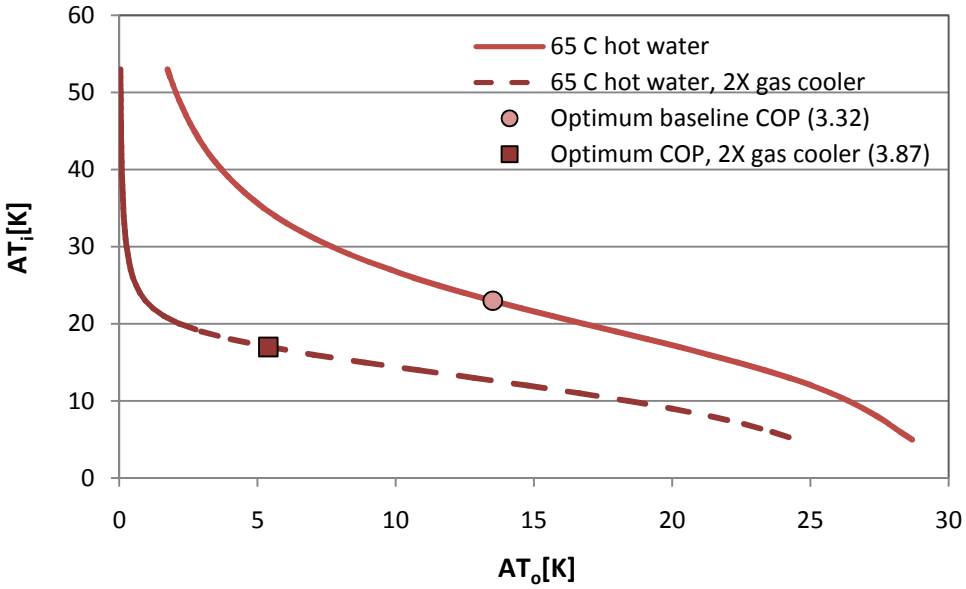

Figure 4: Effect of heat exchanger size on approach temperatures and optimum COP

It is important to understand that approach temperatures on one or both ends of the gas cooler are unavoidable consequences of the mismatch in heat capacity between the CO_2 and the water during their exchange of sensible heat. The specific heat of water is more or less constant, while the specific heat of CO_2 in the supercritical region follows a meandering path. A perfect heat exchanger would eliminate the temperature difference at the "pinch point," somewhere in the middle of the heat

exchanger. A diagram of this heat exchange with the pinch point labeled is shown below in Figure 5.

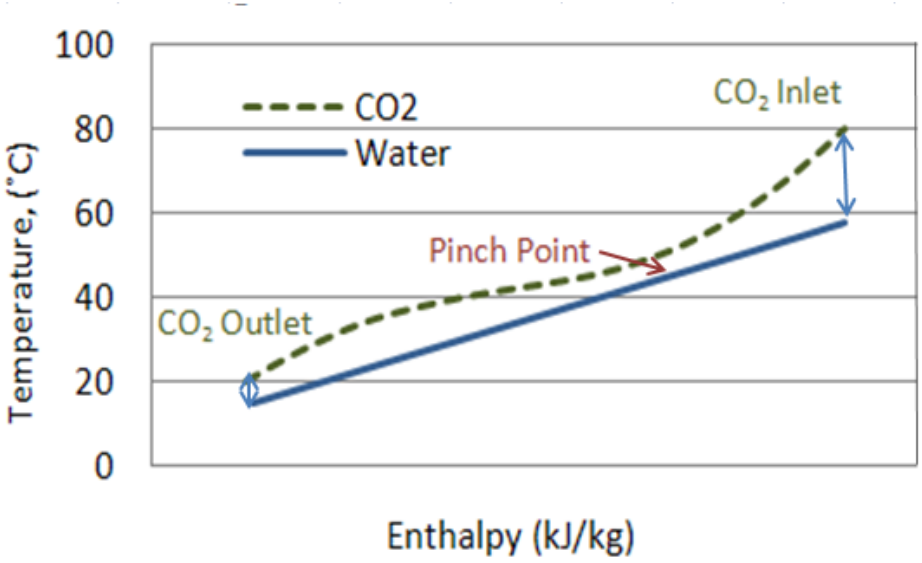

Figure 5: Water and CO_2 temperatures along the length of the gas cooler

3.5 Uncertainty Analysis

The COPs reported in the baseline testing results are the average of the COP as measured on the CO_2 side and the water side of the system. Thus the reported uncertainty in the COP is

$$U_{COP,AVG} = \frac{\sqrt{U_{COP,water}{}^2 + U_{COP,CO_2}{}^2}}{2} \quad (5)$$

The COP is calculated by dividing the capacity by the compressor power, so the uncertainty of either the water side or CO_2 side COP is equal to

$$U_{COPw/c} = COP_{w/c}\sqrt{\left(\frac{U_{Power}}{Power}\right)^2 + \left(\frac{U_{Capacity,w/c}}{Capacity_{w/c}}\right)^2} \quad (6)$$

Since the capacity is equal to the mass flow rate multiplied by the enthalpy difference, Δh,

$$U_{COPw/c} = Capacity_{w/c}\sqrt{\left(\frac{U_{MFR,w/c}}{MFR_{w/c}}\right)^2 + \left(\frac{U_{\Delta h,w/c}}{\Delta h_{w/c}}\right)^2} \quad (7)$$

where

$$U_{\Delta h,w/c} = \sqrt{U_{h,inlet}{}^2 + U_{h,outlet}{}^2} \quad (8)$$

The uncertainty of an enthalpy value is more complicated to calculate. The enthalpy is a function of temperature and pressure, but there is no explicit equation that can be used to calculate the enthalpy. Thus the uncertainty in the enthalpy is calculated by investigating the deviation in the enthalpy caused by varying the pressure and temperature by +/- the uncertainty in each value. In other words, the uncertainty in the enthalpy is taken as the maximum of the four possible cases in Equation 9.

$$U_h = \max\left(\left|h_{T,P} - h_{T+UT,P+UP}\right|, \left|h_{T,P} - h_{T+UT,P-UP}\right|, \left|h_{T,P} - h_{T-UT,P+UP}\right|, \left|h_{T,P} - h_{T-UT,P-UP}\right|\right) \quad (9)$$

Finally, the uncertainties in the measured quantities, U_T , U_P , U_{POWER} , and U_{MFR} are taken as the square root of the sum of squares of the device's systematic error and its random error observed during testing (equal to the standard deviation of the

measured value during steady state condition). Table 4 shows device systematic and random error and the propagation of uncertainty for typical measurement conditions.

Table 4: Typical propagation of uncertainty for baseline measurements

	Systematic Error	Random Error	Uncertainty
Pressure Transducers	23 kPa	8 kPa	24 kPa
Thermocouples	0.5 K	0.04 K	0.5 K
Watt Meter	60 W	1.41 W	60 W
CO2 Mass Flow Meter	0.10 g/s	0.03 g/s	0.10 g/s
Water Mass Flow Meter	0.47 g/s	0.07 g/s	0.48 g/s
h			1.3 - 2.0 kJ/kg
$Capacity_w$			112 W
$Capacity_c$			54 W
COP_w			0.2
COP_c			0.18
$Capacity_{AVG}$			**62 W**
COP_{AVG}			**0.13**

3.6 Results

3.6.1 Parametric Study of Ambient Temperature and Heating Scenario

The results of the ambient temperature and heating scenario parametric study are shown below in Figure 6.

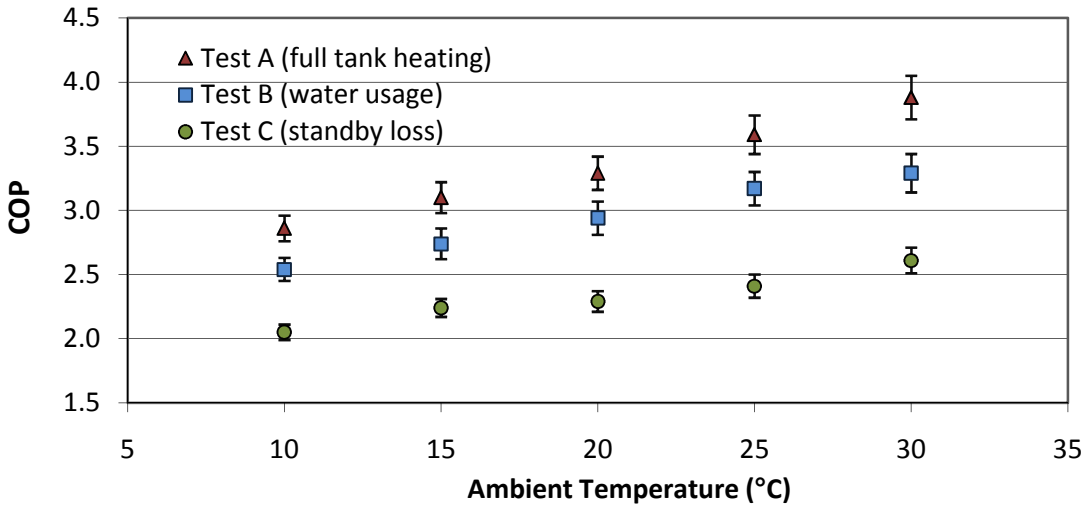

Figure 6: Parametric study of the effect of ambient temperature and heating scenario on COP

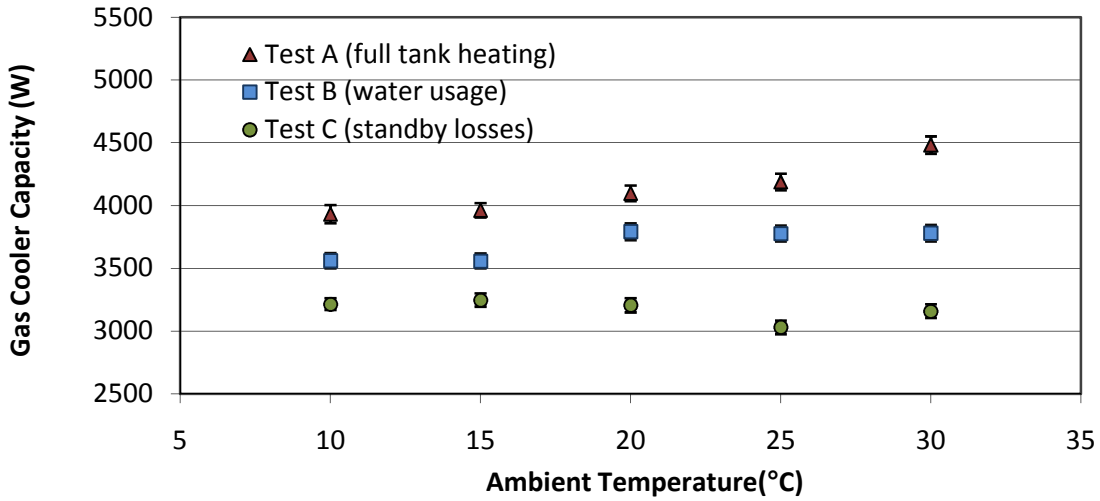

Figure 7: Parametric study of the effect of ambient temperature and heating scenario on capacity

The increase in COP at increasing ambient temperatures was an expected consequence of the increasing evaporating temperature/pressure leading to a decrease in pressure ratio and therefore lower compressor power. The effect on capacity is much more complicated. There were two competing factors that determined the effect on the capacity; the enthalpy difference across the gas cooler and the mass flow rate of

CO_2. The higher suction pressures at higher ambient temperatures caused a higher suction density and therefore a higher flow rate. The opening of the expansion valve at higher temperatures, however, had the effect of lowering the discharge pressure. At lower discharge pressures in the supercritical region, the enthalpy difference for a given CO_2 temperature glide is reduced. For the "A" tests, the higher mass flow rate won out, and the capacity was increased at higher ambient temperatures. For the "B" and "C" tests, the capacity was mostly flat for increasing ambient temperature.

The difference in performance between the different scenarios is directly related with the inlet water temperature to the gas cooler. As the inlet water temperature increases, the CO_2 in the gas cooler can no longer be cooled to as low of a temperature. Thus, the instantaneous COP decreases nearly linearly with increasing inlet water temperature. To relate this back to the heating scenario, during the initial tank heating scenario, the gas cooler is fed cold water from the bottom of the tank for nearly the entire duration of the test (see Figure 8.) During the water usage and reheat test, the gas cooler again is subject to the colder water at the beginning of the test, but this temperature rises earlier in the test. This is because tank stratification is not achieved as well with the cold tap water feed mixing to some degree with the hot water initially at the bottom of the tank (see Figure 9). Finally, during the standby loss test, the tank consistently feeds the gas cooler warm water (see Figure 10). In Figures 8-10, the temperatures at different vertical locations in the tank are plotted, and labeled from 1 to 10, with 1 being the lowest vertical location. These figures show the evolution of the tank temperature profile over time.

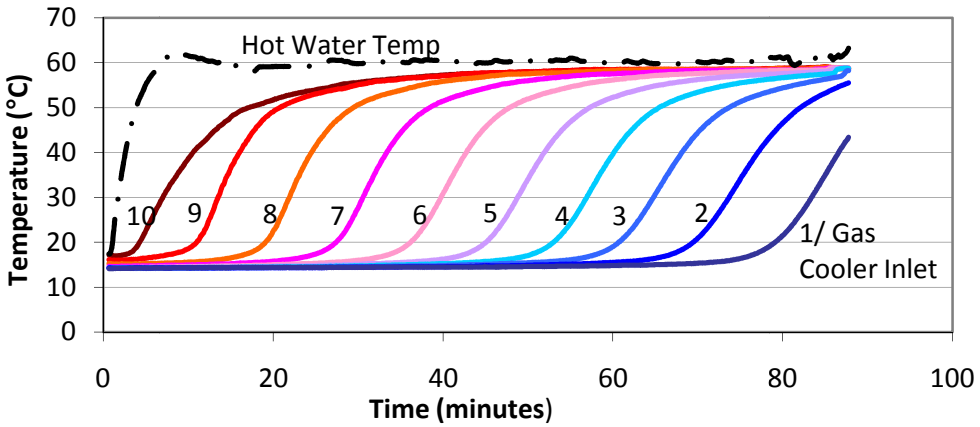

Figure 8: Tank temperature profiles during an initial tank heating ("A" test)

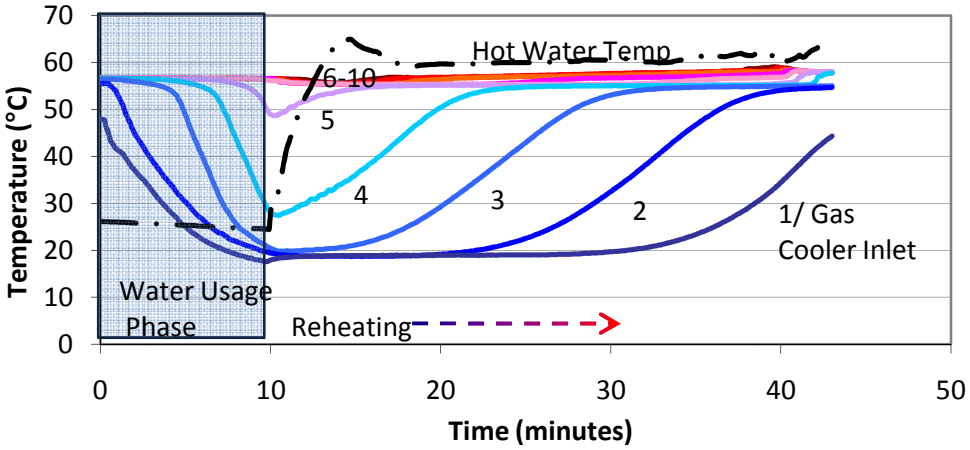

Figure 9: Tank temperature profiles during a water usage and reheating test ("B" test)

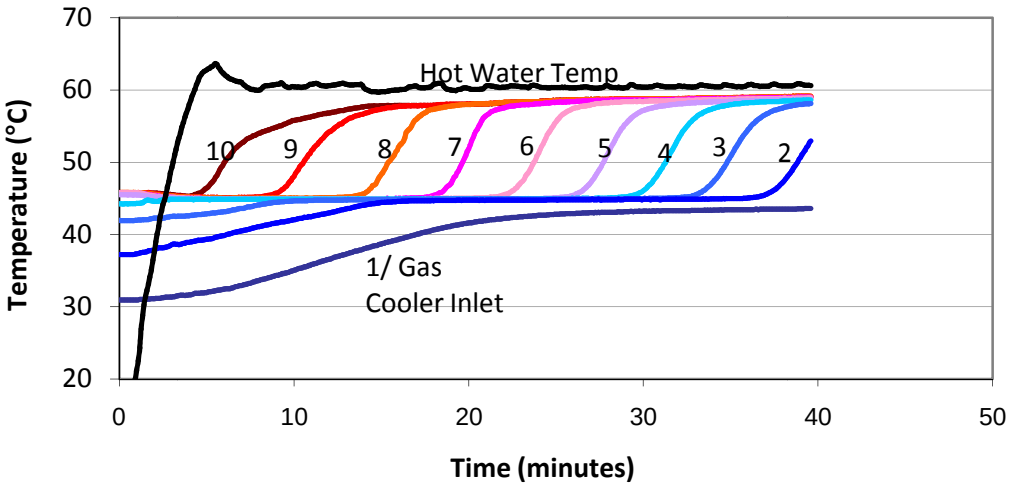

Figure 10: Tank temperature profiles during a standby loss reheating test ("C" test)

For the performance of the system, the key temperature at any given time is the gas cooler inlet temperature, which is fed from the bottom of the tank. Figure 11 below shows the gas cooler inlet temperature during the "B" and "C" test and its effect on COP. In each case, the drop in COP accompanies the rise in inlet gas cooler water temperature. The occasional jumps in COP are due to manual adjustments of the water flow rate to maintain a fixed hot water temperature.

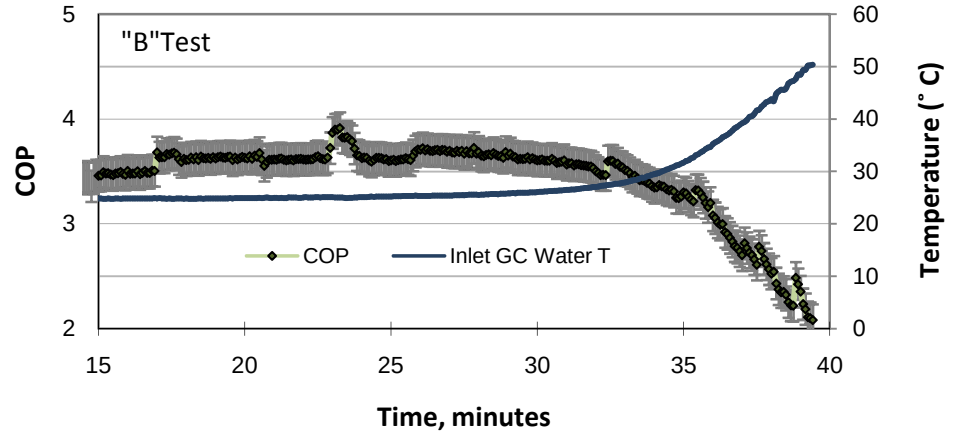

(a) "B"Test

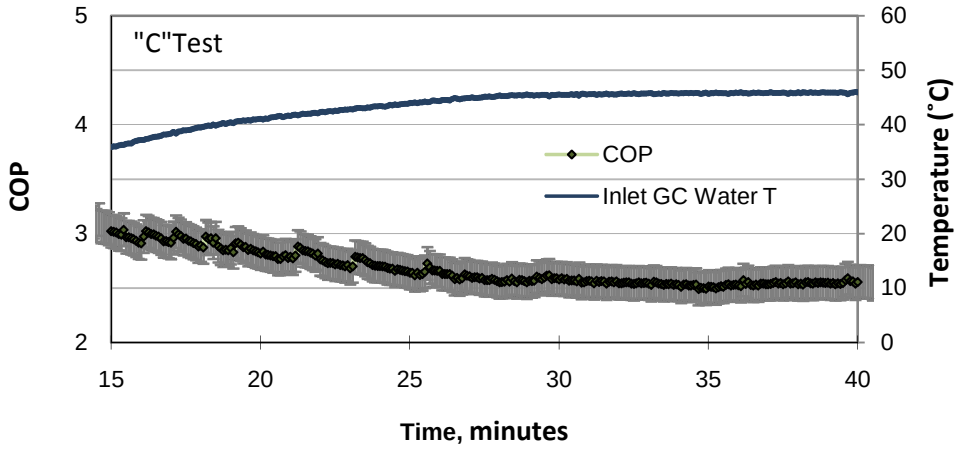

(b)"C" Test

Figure 11: Relationship between gas cooler inlet water temperature and COP ("B" and "C" tests)

3.6.2 Parametric Study of Hot Water Temperature

As described earlier, a second parametric study was performed to determine the effect of changing the hot water temperature on the COP and capacity. Both the heating scenario (Test A) and the ambient temperature (20˚C) were held constant. The study revealed a decrease in COP by about 20% when the hot water temperature was increased from 55 to 70˚C, as shown in Figure 12, below. The capacity peaked at 60°C, and then decreased at higher ambient temperatures, due to the decline in mass flow rate. Modeling was done to analyze the effect of changing the hot water temperature on COP and capacity at different ambient temperatures and heating scenarios.

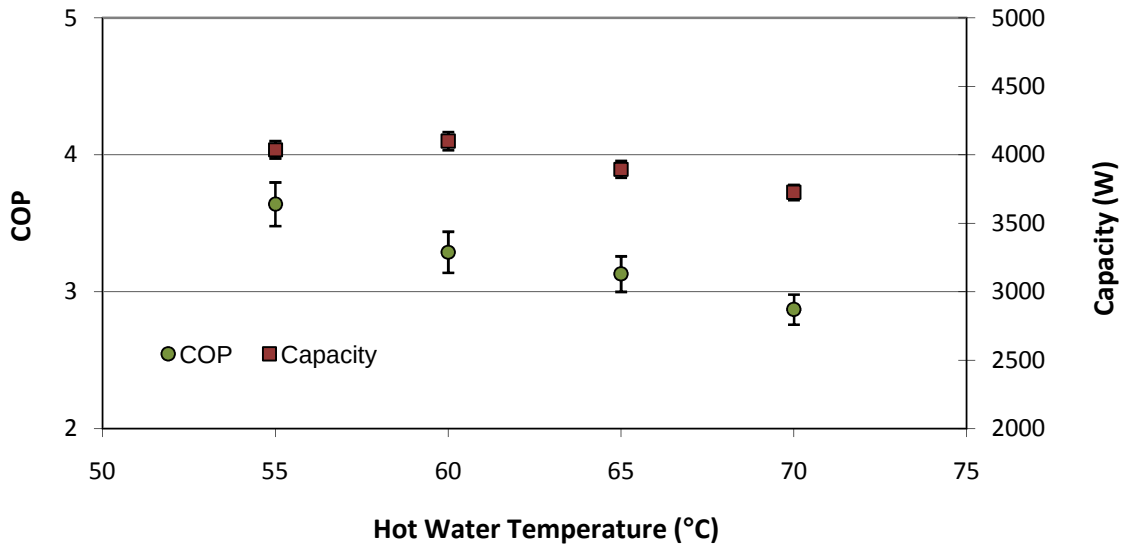

Figure 12: Parametric study on the effect of hot water temperature on COP and capacity

4 Modeling

A model of the HPWH was developed in EES to predict system performance in untested conditions and to perform sensitivity studies of key component parameters on the COP. EES is a convenient tool for the construction of a model of the vapor compression cycle, since each component of the cycle can be defined according to a set of governing equations –either first principle or empirically derived. EES works by solving a set of defined equations simultaneously, so that unknown quantities can be found through an iterative solution algorithm. A model can be created by defining the thermodynamic conditions at state points that exist between cycle components. These state points are analogous to nodes in electronic diagrams. The thermodynamic progression of the refrigerant between those state points can be defined according to governing equations and empirical correlations. EES is additionally useful in such a model because it contains extensive, accurate thermophycial property data for most refrigerants. Thus, if enough information can be determined to uniquely define a state point, EES can provide all relevant thermodynamic properties at that point (temperature, pressure, enthalpy, entropy, density, specific heat, specific volume, thermal conductivity, viscosity and quality), which can then be used in further calculations.

4.1 Description of the Model

The CO_2 gas cooler involves the sensible transfer of heat between CO_2 and water. In the transcritical region, the specific heat of CO_2 is highly variable, so the gas cooler

has to be divided into small segments that each transfer a small portion of the total heat. If the gas cooler is segmented properly, then it can be safely assumed that the specific heat of CO_2 is constant within that segment. Then, for each segment, the log-mean temperature difference (LMTD) method can be used to approximate the heat transferred in that segment and the appropriate refrigerant and water temperatures entering and leaving that segment. In this model, the gas cooler was divided into 10 segments by heat transfer area. The decision of 10 segments was a tradeoff between model accuracy and complexity. With too many segments, EES can run into problems converging on a solution, which proves to be cumbersome, especially for parametric studies. Figure 13 shows the model's error in estimating gas cooler capacity as a function of the number of model segments. In this figure, the capacity for an infinite number of segments is unknown, so the 20 segment case is taken as the reference case and assigned a 0% error.

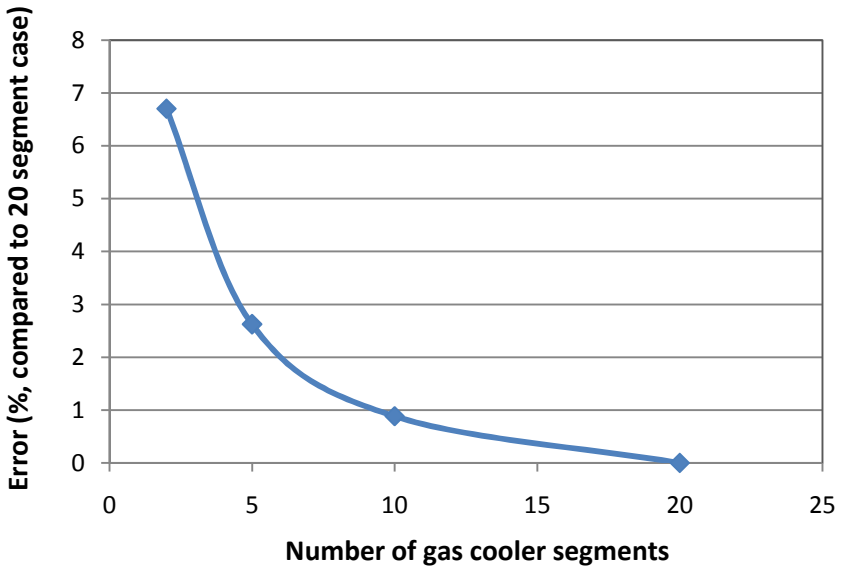

Figure 13: Sensitivity study: Model error in estimation of gas cooler capacity

The equation for heat transferred in each segment is

$$\frac{UA_{gc}}{10}\left(LMTD_i\right) = Q_i \qquad (10)$$

where UA_{gc} is a term for the empirically determined effectiveness of the gas cooler that is conceptually the average overall heat transfer coefficient multiplied by the heat transfer area, Q_i is the heat transferred in the current segment and

$$LMTD_i = \frac{\Delta T_i - \Delta T_o}{\ln\left(\Delta T_i / \Delta T_o\right)} \qquad (11)$$

where ΔT_i is the temperature difference between the CO_2 and the water at the inlet of the segment and ΔT_o is the temperature difference between the CO_2 and the water at the outlet of the segment. Equation 10 can be solved simultaneously with the following two equations

$$Q_i = \dot{m}_c \left(h_{c,i+1} - h_{c,i}\right) \qquad (12)$$

$$Q_i = \dot{m}_w \left(h_{w,i+1} - h_{w,i}\right) \qquad (13)$$

The inputs to the overall gas cooler model are the inlet water temperature, the hot water temperature, and the compressor discharge CO_2 temperature, and the outputs are the water mass flow rate and the CO_2 gas cooler outlet temperature.

To come up with an empirical relation for UA_{gc}, the gas cooler model was essentially run backwards, so that the inputs were the inlet and outlet CO_2 and water

temperatures and the CO_2 mass flow rate (observed steady state values during full heating tests), and the outputs were the water mass flow rate and the UA_{gc} that would be necessary to achieve the input conditions. The UA value for a heat exchanger is not necessarily constant, since the "U" of UA is the overall convective heat transfer coefficient. The overall heat transfer coefficient was hypothesized to increase with the velocity of both the CO_2 flowing in the microchannels and the velocity of the water flowing over those channels. Since the effect of changing either flow rate could not easily be isolated, the calculated UA_{gc} from the model was plotted against the sum of the two flow rates (Figure 14). From a regression analysis of the linear curve fit of the collected data points, this seemed to be an excellent modeling approach.

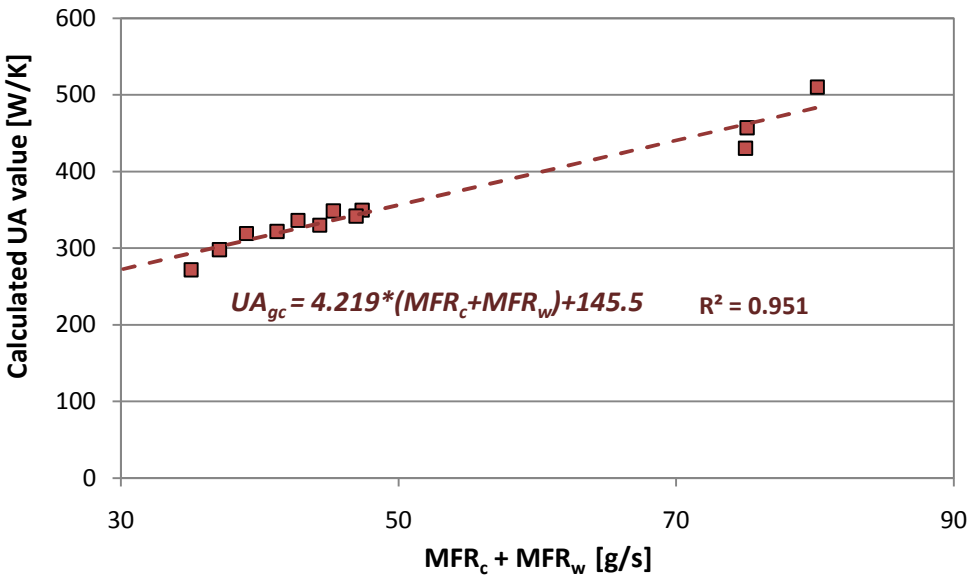

Figure 14: Empirical gas cooler UA as a function of the sum of CO_2 *and water flow rates*

The evaporator uses a simpler heat transfer model that uses the inputs of ambient temperature, the degree of superheat at the evaporator outlet, and the CO_2 enthalpy at

the evaporator inlet to estimate the required saturation temperature and pressure, according to the following equations:

$$Q_e = UA_e\left(T_{ambient} - T_{sat,e}\right) \tag{14}$$

$$Q_e = \dot{m}_c\left(h_{c,e,o} - h_{c,e,i}\right) \tag{15}$$

For the evaporator, an empirical relation for UA_e was determined in a similar fashion as for UA_{gc}. In this case, the temperature at the inlet to the evaporator was changed to an input and UA_e was made an output of the model. The model was then run with empirical data from the same set of test conditions. During baseline testing, the air velocity across the coils of the evaporator was kept constant. The CO_2 mass flow rate changed to some degree, but since the CO_2 side convective heat transfer coefficient is much higher than the air side heat transfer coefficient, the overall heat transfer coefficient should be relatively insensitive to changes in CO_2 mass flow rate. Therefore the UA value should theoretically be fairly constant. Equation 14, however, assumes that the temperature difference between the CO_2 and the air is constant. For most of the length of the evaporator, it is more or less constant. At the end of the evaporator, however, the refrigerant becomes completely evaporated and is then heated sensibly. Thus, in this region of the evaporator, the temperature difference becomes more and more reduced. Higher superheats can be interpreted as a larger region of the evaporator containing vapor refrigerant undergoing sensible heat transfer. For these higher superheats, the expectation is that the calculated UA value would be lower. Thus, using a correlation for the UA as a function of superheat (see Figure 14) can help

to account for the inaccuracy of the assumption. Unfortunately, the evaporator is otherwise very difficult to model.

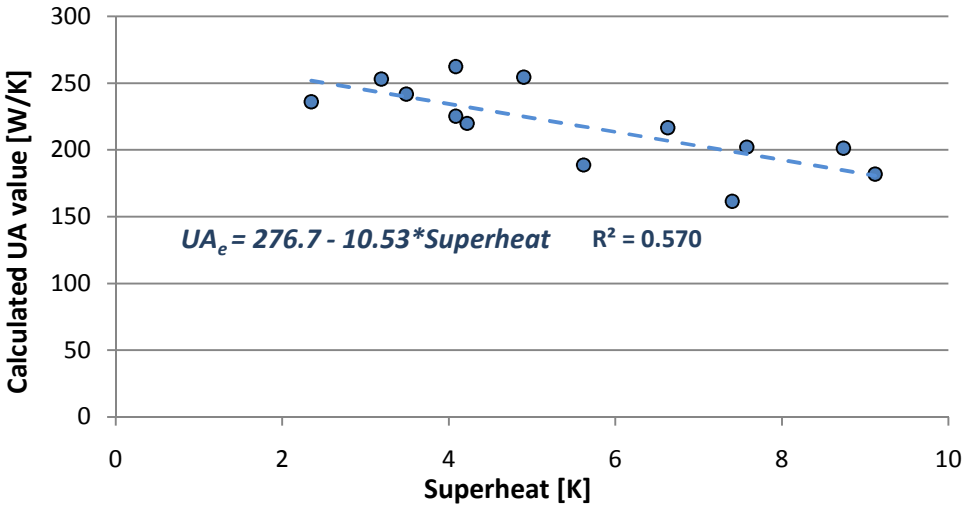

Figure 15: Empirically derived UA value for the evaporator as a function of evaporator superheat

The compressor model is defined according to the diagram in Figure 16. The compressor was a two-stage rotary compressor that was used essentially as a single-stage compressor during baseline testing. The shell of the compressor contains the intermediate stage refrigerant. Thus, all heat rejection from the compressor takes place in the intermediate stage. The compressor model uses three definitions of compressor efficiency (Equations 14-16) to define key system parameters. The numerical subscripts in the equations refer to the state points in Figure 16.

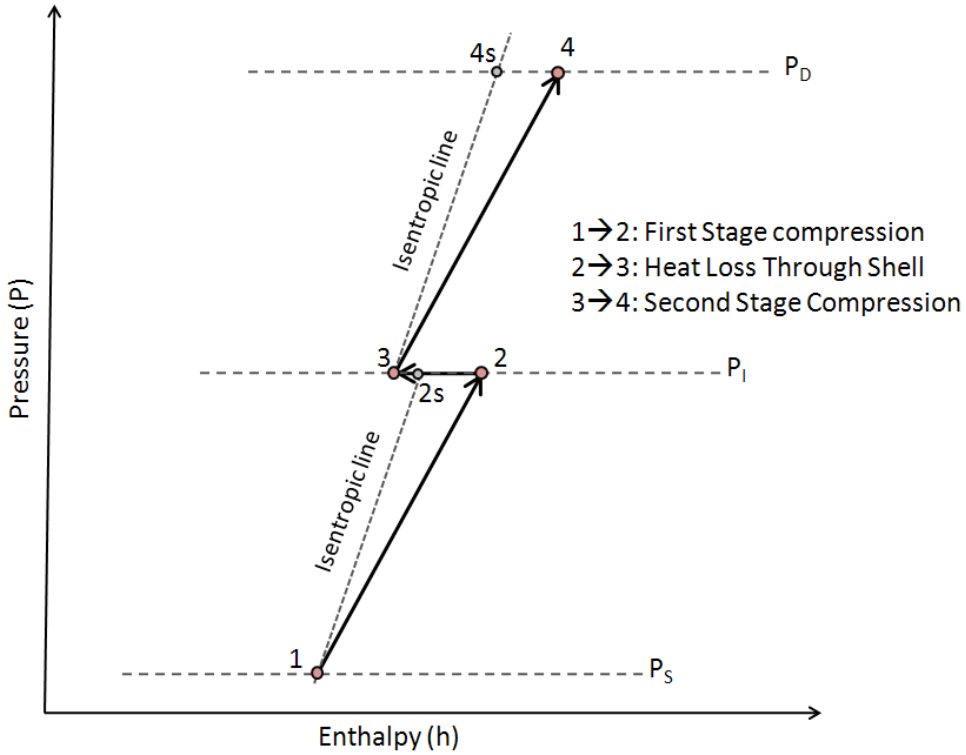

Figure 16: Conceptual diagram of compressor model used in EES HPWH full system model

$$\eta_{vol} = \frac{\dot{m}_c}{V \cdot \omega_{comp} \cdot \rho_1} \tag{16}$$

$$\eta_{ise} = \frac{h_{2s} - h_1}{h_2 - h_1} = \frac{h_{4s} - h_3}{h_4 - h_3} \tag{17}$$

$$\eta_{mec} = \frac{\dot{m}(h_4 - h_1)}{W_{comp}} \tag{18}$$

The compressor mechanical, isentropic, and volumetric efficiencies were modeled as functions of the compressor's pressure ratio (see Figures 17-19), based on measured compressor power and state points derived from baseline testing of the

system. Linear equations for each type of efficiency were then used in the model to predict the system state points and power consumption for new sets of test conditions.

The volumetric efficiency (Equation 16) is used along with the density at the compressor suction, ρ_1, the compressor rotational speed,ω_{comp}, and the compressor displacement volume, V, to determine the CO_2 mass flow rate. The isentropic efficiency (Equation 17) is used in the first stage to determine the temperature at state point 2, based on a known intermediate pressure. It is also used in the second stage to determine the discharge pressure, based on a known discharge temperature. The isentropic efficiency was assumed to be equal during each stage, because there was no way of measuring the temperature at the outlet of the first stage. Finally, the compressor mechanical efficiency (Equation 18) is used along with the enthalpy difference across the compressor and the mass flow rate to determine the electric power required. The amount of heat rejected from the compressor shell is assumed to be 95% of the input electrical energy that was not delivered to the CO_2 (the remaining 5% is assumed to be dissipated to the surrounding magnetic field as eddy currents from the motor).

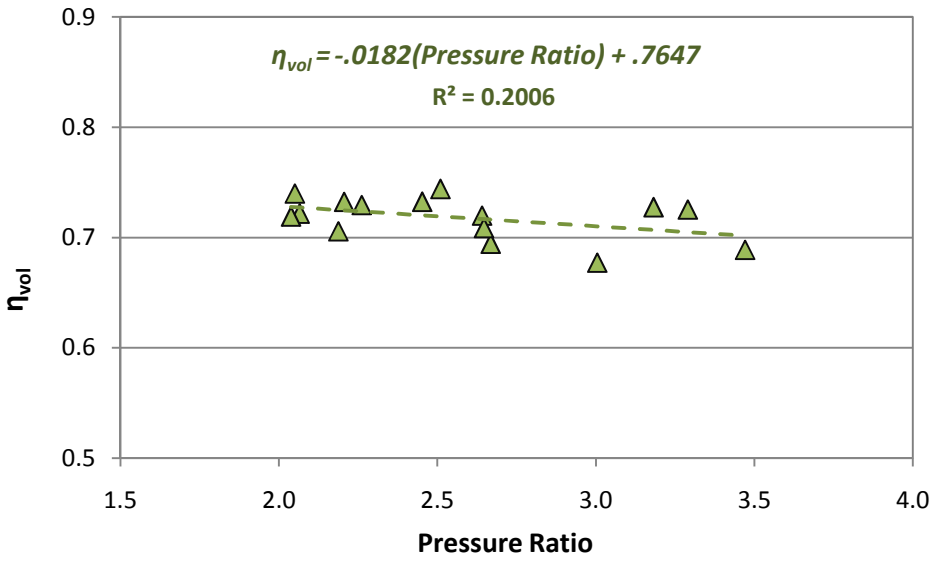

Figure 17: Empirically derived volumetric efficiency at steady state for the baseline tests

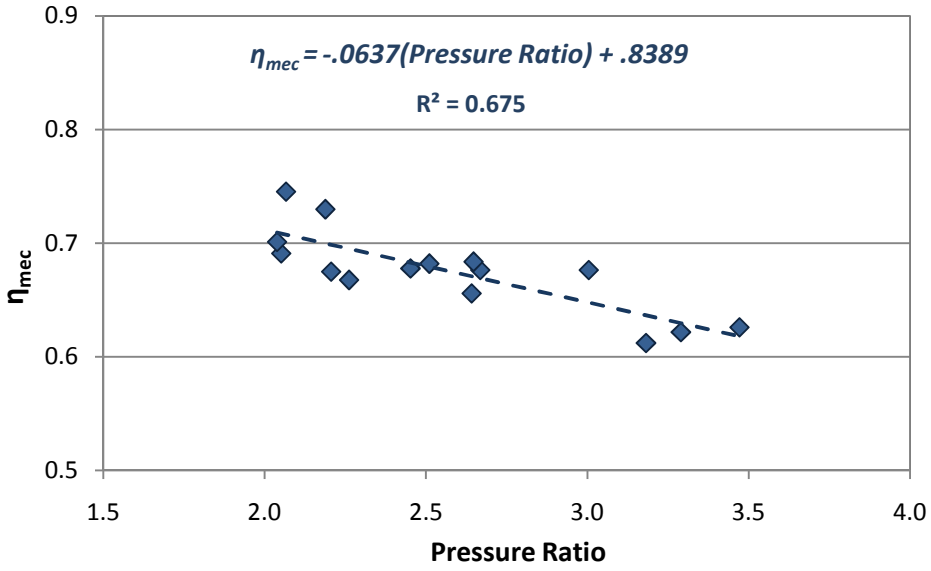

Figure 18: Empirically derived mechanical efficiency at steady state for the baseline tests

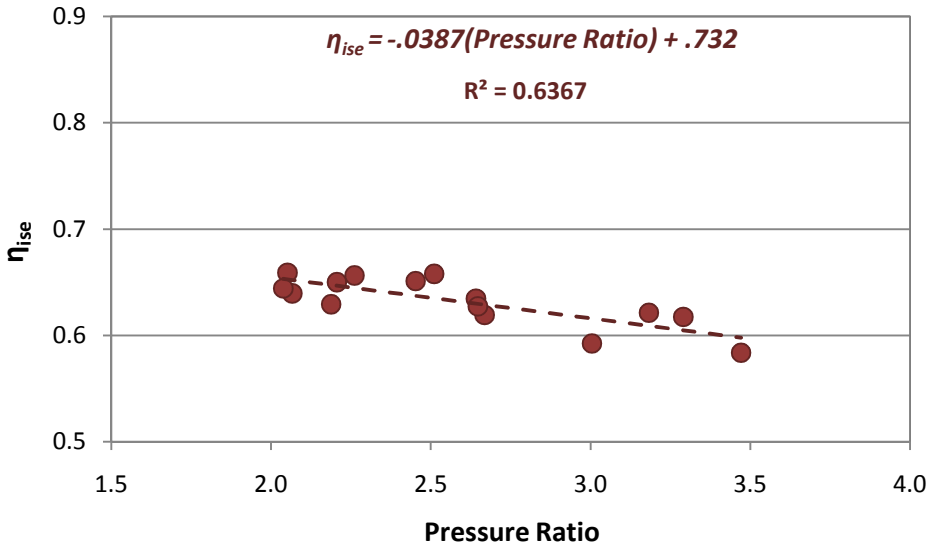

Figure 19: Empirically derived isentropic efficiency at steady state for the baseline tests

Refrigerant side pressure drop in each of the heat exchangers was modeled by applying the empirical relationships shown in Figure 20. The figure was created by plotting the difference in pressure between the inlet and outlet of each heat exchanger every second during a test in which the mass flow rate was reduced from 28 to 8 g/s by reducing the compressor speed. Data points were also taken at 0 g/s with the compressor turned off. Since the gas cooler was broken into 10 segments in the model, the pressure was assumed to drop linearly from the inlet to the outlet of the gas cooler, for the purpose of calculating the pressure in each segment.

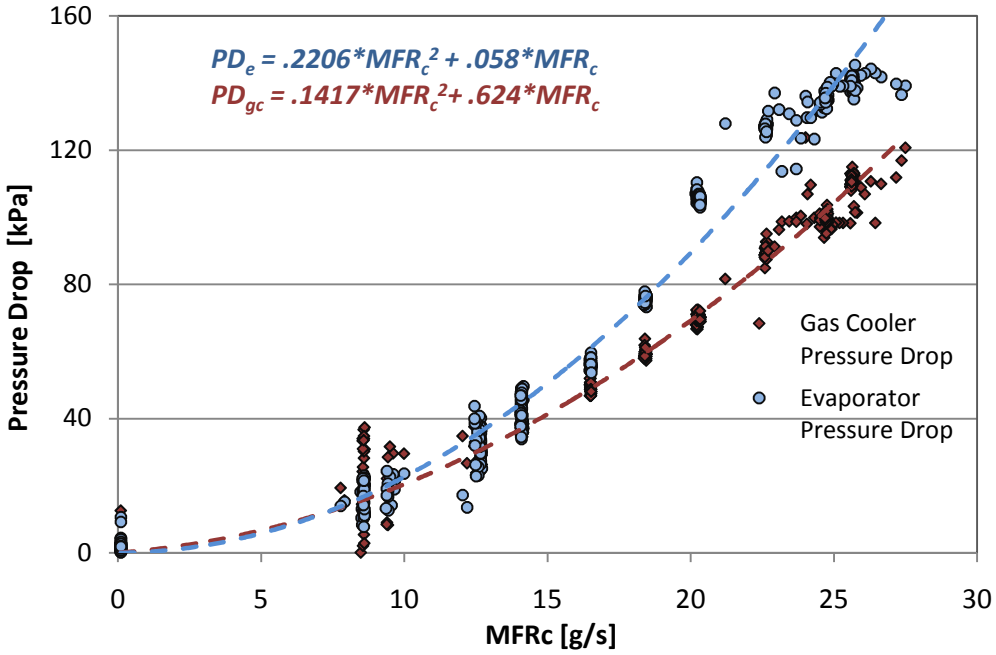

Figure 20: Empirical expressions for pressure drop as a function of CO_2 mass flow rate

4.2 The Potential of the CO_2 Cycle for Heating Water

The EES CO_2 cycle model was used to examine the potential of the CO_2 cycle for heating water and to explore the sensitivity of component performance improvement on COP. Five scenarios were analyzed in the model:

- The baseline system
- System with a gas cooler twice as large
- System with an evaporator twice as large
- System with a compressor having 90% mechanical efficiency
- System with each of the three component enhancements listed above.

For each scenario, four curves were created, representing ambient temperatures from 0 to 30°C. Four modeled data points were plotted for each ambient temperature, ranging from 55 to 70°C hot water temperature. Each point is the optimum COP from a parametric study of AT_i vs. COP. The approach temperature at that optimum point is written next to each point on the graphs to give insight into the discharge temperature to target when trying to optimize performance.

Figure 21 shows the results in the baseline scenario. The COP's are a bit higher in the model than for experimental results, since the conditions at each point in the model are fully optimized, whereas this may not have been entirely feasible during testing. When the baseline model was run with the exact input conditions experienced during testing, the error between the model and the real system was always less than 3%.

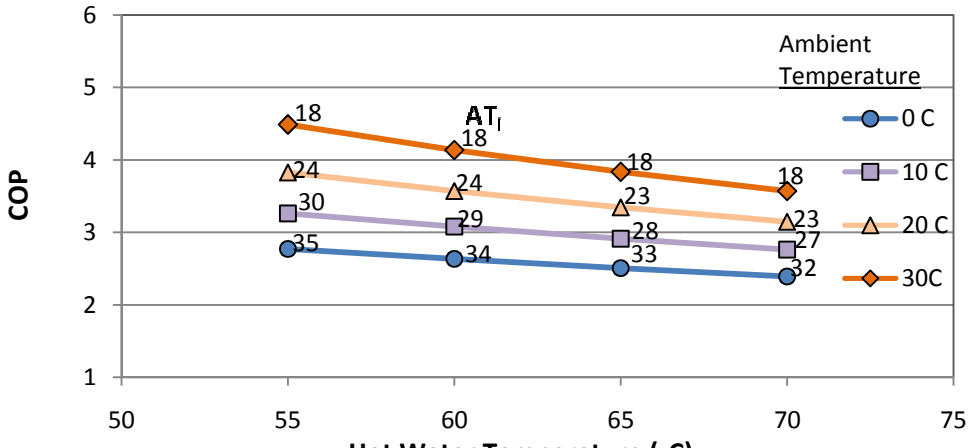

(a)"A" test

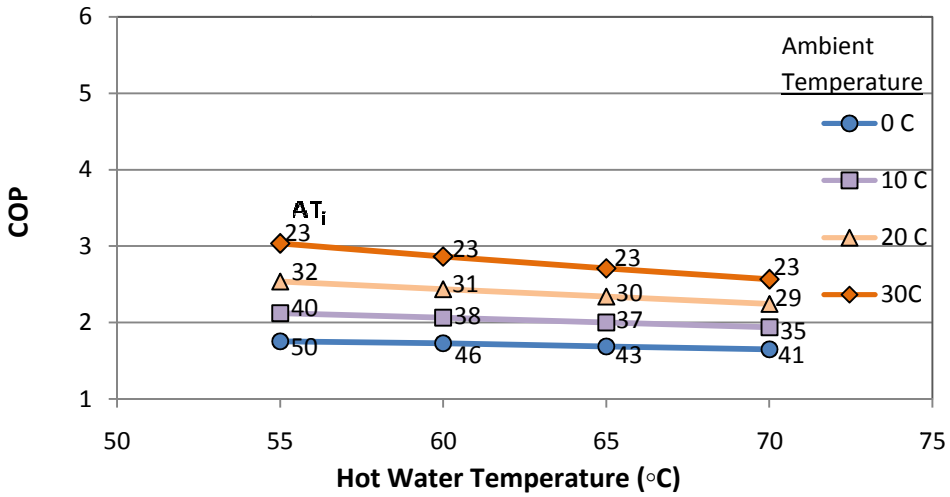

(b)"C" test

Figure 21: Optimum baseline system performance for "A" and "C" tests

The next set of graphs illustrates the results of Scenario 2: a system with a gas cooler twice as large. This scenario was modeled such that the UA value of the heat exchanger was twice that of the baseline system. Additionally, the gas cooler pressure drop was increased by a factor of two, since pressure drop is roughly proportional to the length of tubing. For the "A" test, the performance improvement ranged from 11-19% over the baseline conditions. For the "C" test, however, the performance enhancement was only 1-11% with an average of only about 5%. In the "A" test, the optimum CO_2 inlet approach temperature dropped by about 20%. In the "C" test, the temperature dropped 3-6K, compared to the baseline system.

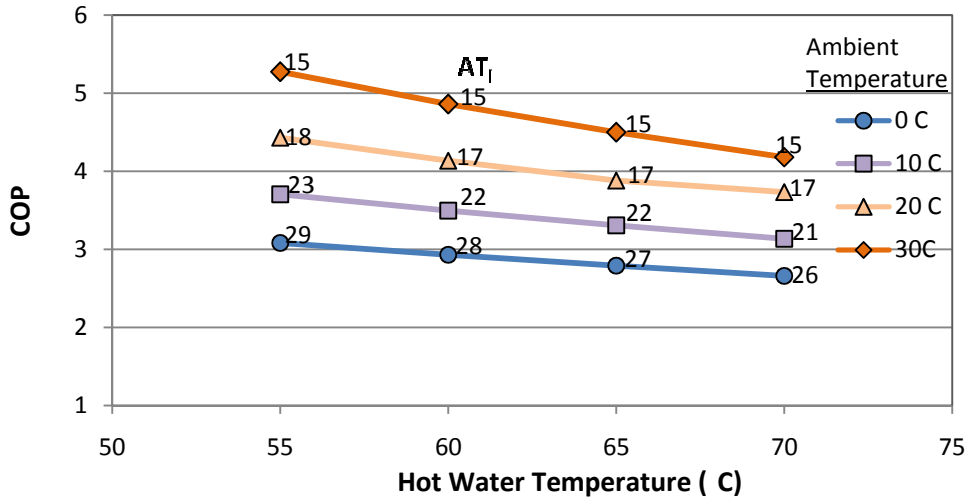

(a) "A" Test

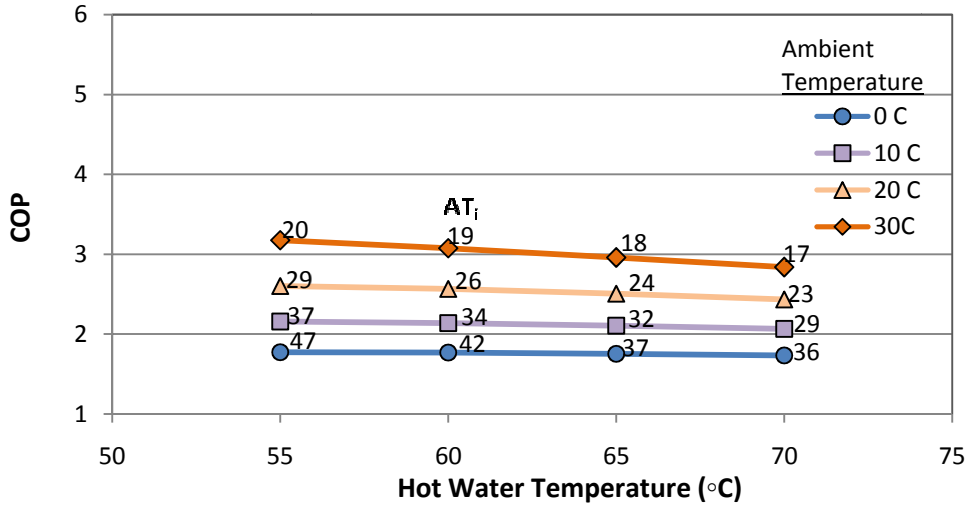

(b) "C" Test

Figure 22: Scenario 2: System with gas cooler twice the size (2x UA, pressure drop)

To understand the reason for the lackluster performance enhancement for the "C" test, refer to Figure 23 below, which shows the CO_2 and water temperatures in the gas cooler during a sample baseline "C" test. With the huge temperature difference at the CO_2 inlet side, nearly all of the heat gets transferred very early in the length of the heat exchanger, and the temperature difference and heat transfer collapses at the tail end. Increasing the heat exchanger size is essentially the same as adding additional

length to the right of the current graph. Obviously, there is not much more to be gained in doing so. This begs the question: if most of the gas cooler is essentially going unused under these conditions, then how does this represent the optimum COP? An explanation lies in the fact that there is not much heat that can be rejected from the CO_2 when it cools from 75 or 80°C down to 45°C. To obtain a sufficiently high enthalpy difference in the gas cooler, the high side of the cycle needs to operate at high temperatures and pressures.

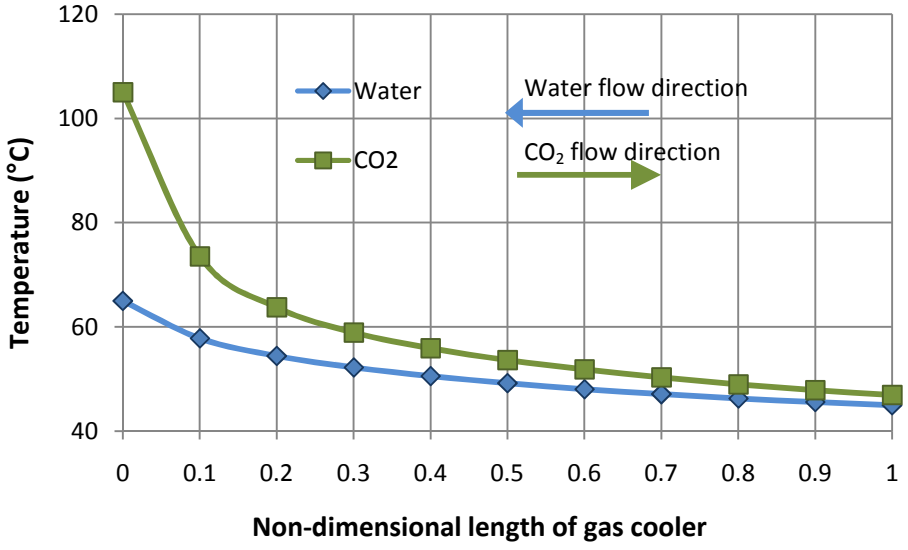

Figure 23: CO_2 *and water temperature distribution in the baseline gas cooler during a sample "C" test*

Figure 24 shows the results from Scenario 3, which was the baseline system with an evaporator that was twice the size (again, in terms of UA and pressure drop). In this scenario, the performance enhancement was more uniform than for Scenario 2, with an 8-14% improvement for the "A" test and a 5-9% improvement for the "C" test. The system always benefits from being able to operate at a higher suction pressure,

afforded by the larger evaporator. Under certain conditions, however, the gains can be muted to some degree by a higher suction pressure pushing the optimum discharge pressure far above the critical point, where the specific heat of the supercritical CO_2 is lower.

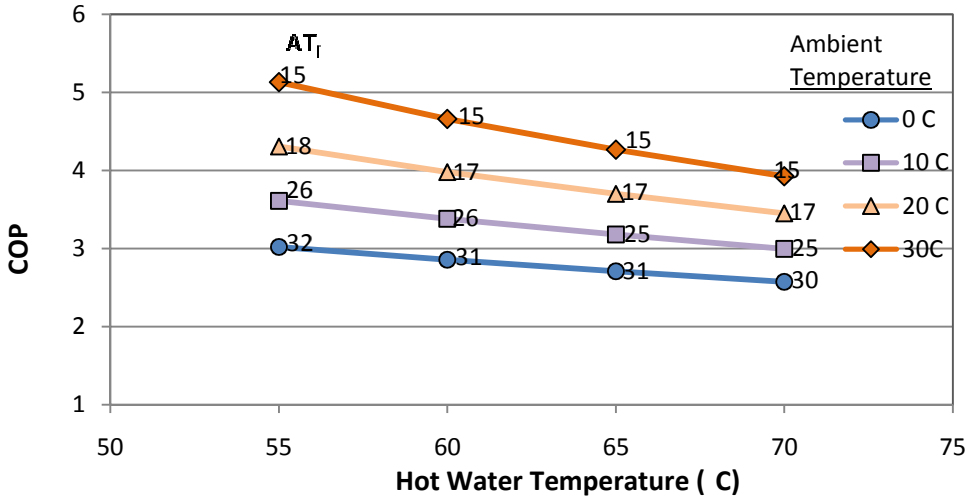

(a) "A"Test

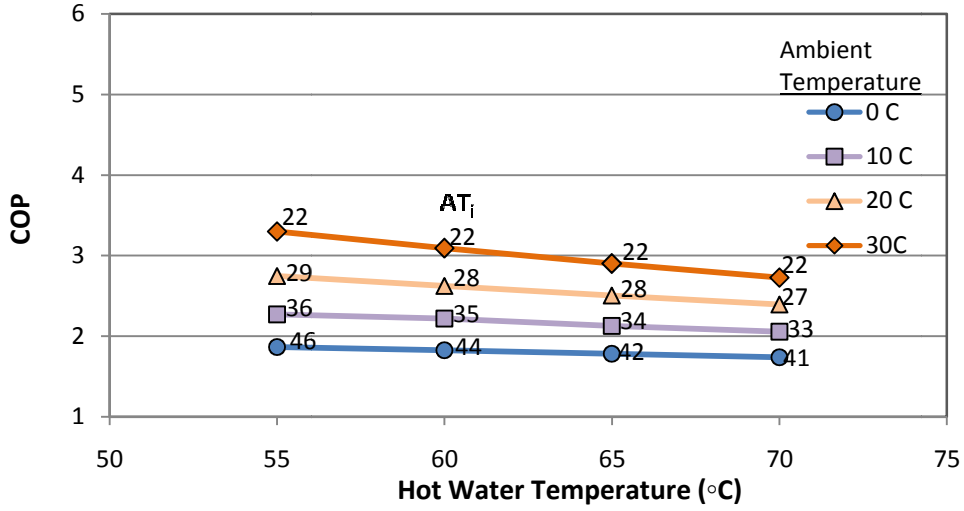

(b) "C" Test

Figure 24: Scenario 3: System with evaporator twice the size (2x UA, pressure drop)

Conceptually, the mechanical efficiency is the fraction of the electrical energy that gets delivered as work and heat to the CO_2 stream. Of the fraction that is not delivered to the CO_2 stream, the vast majority is converted to heat that is rejected from the compressor shell. In cooling applications, this rejected heat from the compressor is useful because it reduces that cooling of refrigerant that must be done in the condenser. For heating applications, however, the condenser (or gas cooler) heat is the useful product of the cycle. If the shell of the compressor were insulated, the frictional heat losses from the compressor would have nowhere else to go besides the CO_2 stream, thus allowing this otherwise lost heat to be captured. Insulating the compressor is modeled in Scenario 4 as an increase in the mechanical efficiency to 90%.

COP enhancement from the increased mechanical efficiency ranged from 8-16% for the "A" test and 9-19% for the "C" test. This modeling indicates that for heating cold water, the most effective performance enhancement is to increase the effectiveness of the gas cooler. For reheating warm water, increasing the compressor's mechanical efficiency is the best course of action. There is an important caveat to the increase in mechanical efficiency – it comes with an increase in the optimum AT_i. At some points, the optimum discharge temperature is well over 100°C. Such high temperatures are likely to cause damage to the compressor in the long run. Therefore, if the compressor is insulated, the system should be run at safe discharge temperatures, in some cases meaning sub-optimal operation.

To test the assumption that insulating the compressor would lead to an increase in mechanical efficiency without significantly influencing the other compressor efficiencies, a test was performed with the current system's compressor. At a constant 20°C ambient and inlet water temperatures, and a constant 60°C hot water temperature, the system was brought to steady state, and its state points and COP were recorded. With the system running, strips of ½" Armaflex foam insulation (R-2) were applied to the compressor shell, covering the majority of its surface. The system was again allowed to come to steady-state operation. After applying this insulation, the mechanical efficiency increased from 71 to 79%, the isentropic efficiency stayed constant at 60%, and the volumetric efficiency stayed constant at 67%. With the 8% increase in mechanical efficiency, the compressor discharge temperature increased by 2K, and the COP increased by 2.5%. The predicted increase in COP from the model under these conditions was 3.0%.

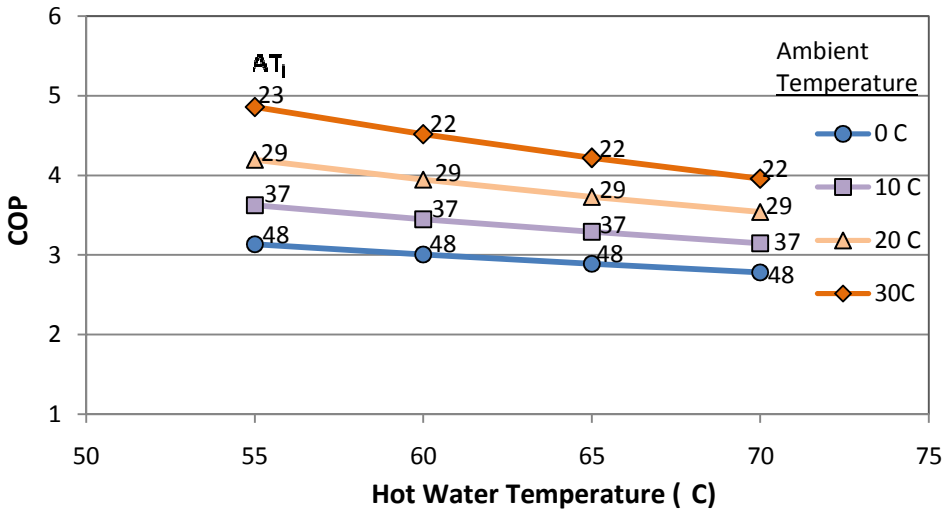

(a) "A" Test

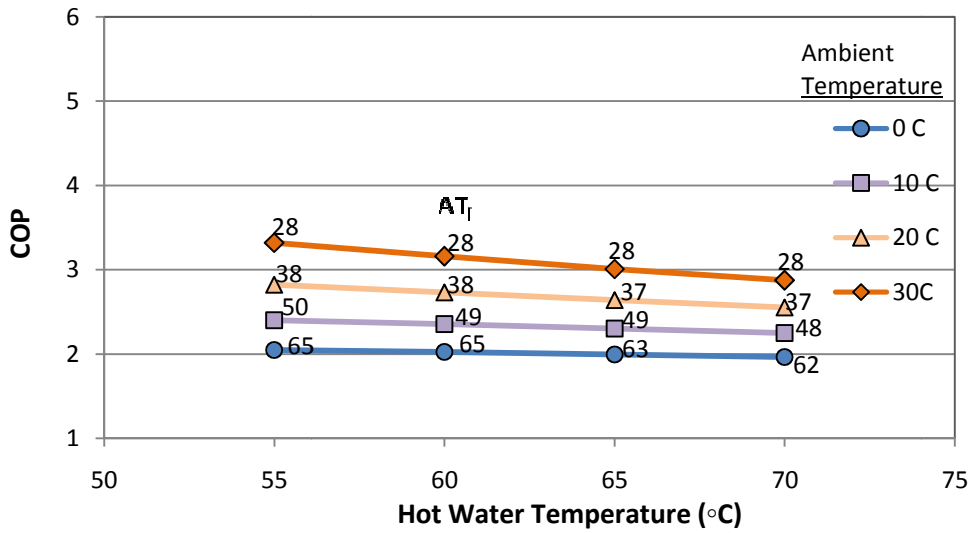

(b) "B" Test

Figure 25: Scenario 4: System with insulated compressor (90% mechanical efficiency)

The final scenario combines the individual component performance enhancements of Scenarios 2-4 into one enhanced system. Overall COP improvement over the baseline system ranged from 23-32% for the "C" test and from 36-50% for the "A" test. Scenario 5 should represent something approaching the practical COP limits for a CO_2 HPWH. Interestingly, the current generation of Japanese CO_2 HPWHs report COP's of 5.1, at 24°C ambient temperature for 65°C hot water and 16°C tap water. Interpolating these test conditions from Scenario 5A yields a COP right around 5.1 or 5.2. Such high performance from the Japanese CO_2 HPWH's is surprising given their compact appearance.

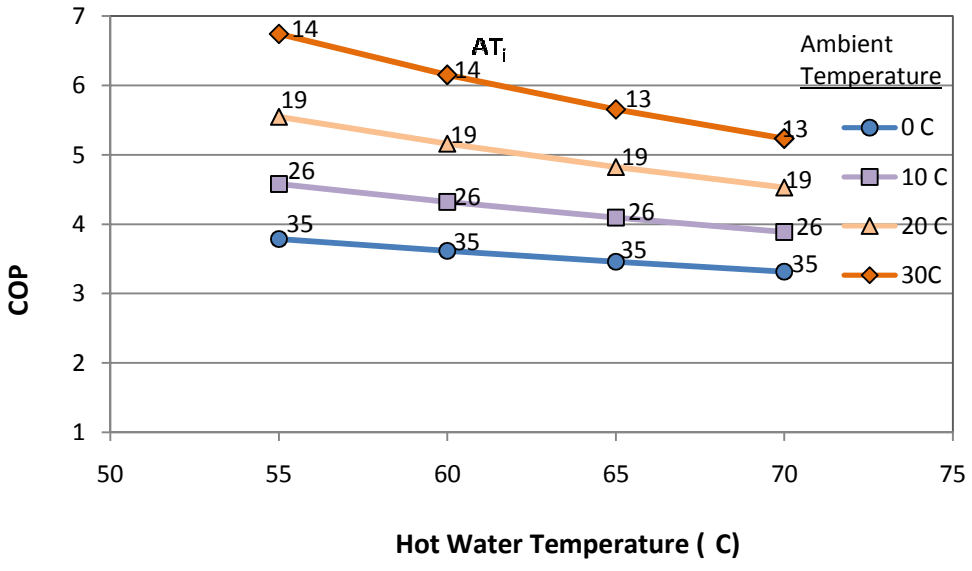

(a) "A" Test

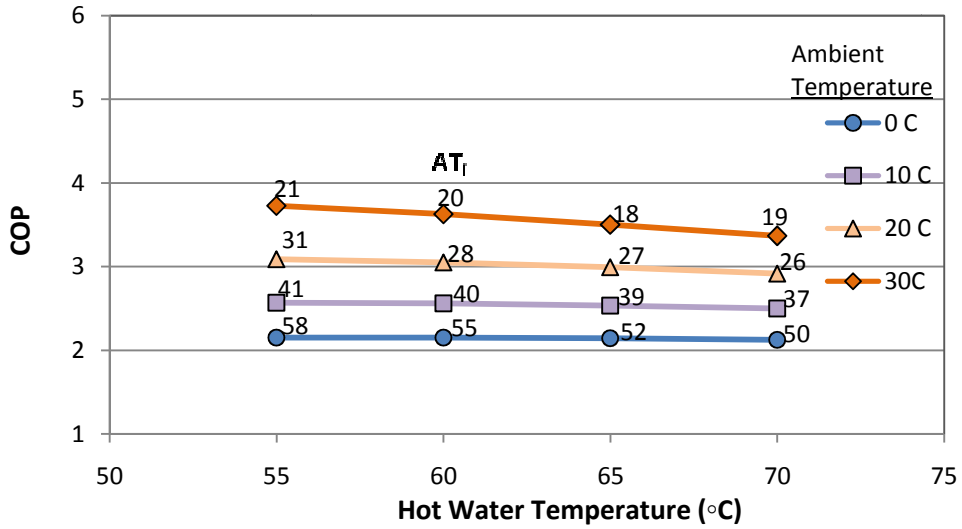

(b)"C" Test

Figure 26: Scenario 5: System with all three performance enhancements

Table 5 is a summary table of the modeling work. The first two columns show the average of the COP for the 16 data points making up each test in each scenario. For scenarios 2-5, these average COPs are compared to the baseline system, and the percent improvement is noted in the second two columns.

Table 5: Summary table for component enhancement modeling

	Average of COP's, ("A" test)	Average of COP's ("C" test)	% improvement ("A" test)	% improvement ("C" test")
Scenario 1: Baseline System	3.26	2.23		
Scenario 2: 2x larger gas cooler	3.76	2.35	**15.0**	5.6
Scenario 3: 2x larger evaporator	3.61	2.39	**10.6**	7.0
Scenario 4: Insulated compressor	3.64	2.53	**11.6**	**13.3**
Scenario 5: All of the above	4.68	2.81	**43.42**	**26.2**

5 Evaluation of Oil Retention

5.1 Description of Oil Retention Measurement Facility

Shown in Figure 27 is a schematic of the test facility for oil retention testing. Here, the main CO_2 circuit is depicted in thick, solid lines, circuits for oil flow are depicted as dashed lines, the water tubing is depicted in dotted lines, and the thin, solid lines are pressure balance lines.

During an oil retention experiment, the oil begins in the oil reservoir, where an oil pump injects the oil into one of 4 locations in the system (inlet of suction line, evaporator, liquid line, or gas cooler) via the toggling of a 4-way valve. From the

injection location, oil navigates the system (counterclockwise in this diagram) until it reaches the pair of oil separators in the suction line. These two separators are the same as those installed at the outlet of the compressor. The oil drains from these separators into the oil level sensing vessel, where the collected volume is measured via a level sensing probe. The probe senses the level of the oil through the capacitance of the probe, which is then interpreted as a volume of oil (through a calibration equation). Pressure balance lines lead from the oil level sensor to the suction line, creating a slightly negative pressure in the oil level sensor with respect to the oil separators. This slight pressure differential ensures proper drainage of oil from the separators into the level sensor. From the oil reservoir, pressure can be balanced to the suction line or the compressor discharge, depending on the injection port. Depending on the injection location, the pressure in the oil reservoir is either slightly negative or slightly positive with respect to the injection location. The pump speed, however, is controlled with a variable speed drive that can be adjusted to achieve the desired mass flow rate of oil, regardless of the pressure differential.

The procedures for calculating the mass of retained oil in the system are discussed in the section on data reduction.

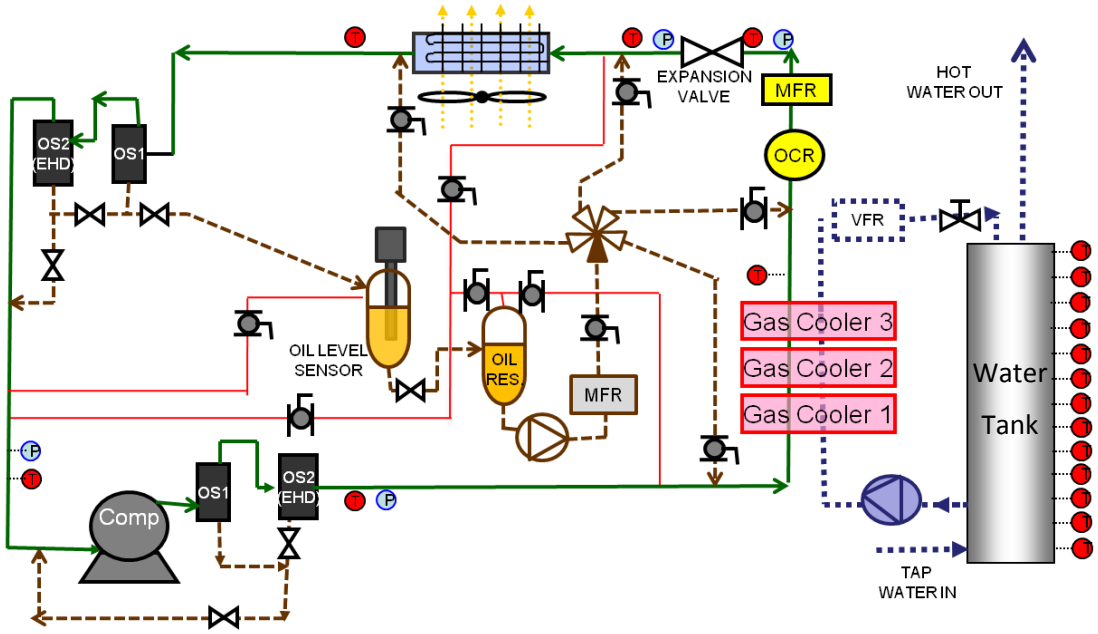

Figure 27: Schematic of oil retention test facility

Specifications for the new components involved in the oil retention testing are detailed in Table 6 below:

Table 6: Instrumentation used in oil retention experiments

Instrument	Type	Manufacturer	Model #	Uncertainty
Oil Level Sensor	Capacitive probe	Omega	LV3000	+/- 0.5%
Oil Mass Flow Meter	Coriolis	Micro Motion	DH025	+/- 0.1% f.s.
Oil Concentration Meter	Capacitive plates	Prototype	N/A	+/- 10% f.s. [9]
LCR Meter	Hand-held	BK Precision	878A	+/-0.1%
High Voltage Power Supply	60 kV	Glassman High Voltage	FX60RS	N/A

5.2 Test Matrix

A test matrix was designed to investigate the role that OMF and CO_2 mass flow rate play in the retention of oil in system components. A full factorial study was chosen wherein 5 different OMFs were tested at two different mass flow rates. The oil mass fractions ranged from 1 to 10% of the overall flow, and the CO_2 mass flow rate ranged from 12-22 g/s, which represented a range of compressor speeds from 35-60 Hz. Oil retention was tested in each of 4 sections of system tubing: a) the suction line, b) the evaporator, c) the liquid line and d) the gas cooler. The variables under study in these experiments were the oil retention (in g/m of tubing), the change in pressure drop (in pressure drop penalty factor) and the change in COP (in %) as a result of the injected oil. The test matrix is summarized in Table 7 below.

Table 7: Test Matrix for Oil Retention Tests

Oil Mass Fraction:	**Mass Flow Rate CO_2**	**Injection Location**	**Dependent Variables**	**Control Variables**
• 1% • 2.5% • 5% • 7.5% • 10%	• 12 g/s • 22 g/s	• Suction line • Evaporator • Liquid line • Gas cooler	• Oil retention • ΔPD_e • ΔPD_{gc} • Δ COP (%)	• System high/ low side pressures (9MPa, 4.5 MPa) • Ambient Temp (20˚C)

The makeup of the 4 test sections is as follows:

Suction Line

- 1.1 m of system suction line 9.5mm tubing (7.4mm ID)
- Oil separators
- 1.2 m of oil drainage line

Evaporator

- 28 m of 9.5mm tubing

Liquid Line

- 2.5 m of 9.5mm tubing
- Oil concentration meter
- Mass flow meter
- Expansion valve

Gas Cooler

- 92 m of 0.89mm microchannels (64 channels in parallel)
- 1.8 m of 9.5mm tubing

The evaporator and the gas cooler test sections are fairly homogenous in terms of the type of tubing through which the oil flows. The gas cooler test section does contain 1.8 m of 9.5 mm tubing, but this is overshadowed by the 92 m of microchannels. The suction and liquid line contain a number of characteristically different components that

will lead to widely different flow behavior along these sections. It is therefore difficult to make generalizations about oil retention in these sections based on the data. However, it is nonetheless important to quantify the oil retention in the suction and liquid lines so that the oil retention in the evaporator and the gas cooler can be accurately quantified as well.

5.3 Measurement Procedures

5.3.1 Resetting the System

Before an oil retention experiment is started, the system must be reset to ensure that consistent and reliable test conditions exist for the experiment. First, heating tapes wrapped around the oil level sensing vessel and oil reservoir are turned on two hours before the start of an experiment to drive out dissolved CO_2 from the oil. Next, oil from the oil level sensor is drained into the oil reservoir by opening the connecting valve between the two vessels. This is done with the oil reservoir's pressure balanced with the low pressure side of the system. The oil level sensor is drained until the level approaches the lower end of the sensing probe inside the vessel (which is at roughly 1960mL gross volume). When this is set, the oil reservoir's pressure is balanced with the side of the system into which the oil will be injected; for the suction line and evaporator, this is the low pressure side of the system. For the liquid line and gas cooler it is the high pressure side. Pressures are checked to make sure they are within the limits of 4600-5400 kPa for the low pressure side and 9000-10000 kPa for the high pressure side. The mass flow rate is checked to make sure it is set to the right value. If

the mass flow rate is off, the compressor speed and/or expansion valve are adjusted to set the flow rate while keeping the pressures within the acceptable limits. Finally, the system is left alone for 30-45 minutes to clear out any residual oil in the system tubing and to allow temperatures, pressures, and mass flow rates to settle to their steady state values.

To test the assumption that the system was relatively clear of oil at the start of an experiment, the evaporator was removed from the system after a series of oil retention experiments, followed by a 30-minute period of operation designed to clear out the oil in the system tubing. The evaporator was weighed on a precise scale, flushed with acetone to dissolve any residual oil, and then with compressed nitrogen to evaporate the acetone. The evaporator was then weighed again, and found to be 1.8 grams lighter. 1.8 grams of oil in the evaporator is consistent with the idea of a very small background flow rate of oil in the evaporator, but indicates that there is not any significant oil that is permanently retained there.

5.3.2 Establishing a Pre-injection Baseline

After steady-state has been achieved, but before injection starts, recording begins for a period of 3 minutes to establish the baseline performance. This means finding the average COP, the average pressure drop in the heat exchangers, and quantifying any background oil flow. The background oil flow rate is determined by taking the derivative of the mass of oil in the oil level sensor with respect to time. The mass of oil in the oil level sensor can be calculated from the measured volume based on

the concentration of CO_2 dissolved in the oil and the density of the CO_2-oil mixture. This will be discussed later in Chapter 5.4.1.

5.3.3 Injecting oil

Oil injection begins by opening the 4-way oil injection valve to the location of the injection port of interest. The oil gear pump is turned on and the pump speed is quickly adjusted with a knob on the pump's control box to match the oil mass flow rate to the value that is necessary to achieve the desired oil mass fraction (for example, at 22 g/s and a 5% oil mass fraction, the oil pump is tuned to pump oil at 1.1 g/s).

During the oil injection phase, the oil is pumped from the oil reservoir, through the gear pump and the oil mass flow meter, then through the 4-way valve to the injection port of interest. The oil mass flow rate is monitored during the test to make sure the rate of oil injection is as steady as possible. In practice, the measured oil mass flow rate fluctuates +/- 0.2 g/s from the nominal value. This seems to be due to compressor vibration interfering with the vibration of the Coriolis mass flow meter. When the compressor is off, the measured oil mass flow rate is +/- 0.05 g/s, and in the case that the compressor speed approaches 40 Hz, the mass flow meter can read +/- 8 g/s, indicating severe vibrational interference. Given the unsteady mass flow rate readings and the fact that we are very concerned with accurately measuring the total mass of oil injected, it is important to keep the measurement timestep in LabVIEW as small as possible.

After oil begins to collect in the oil level sensor, the slope of the collected oil reaches a steady state value. This can occur within several seconds for the 22 g/s tests, or within 30 seconds or so for the 12 g/s tests. The steady state retention period of the test begins at this point. It is important to sustain this period long enough to accurately measure the oil retention, but not too long, since the oil injection can initiate transient system behavior (see Chapter 5.4.2). Generally, a period of 5-10 minutes is acceptable. This time may also be limited on the upper end by the capacity of the oil level sensor. The volume range that is measureable with the oil level sensor's probe is 1,960-2,900 mL, or a net volume of 940 mL. In the case of the 10% OMF test at 22 g/s, this can limit total injection time to about 7-8 minutes.

5.3.4 Establishing a Post-extraction Baseline

After the steady state retention period has elapsed for a sufficient amount of time, the oil pump is shut off and the valves to the injection ports are closed. The oil will then slowly make its way from the system tubing into the oil separators, and drain into the oil level sensing vessel. The slope of the oil extraction curve will settle in the course of a couple minutes to a steady background flow rate, usually around 0.05 g/s, which is typically far below the rate of injection. Once it is clear that the slope of the extraction curve has leveled off, a second set of baseline measurements is taken, again for three minutes. This second baseline is the post-extraction period.

5.4 Challenges and Uncertainties in Oil Retention Measurement

5.4.1 CO_2-PAG Oil Solubility Effects

As previously mentioned, CO_2 dissolves in the PAG compressor oil used in this testing. The amount of CO_2 that will dissolve in the oil is a function of temperature and the pressure. Generally, as temperatures are decreased and pressures are increased, the equilibrium concentration of CO_2 in a volume of PAG oil will increase and vice versa. How fast this equilibrium occurs depends on the mixing dynamics of the CO_2 and the oil. While flowing through the system tubing, the oil exists as a thin film or as small droplets, each with a high ratio of surface area to volume, and will reach a given equilibrium almost instantaneously. Inside the oil reservoir or oil level sensor, there exists a large, stable volume of settled oil, and the equilibrium can take a period of several hours to establish (although pressure related changes seem to happen more quickly.) This is the same phenomenon that occurs when a can of soda (which is basically CO_2 dissolved in water under pressure) is opened. In this example, it may also take a period of hours for all of the CO_2 to dissolve out of solution.

The exact Wt.% of CO_2 in the oil reservoir or in the oil level sensor cannot be known, so it is always assumed that the CO_2 and oil are at a steady state at a given temperature and pressure. The steady-state equilibrium Wt.% of CO_2 in PAG-ND8 oil is shown below in Figure 28.

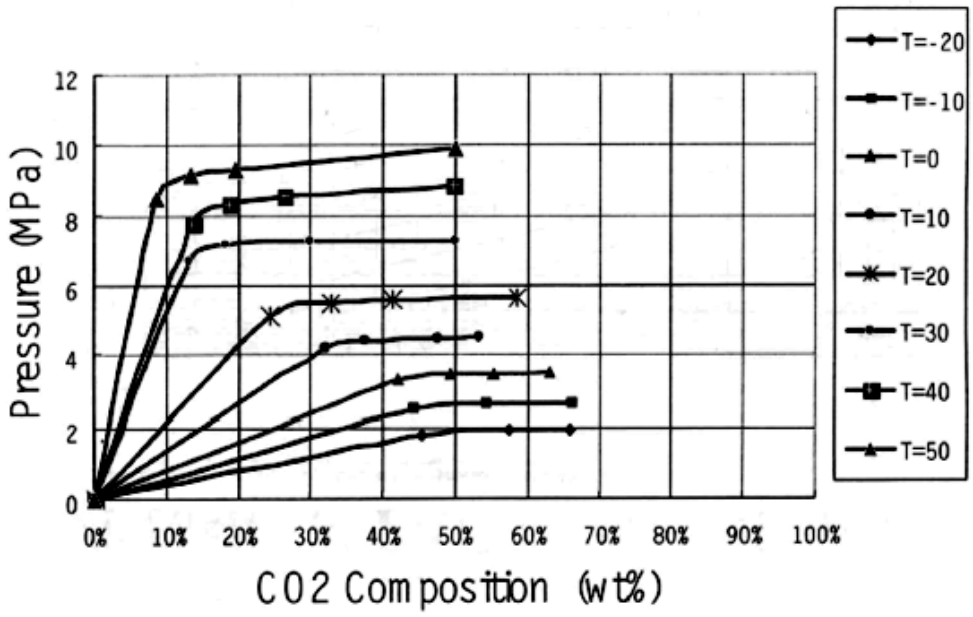

Figure 28: Weight percentage of CO_2 *in PAG-ND8 oil as f(P,T)[9]*

What the graph shows is that for a given temperature, the CO_2 Wt.% increases linearly up to a certain point (with increasingly steeper slopes at higher temperatures), and after a certain turning point, the CO_2 Wt.% can increase dramatically until it reaches 50-70%. Thus, it is very important to keep the oil in the two large vessels at a high enough temperature to ensure that it stays below this turning point. Otherwise, the vessels can siphon off large quantities of oil and the uncertainty of CO_2 Wt.% in the oil can increase exponentially. The quantity of CO_2 dissolved in the oil in the oil level sensor and oil reservoir is estimated by Equation 19, where P_{oil} is in kPa and T_{oil} is in ^{o}C.

$$\mathrm{CO_2\ Wt.\%} = \frac{P_{oil}}{546 + 17.69\left(T_{oil} - 30\right)} \tag{19}$$

5.4.2 Injection –induced Transient System Behavior

One of the most difficult challenges in reporting accurate oil retention measurements is the fact that injecting oil can induce transient behavior of the system, notably in the high and low side pressures and the mass flow rates. The observed effect starts when oil is injected in the system, and lasts until all of the oil has been collected in the oil level sensing vessel. During the period of injection and extraction of oil, the high and low side pressures and the mass flow rate drop fairly linearly with time. In addition, the discharge temperature tends to increase, the expansion valve outlet temperature decreases, and the evaporator outlet temperature increases. The increase in evaporator outlet temperature is in response to the decreased mass flow rate and increased temperature difference in the evaporator causing an increase in superheat.

The hypothesized reason for the mass flow rate and pressure decrease is a change in the volume of the high and low pressure side of the system available for the CO_2 to occupy. As oil is injected into the system, the volume of oil in the oil reservoir drops, and the void is filled with CO_2 that is siphoned off of the discharge line (if the pressure balance line is connected to the high pressure side of the system, e.g. in gas cooler or liquid line injections). At the same time, the oil level sensor is filling with oil at nearly the same rate, and the decreasing available volume in that vessel forces CO_2 into the suction line. Because the CO_2 filling the oil reservoir is at a higher density than the CO_2 leaving the oil level sensing vessel, the net effect between the two vessels is an increase in CO_2 mass. This quantity of CO_2 is thus CO_2 that has been taken away from

the main vapor compression cycle and is stored in the two oil vessels. Assuming the change in volume is equal and opposite in the oil reservoir and oil level sensing vessel, the net increase in mass between the two vessels during the test is equal to:

$$\Delta m = \Delta V\left(\rho_{R,f} - \rho_{LS,0}\right) \tag{20}$$

where ΔV is the change in volume, $\rho_{R,f}$ is the density of CO_2 in the oil reservoir after the test, and $\rho_{LS,0}$ is the density of CO_2 in the oil level sensor before the test.

A sample experiment, in which oil was injected to the inlet of the gas cooler, is shown below in Figure 29. This test featured a volume change of around 600 ml, and an estimated mass increase of 82g within the oil reservoir and oil level sensor. The reductions from before the test to after the test are the following: suction density: -14.4%, mass flow rate: -11.0%, suction pressure: -7.4%, discharge pressure: -3.5%.

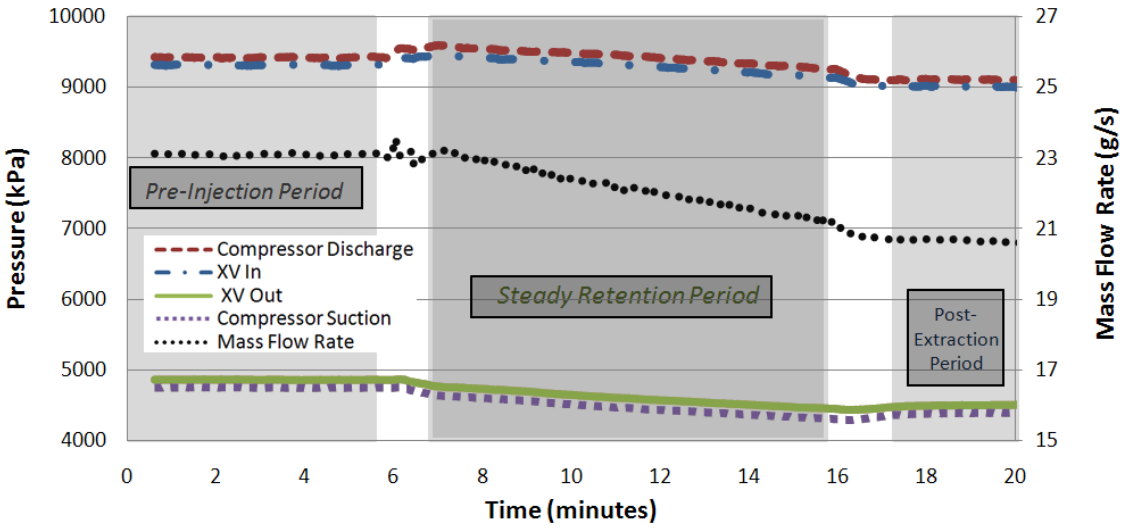

Figure 29: System pressures and mass flow rate during a 22 g/s test at 0.05 OMF

The important implication of this effect is that the experiments in which oil is injected into the gas cooler or the liquid line are not performed at constant pressures and mass flow rates, and thus the measured quantities of oil retention, pressure drop increase, and COP degradation are not constant either. The solution is to average these quantities during the steady state retention period, thereby ensuring that the magnitude of the change in their values is minimized.

5.4.3 Extraction Efficiency

Not all of the oil that enters the oil separators is effectively separated from the CO_2 stream. The ratio of the mass of oil separated from the mass entering the separators is known as the extraction efficiency. It was anticipated that with the use of an EHD separator as a second stage in the oil separation process, the separation of CO_2 and oil would be nearly complete. The prototype EHD, however, was not effective at separating the oil. After a discussion with the developers of the EHD technology, it is believed that a different geometry with a narrower body, narrower inlet tubing, and a thinner electrode would be necessary to achieve effective separation. The combined extractor efficiency observed from the oil retention tests was approximately 60% for the 12 g/s tests and 70% for the 22 g/s tests. There was no statistically significant change in efficiency at different oil mass fractions. This observation differed from the observations of L. Cremaschi's [9] oil retention tests for R22/mineral oil at 46-66 g/s. In his tests, Cremaschi observed a 99% extractor efficiency above 0.05 OMF, around 80% between 0.02 and 0.05 OMF, and as low as 50% for 0.01 OMF. Increasing extractor

efficiency at increasing mass flow rates, however, is an expected result, since the faster flow will induce a stronger vortex in the centrifugal oil separator.

Extraction efficiency can be accounted for in calculating the oil retention. However, if the extraction efficiency changes during a test due to changes in the flow dynamics inside the oil separator, then this will adversely affect the measured oil retention, since a constant extraction efficiency is assumed. The only way to reduce this type of error is to bring the nominal extraction efficiency closer to 100%.

5.5 Data Reduction Procedures

5.5.1 Oil Retention Mass

A series of calculation procedures enables the transduction of raw measurements of oil mass flow rate and volume of extracted oil to the mass of oil retained. The process begins with these raw measurements, shown in Figure 30. Note that the mass flow rate of injected oil has been converted to the total mass of injected oil at a given time step n, by integrating the mass flow rate with respect to time, according to Equation 21.

$$m_{\text{total oil, injected, n}} = \sum_{n=1}^{N} \left(\dot{m}_{CO_2-oil,n} \cdot \Delta t_n \right) \tag{21}$$

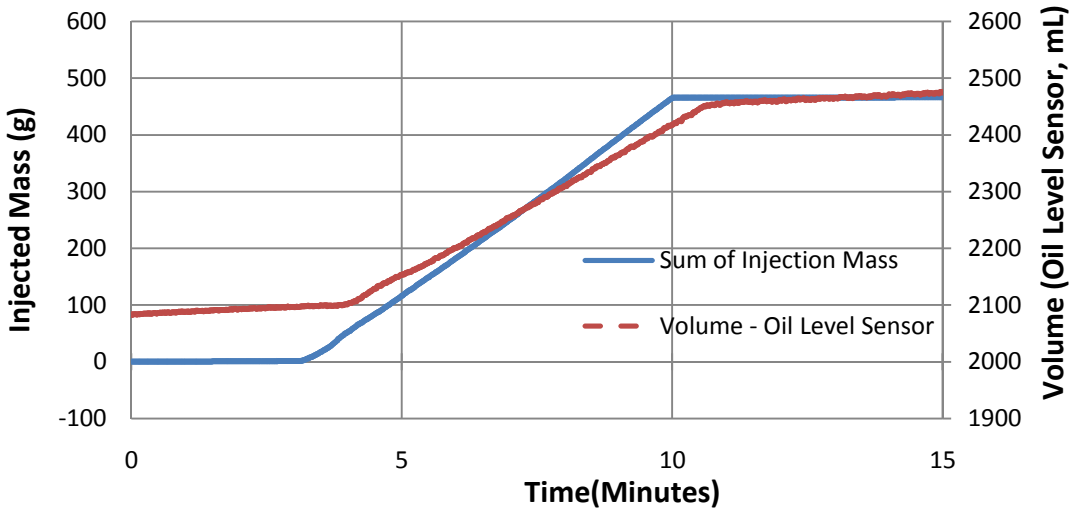

Figure 30: Sample raw measurements: injected mass of oil and oil level sensor volume

The next step is to convert these measurements to their corresponding mass of pure oil by accounting for CO_2 dissolution in the oil.

$$m_{\text{pure oil, injected, n}} = \sum_{n=1}^{N}\left(\left(\dot{m}_{C,n} + \dot{m}_{oil,n}\right)\cdot\left(1-\frac{CO_2Wt.\%_{,n}}{100}\right)\cdot\Delta t_n\right) \quad (22)$$

$$m_{\text{pure oil, extracted, n}} = \left[\rho_{C/oil,n}\cdot V_{LS,n}\cdot\left(1-\frac{CO_2Wt.\%_{,n}}{100}\right)\right]-\left[\rho_{C/oil,0}\cdot V_{LS,0}\cdot\left(1-\frac{CO_2Wt.\%_{,0}}{100}\right)\right] \quad (23)$$

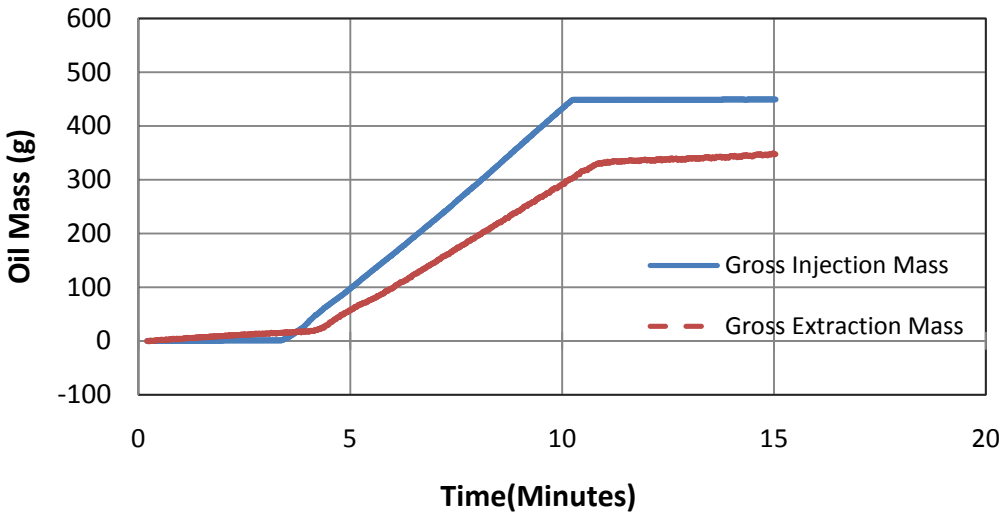

Figure 31: Mass of pure oil from previous raw measurements

If a mass balance of pure oil is applied across the test section, the relationship is the following:

$$m_{oil,injected} + m_{oil,background} = m_{oil,extracted} + m_{oil,bypass} + m_{oil,retained} \quad (24)$$

The oil entering a test section is the sum of the injected oil and any oil that is already present (background flow). As previously discussed, a background flow rate can be deduced from the extraction curve and assigned a linear equation with respect to time. The oil leaving the separators is either collected in the oil level sensor or bypasses the separators and continues flowing to the compressor. The difference between the oil that has entered the test section and the oil that has left the test section is the mass of retained oil. Moving terms around and applying the definition of extractor efficiency, the equation for the oil retention is the following, where all masses listed are pure oil masses:

$$m_{oil,retained} = m_{oil,injected} - \left(\frac{m_{oil,extracted} - m_{oil,background}}{\eta_{separators}} \right) \quad (25)$$

Shown in Figure 32 is a plot of the pure oil injected and the quantity of the extracted oil minus the background oil flow, divided by the extractor efficiency (or in other words, the mass of injected oil that has left the separators). The difference between these two quantities is the mass of retained oil, plotted on the right axis.

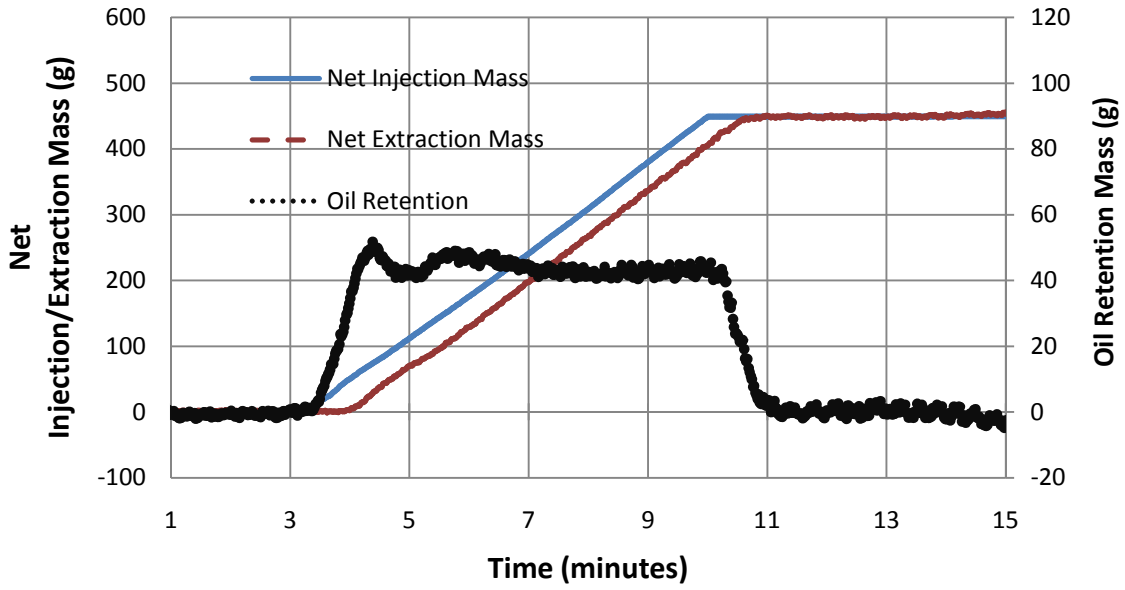

Figure 32: Pure mass of injected oil, injected oil leaving the separators, and oil retention

The extractor efficiency is calculated after an experiment is over and relies on the assumption that all of the oil that was injected eventually clears out of the test section at the end of an experiment, bringing the retention of injected oil back down to zero (which is a fair assumption, considering the findings from 5.3.1). Oil retention for a

given condition is calculated by averaging the calculated oil retention over the steady state retention period. Ideally, the oil retention should be a constant, but since the oil can induce transient behavior in the system, in reality, there may be some drift.

5.5.2 Increase in Pressure Drop

One of the important consequences of oil retention that is being studied is the increase in pressure drop. This increase in pressure drop is caused by the oil film on the tubing's inner wall, causing a reduction in the diameter of the passage through which the bulk CO_2 can flow. In these experiments, a non-dimensional pressure drop penalty factor (PDPF) is defined by dividing the average pressure drop during the steady state injection period by the average pressure drop during the pre-injection and post-extraction periods. An example of the transient pressure drop during an oil retention experiment is shown below.

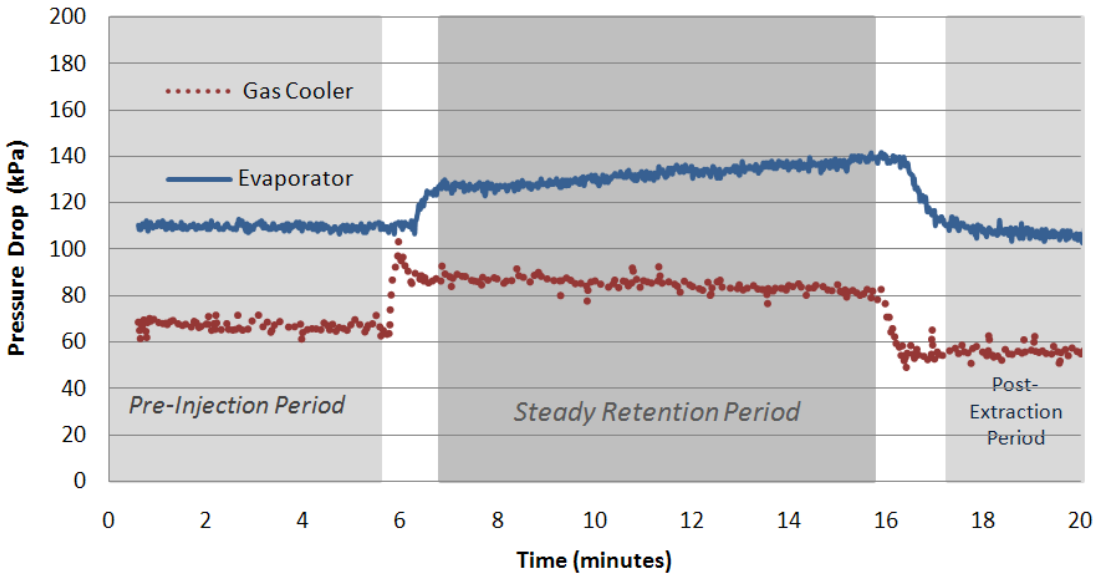

Figure 33: Pressure drop in the evaporator and gas cooler during a 22 g/s, 0.05 OMF experiment.

5.5.3 COP Reduction

The COP reduction is the difference in COP during steady state oil retention versus when the system is free of oil. The best measurement of the COP during injection is the COP near the end of the injection, since the COP takes time to settle on a new value after injection begins. This COP is compared to the COP several minutes after the injection/extraction has been concluded, and all the oil has been collected in the level sensor. The COP after the injection was chosen as a point of comparison because the oil-free COP after the injection is generally a bit different than the oil-free COP before the injection since the pressures and temperatures in the system have been altered. The COP is always measured on the water side for this calculation because the CO_2 side COP measurement uses a property routine for pure CO_2, and during injection, there is a mixture of CO_2 and PAG oil in the gas cooler. An example of transient COP during an oil retention experiment is shown below in Figure 34.

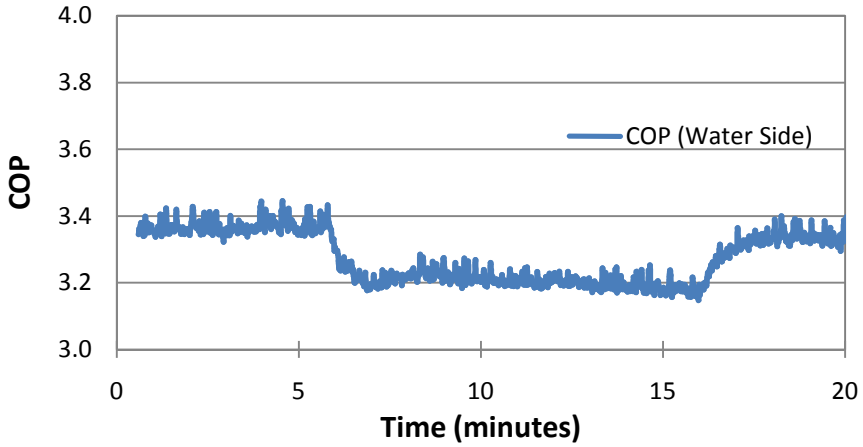

Figure 34: Water side COP measurements during a 22 g/s experiment at 0.05 OMF

5.6 Uncertainty Analysis

Oil retention is not a measured value but is instead a calculation that relies on a number of assumptions and includes a lot of unknown uncertainties (such as the uncertainty induced by a changing extraction efficiency, and the uncertainty of the CO_2 concentration in the oil). Thus, calculation values are modeled as a stochastic process, and the error for each individual test is the standard deviation about the true value. An estimate of the standard deviation of oil retention, pressure drop increase, and COP degradation is found by assuming pooled variance of each variable at different oil mass fractions, and carrying out repeated experiments to estimate the variance at each point. The calculated standard deviations of each of the dependent variables are displayed below in Table 8.

Table 8: Standard deviation of reported oil retention variables using pooled variance

Oil Retention (g)		
Port	**σ(12 g/s)**	**σ(22 g/s)**
Suction Line	2.6	4.9
Evaporator	5.2	6.6
Liquid Line	6.3	7.1
Gas Cooler	8.9	9.7
Pressure Drop Increase (PDPF)		
Test Section	**σ(12 g/s)**	**σ(22 g/s)**
Gas Cooler	0.086	0.046
Evaporator	0.114	0.061
Cop Degradation (%)		
overall	1.3	0.7

The true value also has uncertainty associated with it, which is characterized by the standard error of the mean (Equation 26)

$$U_{OR,mean} = \frac{\sigma}{\sqrt{n}} \tag{26}$$

Thus, the total uncertainty of a data point is the sum of the uncertainty about the mean and the uncertainty of the mean itself, or

$$U_{OR} = \sigma + \frac{\sigma}{\sqrt{N}} \tag{27}$$

The mean value is calculated as a power function curve fit of oil retention for a given injection port at a given mass flow rate as a function of oil mass fraction. Using a regression analysis, the power function gives the best fit about the calculated oil retention values and also matches well with the shape of the oil retention curves reported by Cremaschi [14] and Lee [9].

The total retention at a given port at a given OMF has a value OR_{mean} and uncertainty $U_{OR,mean}$. The value of oil retention at an individual test section is found through a differential method, wherein the value of oil retention in a given test section is the difference between the value at the injection port for that section, and the value for the next downstream port. For the suction line, there is no downstream port, and the uncertainty is unchanged. However, for each of the other test sections, the uncertainty in the oil retention for that section is increased according to the equations:

$$U_{OR,evaporator} = \sqrt{U_{OR,EVport}^{\ 2} + U_{OR,SLport}^{\ 2}} \tag{28}$$

$$U_{OR,liquid\_line} = \sqrt{U_{OR,LLport}^{\ 2} + U_{OR,EVport}^{\ 2}} \tag{29}$$

$$U_{OR,gas\_cooler} = \sqrt{U_{OR,GCport}^{\ 2} + U_{OR,LLport}^{\ 2}} \tag{30}$$

5.7 Results

Table 9 shows the number of experiments performed for each type of injection experiment during the oil retention evaluation. Experiments were repeated to reduce the uncertainty in the reported oil retention, change in COP, and change in pressure drop. Some experiments were repeated more often than others in order to achieve consistency in the reported values. Also, the 22 g/s experiments were repeated more often than the 12 g/s experiments, because the standard deviation in the oil retention was higher, and more experiments were necessary to reduce the uncertainty to an acceptable level.

Table 9: Number of experiments performed for each oil retention test

		Target OMF				
		0.01	0.025	0.05	0.075	0.1
Type of test	12 g/s gas cooler	0	2	3	2	1
	12 g/s liquid line	0	2	2	2	2
	12 g/s evaporator	0	2	2	2	2
	12 g/s suction line	0	2	2	2	2
	22 g/s gas cooler	3	3	4	3	3
	22 g/s liquid line	3	4	5	3	2
	22 g/s evaporator	2	4	6	2	2
	22 g/s suction line	2	3	4	3	3

5.7.1 Oil Retention Mass

Oil retention mass was first calculated as the total oil retention for a given injection location in grams. Data for duplicates of the same trial were averaged in Figures 35 and 36, which show the results of the 12 and 22 g/s experiments.

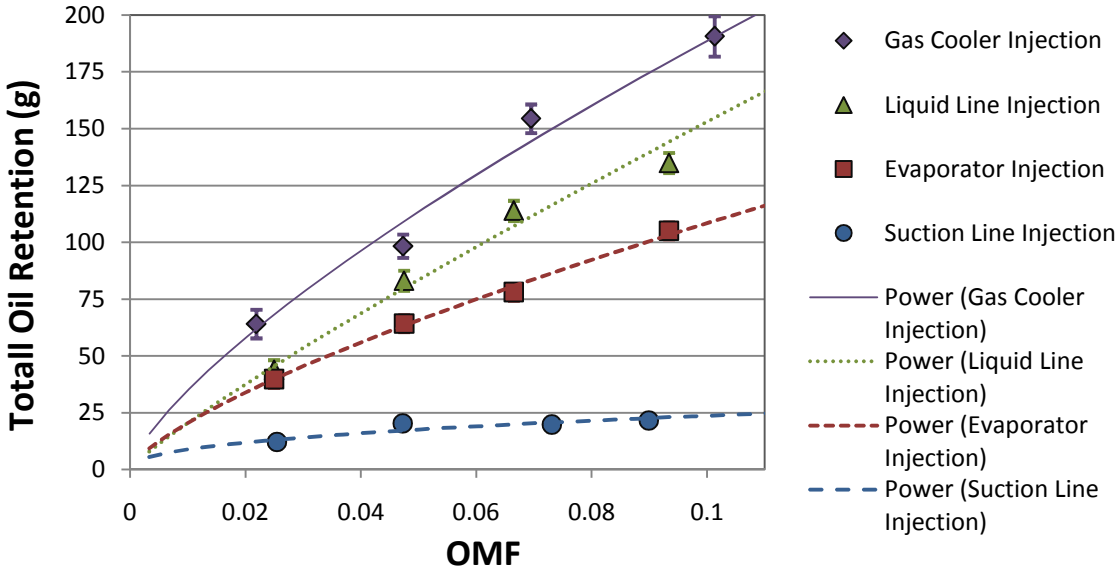

Figure 35: Total oil retention at the four injection ports for 12 g/s MFR

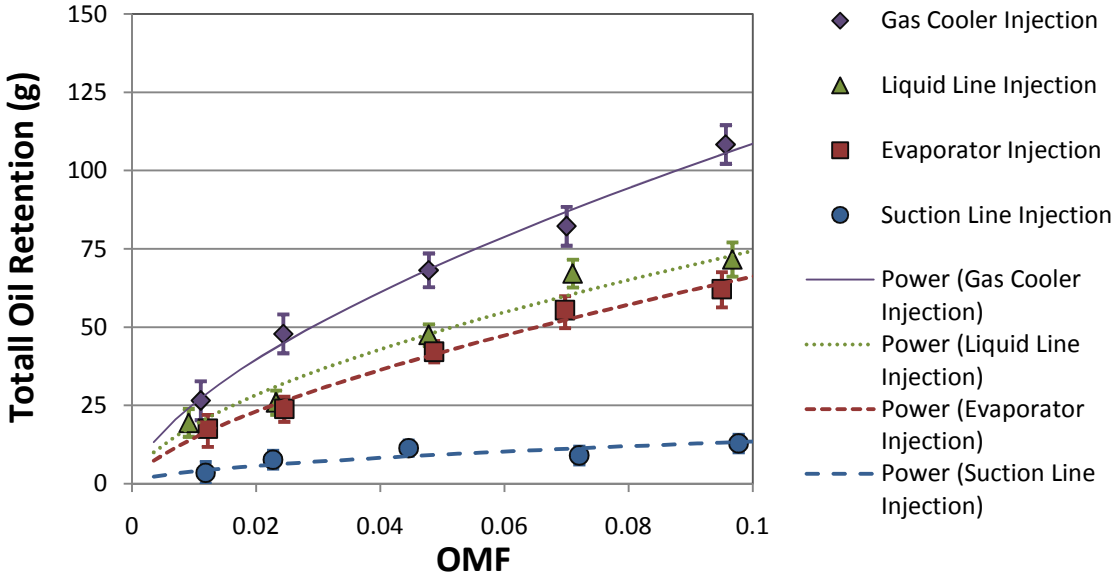

Figure 36: Total oil retention at the four injection ports for 22 g/s MFR

Invariably, the oil retention during the 12 g/s tests was higher than the oil retention during the 22 g/s tests at the same OMF and injection location. On average, the oil retention was 1.7 times higher. The biggest increase was for the suction line, where the oil retention more than doubled. These results underscore the critical importance of the velocity of the bulk CO_2 in dragging the oil film along.

To calculate the oil retention in each of the individual test sections, the oil retention of the next downstream injection site is subtracted from the oil retention at the injection location of interest. This is known as the differential method. To make generalizations about oil retention, it is useful to normalize the oil retention mass. Since oil forms a film on the inner wall of the tubing, it is more informative to normalize the oil retention on a unit-length basis than on a unit-volume basis. Figures 37 and 38 show the normalized oil retention for each test section at the two mass flow rates tested. For these graphs, the lines were calculated by subtracting the trendlines from Figures 35 and 36. The error bars represent the confidence in the differential line, based on the uncertainty in the mean for each of the two lines used to calculate it.

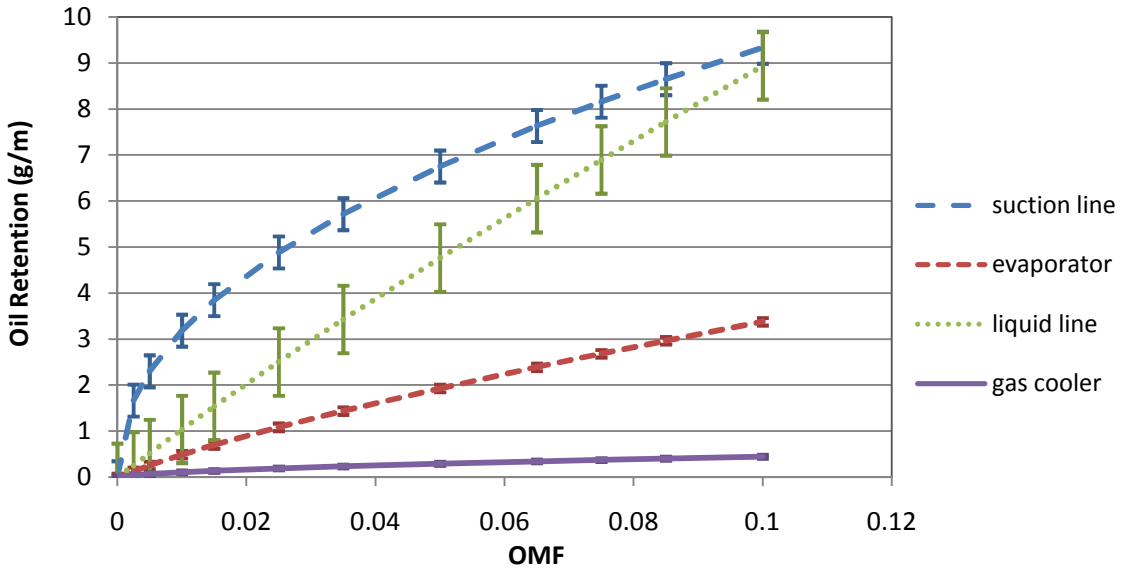

Figure 37: Normalized individual test section oil retention (12 g/s MFR)

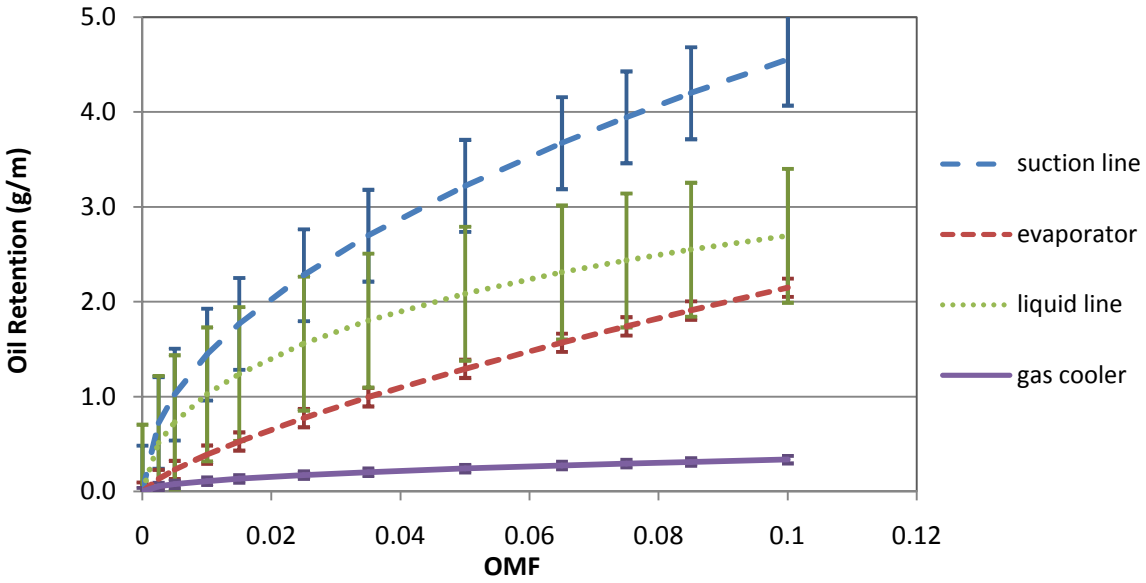

Figure 38: Normalized individual test section oil retention (22 g/s MFR)

The two graphs appear to show consistent results with respect to one another. The suction line, evaporator, and liquid line are all composed mostly of 9.5mm tubing, so it is relatively fair to make a direct comparison among these three lines in each graph

(although the suction line contains oil separators with a much wider diameter, and the liquid line contains two components with slightly wider tubing). One possible explanation for oil retention in the liquid line being higher than in the evaporator would be a bottlenecking of the oil flow upstream of the expansion valve, due to its narrow orifice. There are two possible explanations for the oil retention in the suction line being higher than in the evaporator. First, in the suction line, the oil flow must navigate a vertical upward flow section, which has been shown by Cremaschi [14] to dramatically increase the oil retention, relative to other components and other geometries. Another explanation is that part of the suction line test section is an oil drainage line from the oil separators to the oil level sensor, where flow is much reduced, compared to the main CO_2 circuit. The oil retention in the gas cooler is much smaller than in the evaporator on a unit-length basis because the inner surface area per unit length of the microchannel gas cooler tubing is much smaller than that of the 9.5mm tubing of the evaporator.

5.7.2 Pressure Drop Increase

The increase in pressure drop due to the injected oil is summarized in Figures 39 and 40. The results of this research seem to indicate that the pressure drop in both heat exchangers continues to grow with increasing OMF, but at a decreasing rate. Evaporator PDPF results are taken from experiments at the evaporator, suction line, and gas cooler injection ports, since the oil is retained in the evaporator during each of these tests. The gas cooler PDPF results are taken only from the gas cooler injection tests.

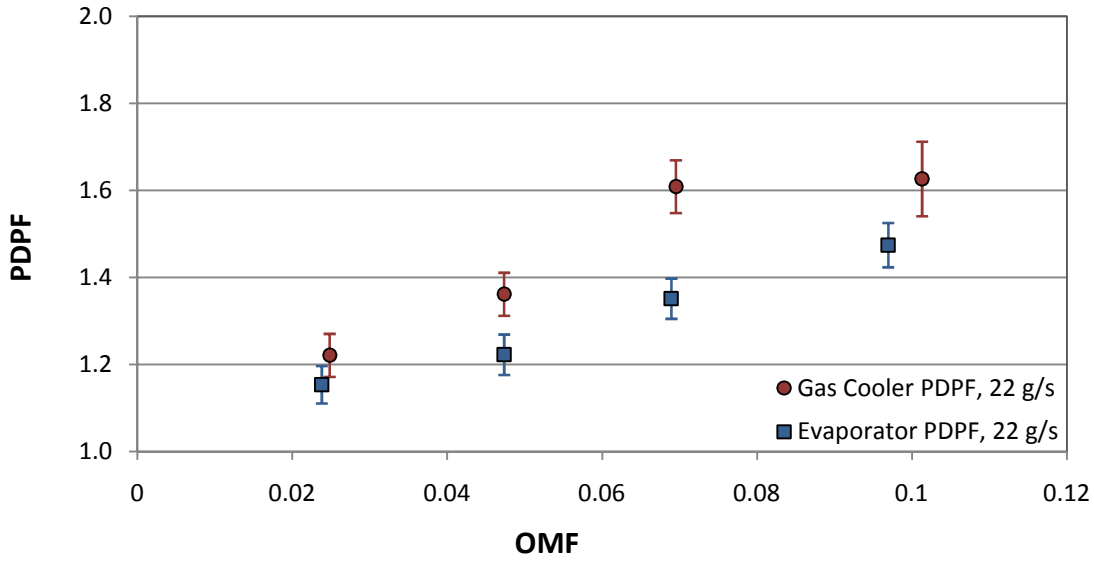

Figure 39: Pressure drop penalty factor at 12 g/s MFR

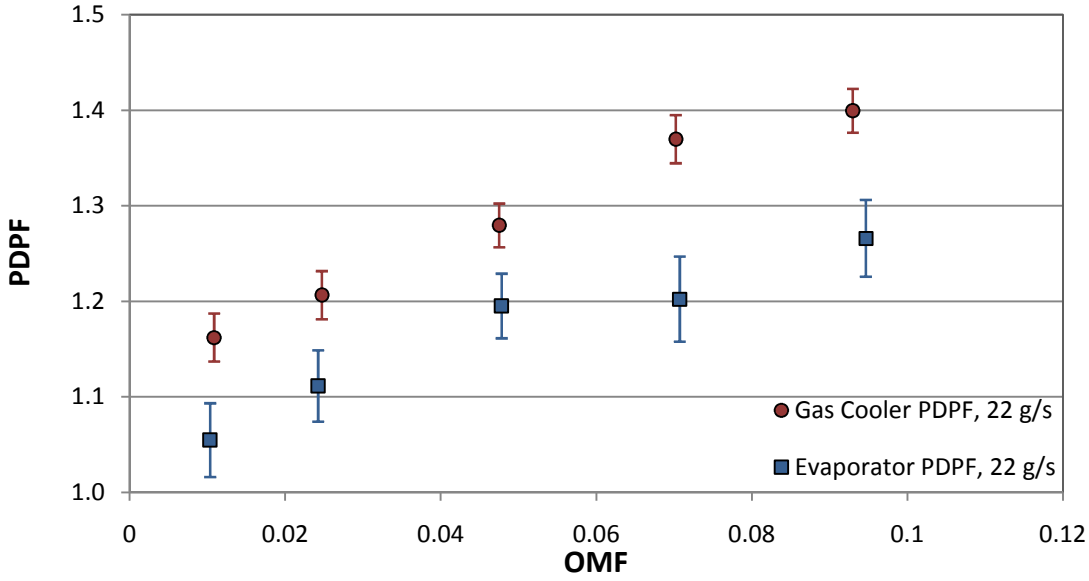

Figure 40: Pressure drop penalty factor at 22 g/s MFR

As expected, the PDPF is higher for the gas cooler than for the evaporator. This is due to the gas cooler's higher surface area to volume ratio causing an oil film that decreases the cross sectional area available for the bulk CO_2 to flow by a higher percentage,

5.7.3 COP Reduction

In a typical vapor compression system there are two mechanisms by which retained oil can reduce the system COP. The first mechanism is through a reduction in the heat transfer coefficient. In the transcritical CO_2 cycle, the relationship between oil mass fraction and heat transfer reduction is very complex. Reduction in heat transfer coefficient is highest near the pseudocritical temperature, and depending on the pressure, can be very small further away from this temperature. The second mechanism is the pressure drop increase. Pressure drop increases raise the pressure ratio and reduce the mass flow rate without any increase in the enthalpy difference across the heat exchanger. In CO_2 systems, pressure drop does not play as big a role as it does for lower-pressure refrigerant cycles, since a given absolute pressure drop represents a lower fraction of the total pressure. Pressure drop, however, is still a significant contributor to the COP reduction.

In this test facility, there are two additional sources of COP reduction due to the injected oil. The first is due to the temperature mismatch between the oil and the CO_2. This mismatch can cause some of the heat rejected in the gas cooler to go towards heating the oil, rather than heating the water. This effect is observed when the temperature of the oil injected to the gas cooler (in these experiments, usually ~20^{o}C) is cooler than the gas cooler's outlet CO_2 temperature (~35-40^{o}C). The other mechanism is the narrowing of the expansion valve orifice as the oil flows through. In practice, a vapor compression cycle with oil could be controlled to maintain a certain pressure ratio

through opening the expansion valve. However, in these experiments, the opening of the expansion valve is disruptive to many of the parameters, and tends to release some of the retained oil behind the expansion valve. Therefore, the expansion valve is kept in its pre-injection position during the experiment.

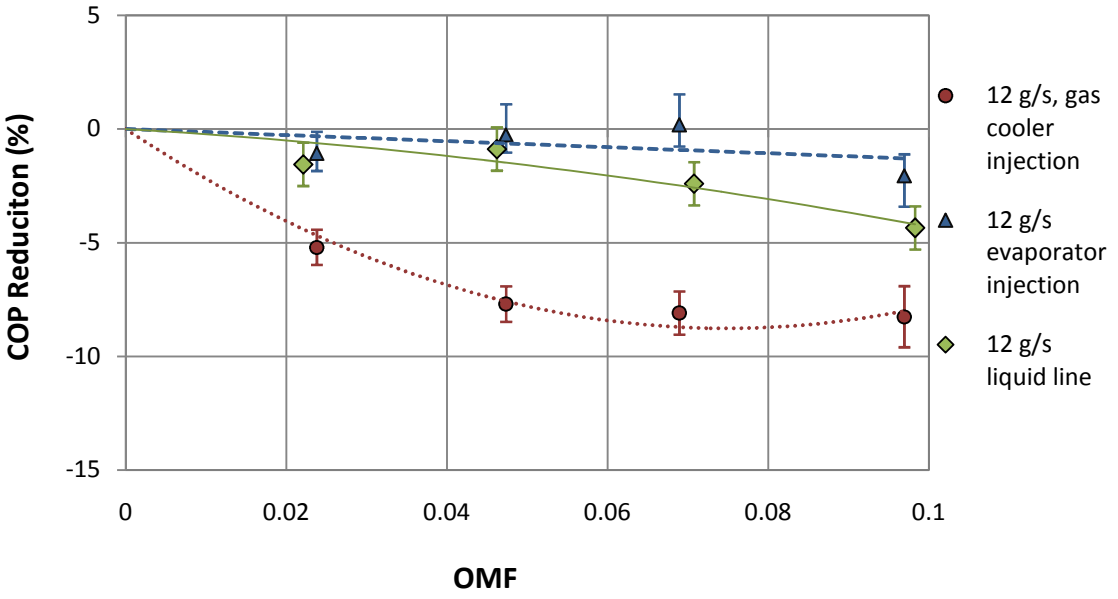

Figure 41: COP reduction for the 12 g/s tests

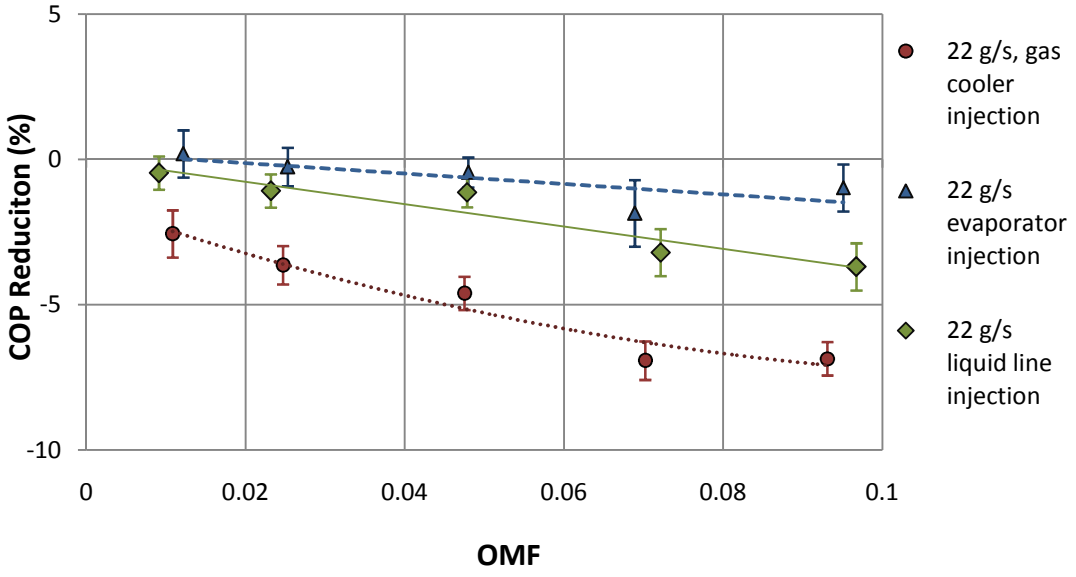

Figure 42: COP reduction for the 22 g/s tests

In Figures 41 and 42, the measured COP reduction due to the injection oil is plotted for three injection ports. The reduction observed during injection to the evaporator is plotted as triangles. The dashed trendlines in each graph for the evaporator show a slight negative slope with OMF. For this injection location, the two possible mechanisms for COP reduction are evaporator pressure drop and decreased heat transfer in the evaporator. Since no noticeable decrease in evaporator superheat was observed, however, it is not believed that reduced heat transfer in the evaporator played a limiting role in COP. The diamond shapes with the solid trend line show the COP reduction for liquid line injection. The only difference between the liquid line injection and evaporator injection in terms of COP reduction is that now the oil must flow through the expansion valve. Thus, there is the potential for the COP to be affected by the narrowing of the expansion orifice. Both curves seem to show negligible effects at OMFs below 5%, and rapidly decreasing COP beyond 5% OMF. Finally, the circles with the dashed trendline show the COP reduction for the gas cooler injection port. Here, in addition to the mechanisms available for the liquid line COP reduction, there is gas cooler pressure drop, gas cooler heat transfer inhibition, and COP reduction due to the injected oil borrowing some of the CO_2's rejected heat.

Based on measurements of the temperature of the oil flowing into the gas cooler and the specific heat of PAG oil (2.05 kJ/kg-K), the change in COP due to the heat of the injected oil could be calculated according to the equation:

$$\Delta COP(\%, oil) = \frac{100 \cdot \dot{m}_{oil} C_{p,oil} \left(T_{oil,injected} - T_{gc,o} \right)}{W_{comp} \cdot COP_0} \quad (31)$$

The effect of the change in pressure drop on the COP was calculated by running the full system model in EES at the observed test conditions twice; once with the average pressure drop measured before/after the injection, and once with the average pressure drop measured during the steady state oil retention period. The percent change in these two modeled cases is considered to be an accurate estimation of the amount of COP reduction due to increased pressure drop in the heat exchangers.

The amount of COP reduction due to expansion valve narrowing was estimated by subtracting a point on the evaporator COP reduction curve from its corresponding point on the liquid line curve. The remaining component of the COP reduction, the degradation due to heat transfer inhibition, was estimated as the total COP reduction minus each of the three other components. This assumes that each mechanism acts independently to reduce the COP, and it introduces a considerable source of error, especially for the heat transfer inhibition estimation.

Figure 43 shows the COP reduction due to the heat of the injected oil and the narrowing of the expansion orifice – the two COP reduction mechanisms that are valid only for this oil retention measurement facility. The injected oil tends to reduce the COP since it is always cooler than the CO_2-oil stream that leaves the gas cooler. This reduction is always less than 1%. (It should be noted that the oil is heated in the oil reservoir to remove CO_2 from the injected oil, but it cools to near room temperature in

the tubing of the oil subsystem before it reaches the injection port.) The narrowing of the expansion orifice is responsible for less than 1.5% COP reduction at 1% OMF, increasing to 1.5-3.5% reduction at 10% OMF.

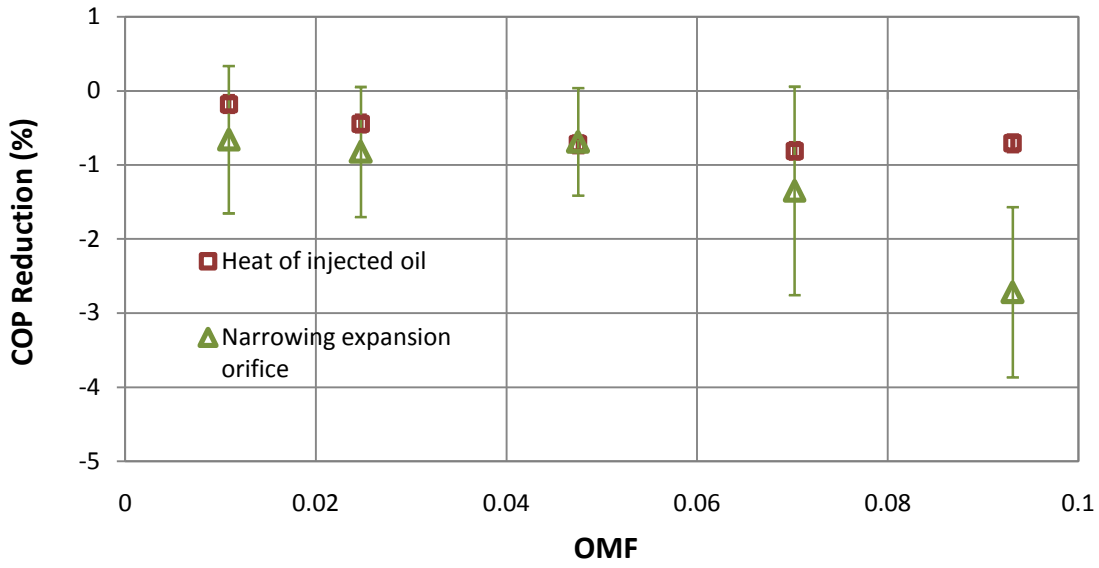

Figure 43: COP degradation due to the heat of injected oil and a narrowing expansion orifice (22 g/s)

Figure 44 shows the effect of remaining two mechanisms of COP reduction; the two mechanisms that would be present in a typical HPWH, in which compressor oil was circulating throughout the system. The increased pressure drop in the heat exchangers caused around a 0.5% reduction in COP at 1% OMF, increasing to a 2% reduction at 10% OMF. It should be noted, however, that with different heat exchangers, this reduction would be somewhat different. There is a lot of uncertainty in the degradation due to heat transfer degradation, but it appears to fall somewhere between 1 and 3%, and is

fairly constant with increasing OMF above 1%. If this is true, it would indicate that the heat transfer degradation is mostly due to a reduction in heat transfer coefficient between the CO_2 and the oil film (compared to a clean tube wall). The additional heat transfer resistance provided by an incrementally thicker oil film as the OMF is increased appears to play a negligible role in COP reduction. These findings match well with the findings of Dang [30] who reported that the reduction in the overall heat transfer coefficient occurs mostly at low oil mass fractions (~1%) and quickly saturates as the OMF is increased.

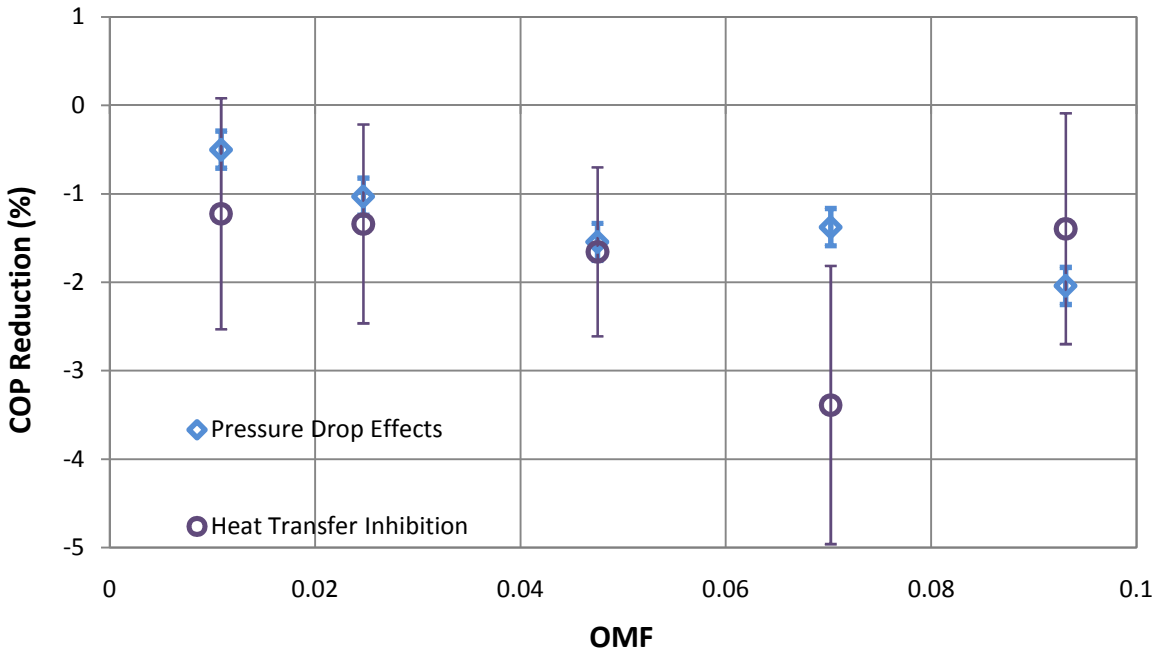

Figure 44: COP degradation due to heat transfer inhibition and pressure drop (22 g/s)

6 Cycle Modifications for Performance Enhancement

6.1 Two-Stage Compression with Internal Heat Exchanger

The final stage of the project was to investigate the potential benefits of design enhancements on the COP. The first design enhancement that was investigated was two-stage compression using an internal heat exchanger (IHX). This cycle has shown significant performance enhancement for cooling applications. The question is whether the same improvement will be observed for the water heating application.

6.1.1 Description of Performance Measurement Facility

A diagram of the components used in the performance measurement facility for the two-stage compression testing is shown below in Figure 45. After the gas cooler, the stream splits in two. One mass flow meter measures the flow rate before the split and another measures the flow rate in the bottom branch. After passing through this mass flow meter, the CO_2 is expanded to an intermediate pressure, thereby reducing its temperature. It then flows in counter-flow with the CO_2 in the first branch, sub-cooling that branch. From there, it flows into the shell of the compressor, where it mixes with compressed gas from the 1^{st} stage of compression. The IHX used was a 30cm long microchannel-microchannel heat exchanger.

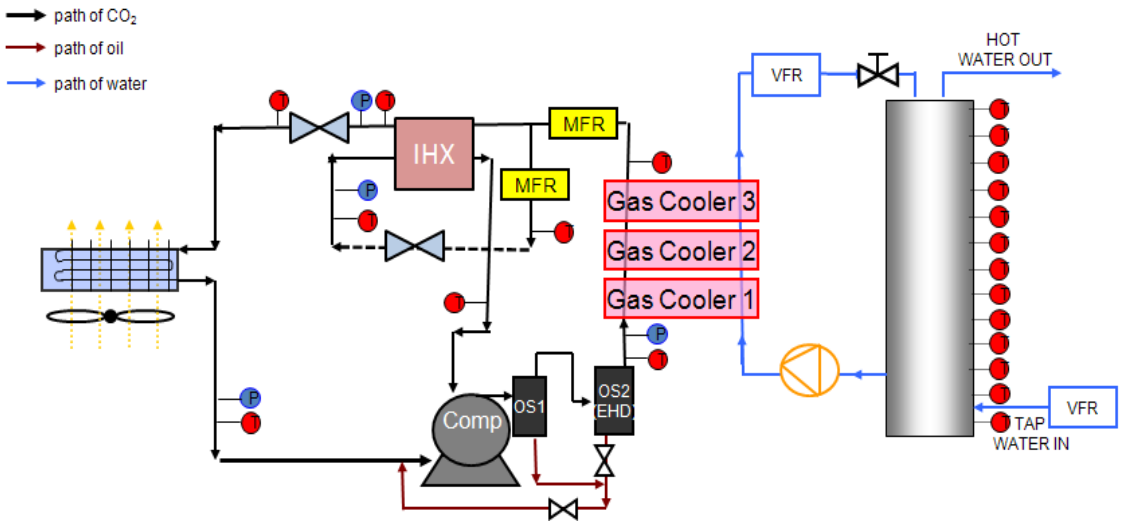

Figure 45: Two-stage compression with internal heat exchanger

The process is depicted on a P-h diagram in Figure 46. This diagram was constructed with actual temperature and pressure measurements during tests from the baseline cycle and the IHX cycle during the 10°C "A" test. The state points are labeled as follows. The label "a" after the number indicates a point on the baseline cycle, and "b" indicates a point on the IHX cycle.

1: Compressor suction

2: 1st stage discharge

3: 2nd stage discharge/gas cooler inlet

4: Gas cooler outlet/IHX inlet

5: Expansion valve outlet/evaporator inlet

6: Compressor 2nd stage inlet

7: Intermediate pressure IHX inlet (IHX cycle only)

8: Intermediate pressure IHX outlet (IHX cycle only

9: High pressure IHX outlet/expansion valve inlet (IHX cycle only)

For the IHX cycle, note that the flow rate of CO_2 in the high pressure branch (3-4) is equal to the sum of the flow rates in the intermediate pressure branch (7-8-6), and the low pressure branch (5-1). This 10°C "A" Test makes for a compelling comparison because the cycle operated at virtually identical state points to the baseline cycle, with the exception of the temperatures in the second stage of compression and within the gas cooler itself. The comparison highlights the tradeoff with the IHX cycle of increased mass flow rate at the cost of gas cooler enthalpy difference.

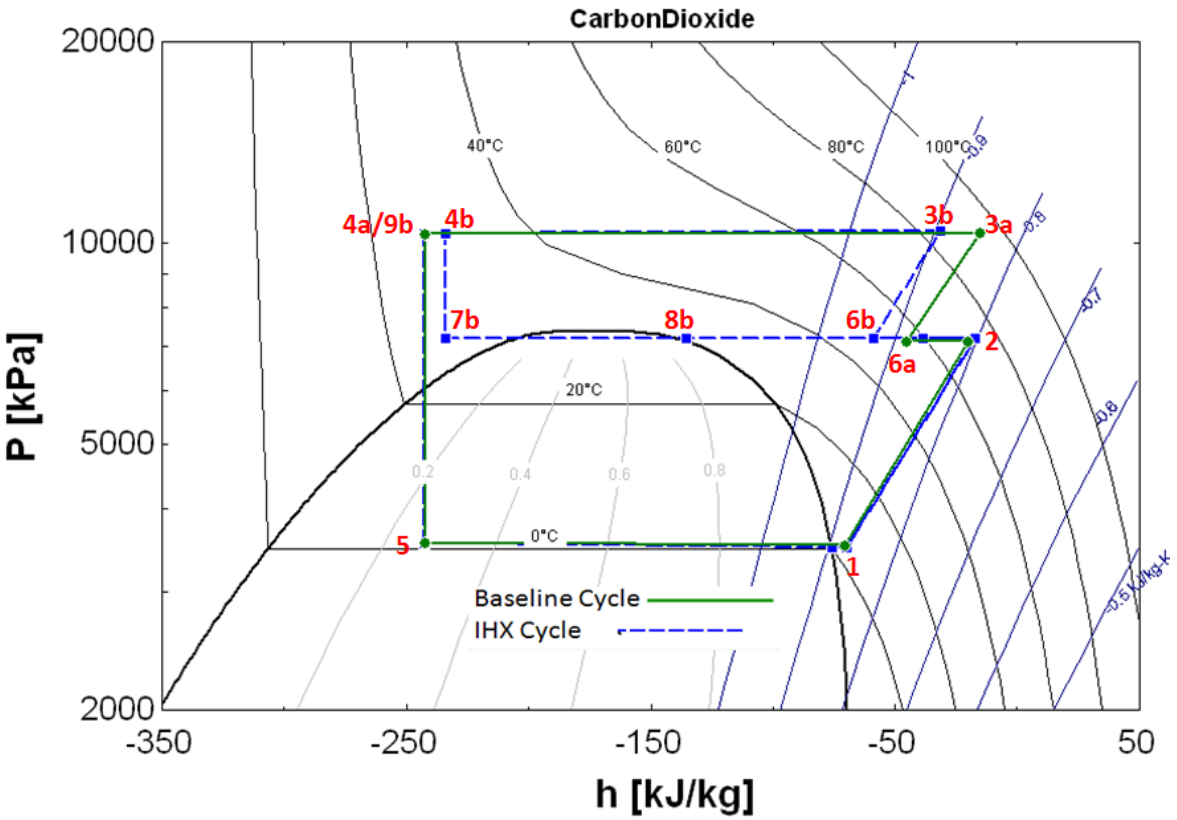

Figure 46: P-h diagram of two-stage IHX cycle vs. baseline cycle for 10°C "A" Test

6.1.2 Modeling

A model was constructed in EES to simulate the two-stage compression cycle with an IHX. This model was made as a modification to the original CO_2 HPWH EES model. The key changes that had to be made to the model were A) the addition of a new heat exchanger, which transferred the heat rejected from state points 4-9 to the diverging stream of CO_2 at state point 7-8 and B) the introduction of the intermediate pressure fluid to the compressor (which increased the mass flow rate in the second stage and reduced the temperature at the inlet to that stage). A new schematic diagram for the compressor is presented in Figure 47:

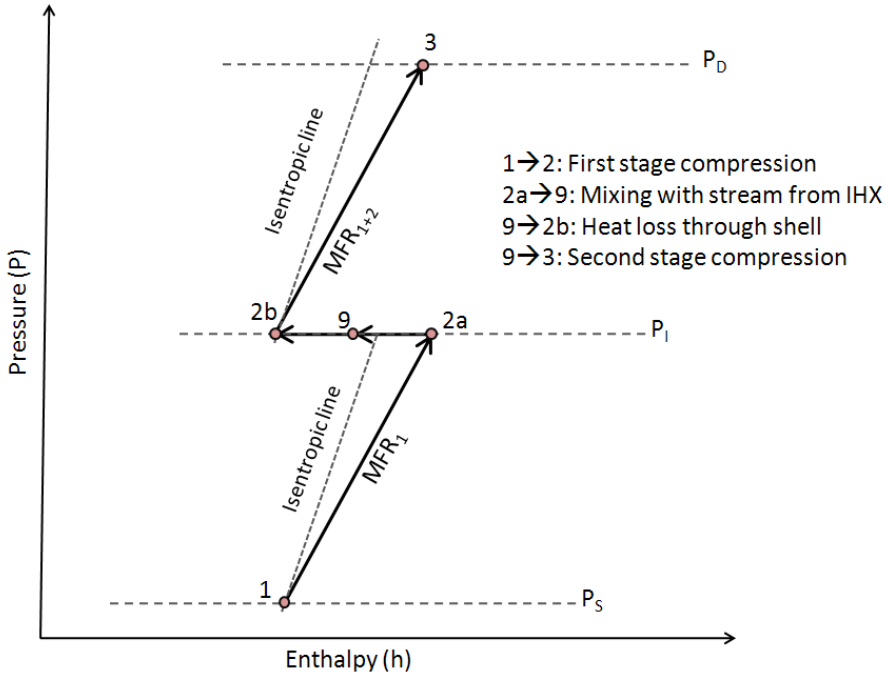

Figure 47: Modification to compressor model for IHX cycle

The compressor mechanical efficiency (Equation 32) was adjusted to account for the new stream of refrigerant, and a second stage volumetric efficiency equation

(Equation 33) was added to predict the intermediate pressure needed to achieve the desired mass flow rate ratio (r_m). The mass flow rate ratio was defined as the mass flow rate in the intermediate branch (MFR_2) divided by to total mass flow rate through the gas cooler (MFR_{1+2}).

$$\eta_{mec} = \frac{MFR_{1+2}\left(h_3 + h_{2a} - h_9\right) - MFR_1 \cdot h_1}{W_{comp}} \tag{32}$$

$$\eta_{vol,2} = \frac{MFR_{1+2}}{V_2 \cdot \omega_{comp} \cdot \rho_{2b}} \tag{33}$$

The model was first utilized to estimate the optimum mass flow rate ratio. At constant inlet water temperature, hot water temperature, ambient temperature, and AT_i, the mass flow rate ratio was varied from 0 to 0.2. There wasn't always an improvement in COP over the baseline, but where there was, the optimum point seemed to be around an r_m of 0.10. A sample curve for r_m vs. COP is shown below for 10°C Ambient temperature.

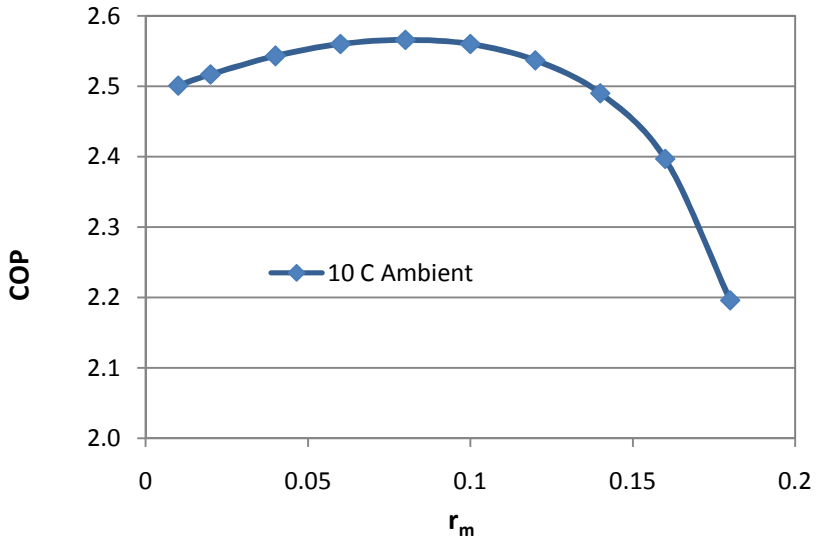

Figure 48: r_m vs. COP for 10°C ambient temperature

Next, holding the mass flow rate ratio constant at 0.1, a parametric study of AT_i vs. COP was performed at several ambient temperatures. It was found that the optimum approach temperature for the two-stage cycle was about 5-10K cooler than for the baseline cycle. The model also predicted that this optimum point would be slightly higher than the baseline for low ambient temperatures, and slightly lower than the baseline for high ambient temperatures. The curves for 10, 20 and 30°C are shown below in Figure 49.

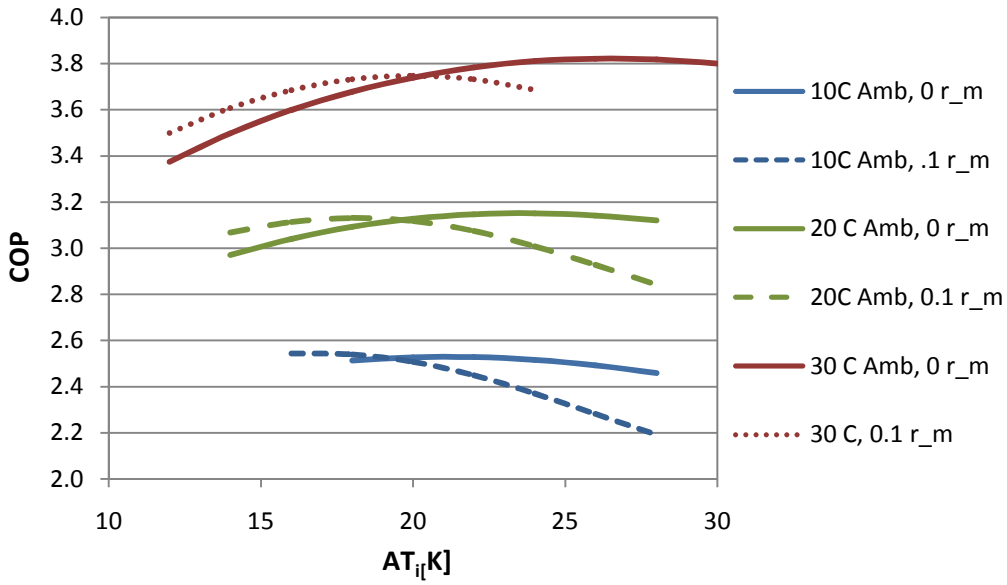

Figure 49: Results of IHX cycle modeling - change in COP with approach temperature

6.1.3 Experimental Results

With insight into optimum operating conditions for the two-stage cycle from the model results, a series of full heating experiments was performed to investigate the actual performance of the IHX cycle with respect to the baseline cycle. The following full heating experiments were performed for the baseline cycle and the two-stage cycle with IHX:

- 10°C Ambient, "A" test
- 10°C Ambient "C" test
- 30°C Ambient "A" test
- 30°C Ambient "C" test

These four experiments represented the four “corner points” of the original baseline parametric study of ambient temperature and heating scenario. Thus, these experiments should reveal the regions of maximum and minimum benefit for the IHX cycle within this temperature range. The “A” tests were performed at the available tap water temperature of 20°C, and for 60°C hot water. The results of the study are shown below in Table 10.

Table 10: Comparison of COP for baseline cycle vs. IHX cycle

	Baseline System COP	Two-Stage w/ IHX (r_m = 0.1)	% Improvement (IHX)
10°C, "A" test	**2.62** *+/- 0.10*	**2.62** *+/- 0.10*	**0.1** *+/- 3.7%*
10°C, "C" test	**1.82** *+/- 0.07*	**1.96** *+/- 0.07*	**7.5** *+/- 3.7%*
30°C, "A" test	**3.67** *+/-0.16*	**3.59** *+/-0.16*	**-2.1** *+/- 4.4%*
30°C, "C" test	**2.66** *+/-0.12*	**2.66** *+/-0.12*	**-0.2** *+/- 4.9%*

The only significant performance improvement observed was for the 10°C "C" test. At all other points, the measured improvement was within the uncertainty of the test, indicating no substantial change in performance one way or the other.

There are three quantities that affect the calculated COP; the compressor power, the enthalpy difference across the gas cooler, and the mass flow rate. To understand where the benefit of the IHX cycle lies, it is useful to analyze each contribution to the COP (compressor power, mass flow rate, and enthalpy difference) individually.

One expected result of the two-stage cycle was an increase in compressor efficiency via reduction of the temperatures within the compressor. Figures 50-53 show the calculated compressor efficiencies at steady state for the baseline cycle vs. the IHX cycle during these experiments. The figures seem to indicate that the first stage volumetric efficiency, the isentropic efficiency, and the mechanical efficiency were nearly identical. Only the second stage volumetric efficiency increased, by a modest 1-2%. Thus, there doesn't appear to be any real mechanism for reduction of compressor power, and indeed, the compressor power increases slightly in the two-stage cycle due to an increase in mass flow rate in the second stage. As a side note, superimposed on Figures 50-53 are measured compressor efficiencies during baseline performance evaluation, which was performed 8 months prior to this set of tests. There seems to have been some degradation in both the first stage volumetric efficiency and the isentropic efficiency since that time.

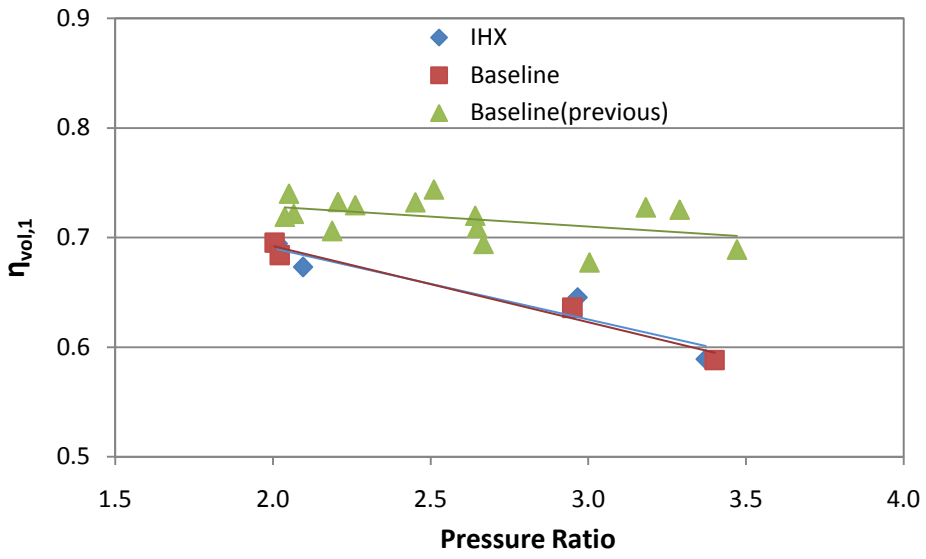

Figure 50: Comparison of first-stage volumetric efficiency for IHX cycle vs. baseline cycle

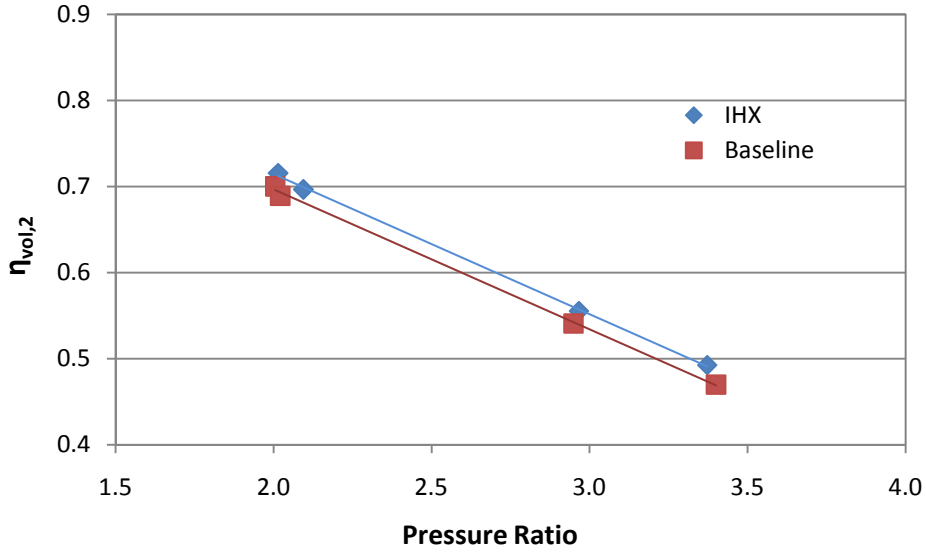

Figure 51: Comparison of second-stage volumetric efficiency for IHX cycle vs. baseline cycle

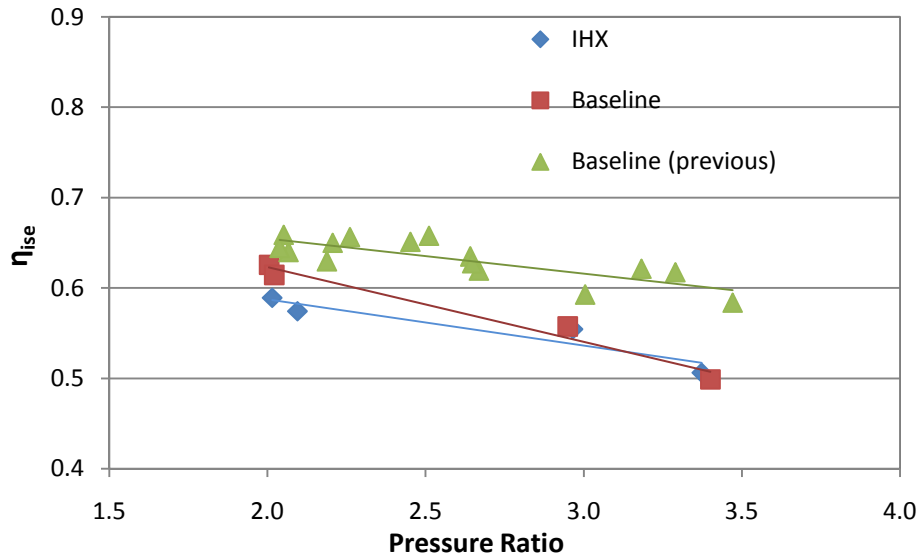

Figure 52: Comparison of isentropic efficiency for IHX cycle vs. baseline cycle

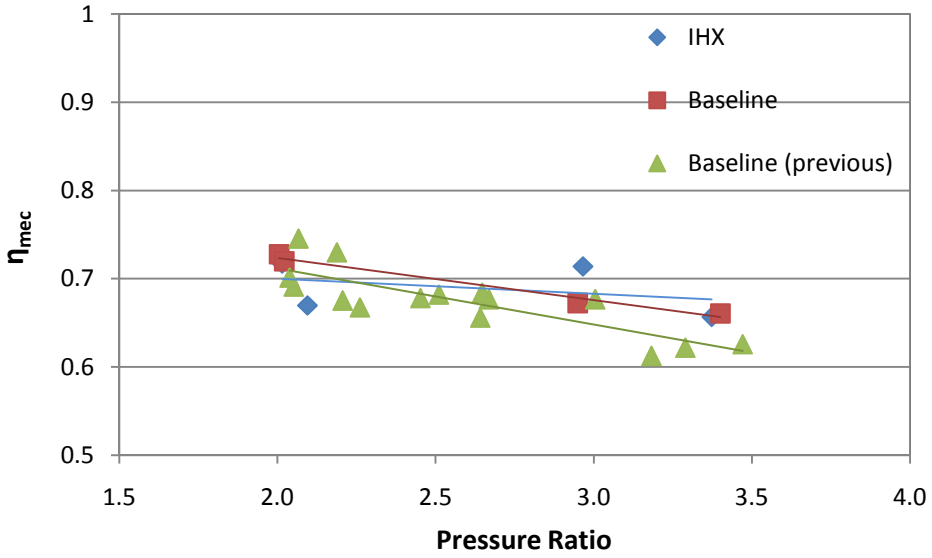

Figure 53: Comparison of mechanical efficiency for IHX cycle vs. baseline cycle

The two remaining contributors to the COP are the mass flow rate and the enthalpy difference across the gas cooler. The mass flow rate increases about 10% in each experiment over the baseline case. This is because the intermediate pressure

stream, which is set to 10% of the total gas cooler flow rate, increases, with no substantial effect on the flow rate through the evaporator. This increase in mass flow rate always tends to increase the COP.

The enthalpy difference in the gas cooler appears to be a real key factor. The introduction of the cooler stream into the second stage of the compressor tends to cool the discharge temperature by about 5K, at a constant discharge pressure. Coincidentally, this temperature reduction matches well with the optimum COP condition for the IHX cycle (see Figure 49). When the AT_i is low, as was the case for the 30°C "A" test, a reduction in discharge temperature caused a significant increase in the AT_o (~2.5K). This pinched the CO_2 enthalpy difference on both ends of the gas cooler. When the AT_i was very high (as in the 10°C "C" test), there was no significant drop in the AT_o, and thus the enthalpy difference was only squeezed on one end. It is these kinds of conditions that appear somewhat favorable for the IHX cycle – allowing the increase in mass flow rate to outweigh the reduction in enthalpy difference in the gas cooler. With such limited scope, however, the findings do not appear to be any kind of mandate for the use of this cycle in CO_2 HPWH's.

6.2 Suction Line Heat Exchanger

6.2.1 Description of Performance Measurement Facility

Another option for an internal heat exchanger is to use it as a suction line heat exchanger (SLHX). An SLHX takes heat from the CO_2 stream at the outlet of the gas cooler and uses it to provide superheating to the refrigerant leaving the evaporator. In

this cycle, the compressor returns to its single-stage operation, as in the baseline system testing. A schematic of the new test facility is shown below in Figure 54.

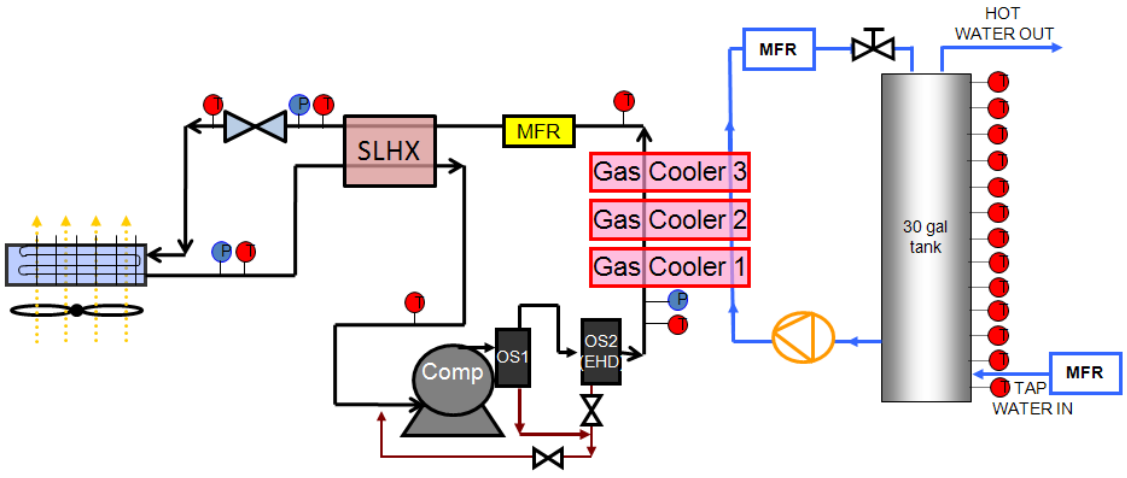

Figure 54: System schematic with suction line heat exchanger (SLHX)

The same series of experiments was performed for the SLHX cycle as for the baseline cycle and IHX cycle discussed in Chapter 6.1.3. A clever series of valves allowed the performance measurement facility to be run as a baseline vapor compression cycle, a two-stage cycle with IHX, and a single stage cycle with SLHX. The valve structure allowed the lower branch of the internal heat exchanger in Figures 44 and 53 to accept CO_2 from and deliver it to different locations in the cycle, in order to achieve the desired configuration. Thus, the series of SLHX tests could reliably be performed at the same CO_2 charge as the IHX cycle tests and the baseline cycle tests, since the test facility did not have to be physically altered in any way.

The benefit of the SLHX for water heating in the CO_2 cycle is two-fold. First, it enables the evaporator to be devoted entirely to the task of evaporation by taking over

the role of superheating. As was shown in Figure 15, superheating lowers the effectiveness of the evaporator by introducing a region at the end of the evaporator with a reduced temperature difference with respect to the air. The SLHX can provide substantial superheating to the inlet of the compressor. For this facility, at the optimum COP conditions, the superheat was 19K. This superheating facilitates the second method for performance enhancement. At a given suction pressure, as the suction temperature increases, the pressure required to compress the gas to the desired discharge temperature can be greatly reduced. This can be seen from the 80 and 100°C isotherms on the P-h diagram in Figure 55. For the 10°C "A" test conditions, the optimum COP was identified at a point with a lower discharge pressure but a higher discharge temperature than the corresponding baseline testing discharge point. A comparison of the baseline and the SLHX cycle are shown below in the P-h diagram of Figure 55. The notable changes in the cycle, as far as the COP is concerned are the slightly increased enthalpy difference in the gas cooler (points 3-4) and the decreased pressure ratio (P3/P1).

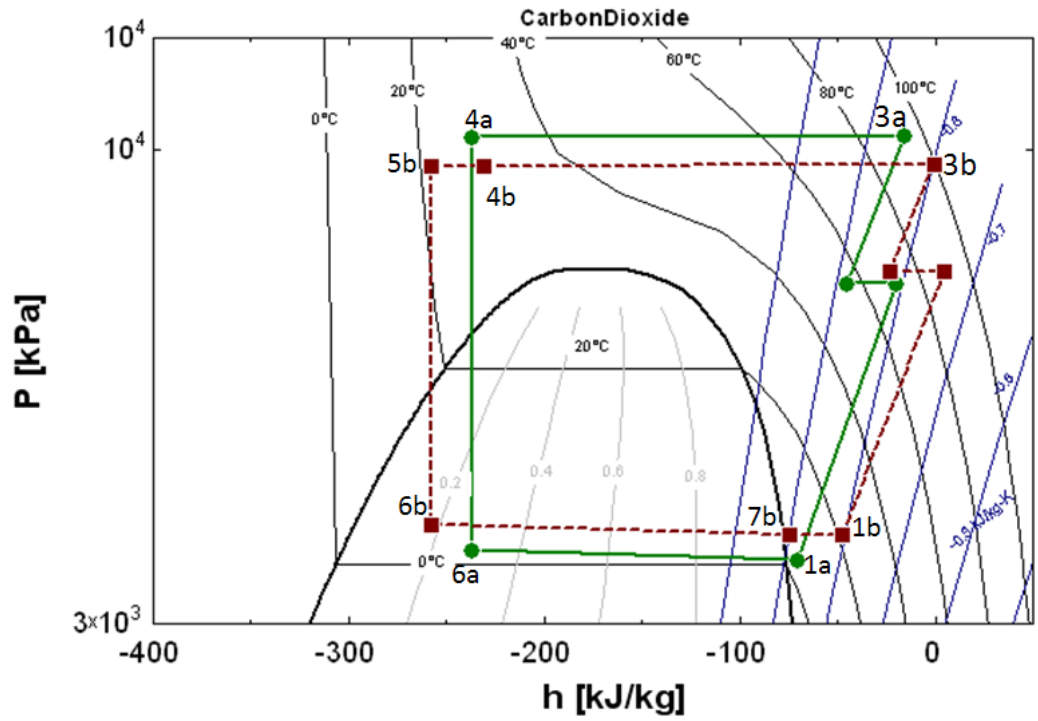

Figure 55: P-h diagram of baseline cycle (solid line) and SLHX cycle (dashed line) during 10°C "A" test

6.2.2 Experimental Results

The overall COP for the SLHX heating tests is summarized in Table 11, and compared with the baseline cycle. In these tests, there was a significant improvement over the baseline cycle for the 10°C ambient tests, and an insignificant change from the baseline at the 30°C conditions. The SLHX seems to perform best when superheat is a limiting factor for the baseline case. In these conditions, the SLHX allows the evaporating temperature/pressure to be raised. The optimum discharge temperature is somewhat higher at a lower discharge pressure, and there is little net effect on the capacity. Meanwhile, the pressure ratio has been significantly reduced, so the COP goes

up quite a bit. Since the charge was optimized for the 10°C "A" test, and since a constant charge was used throughout these tests, the system was essentially undercharged for the 30°C tests. The optimum COP for the baseline tests was achieved at superheats approaching 10K. Introducing the SLHX did little to help the cycle under these conditions, because the discharge pressure had to be maintained at a high enough level to support a high system capacity. Vapor compression systems typically use charge management devices like accumulators, which store liquid refrigerant at low ambient temperatures, and release some of that charge as vapor at higher ambient temperatures. With good charge management, the SLHX should be able to provide performance enhancement across a broader range of ambient temperatures.

Table 11: Comparison of COP for baseline cycle vs. SLHX cycle

	Baseline System COP	SLHX cycle COP	% Improvement (SLHX)
10°C, "A" test	**2.62** *+/- 0.10*	**2.84** *+/- 0.12*	**7.9** *+/- 4.1%*
10°C, "C" test	**1.82** *+/- 0.07*	**1.88** *+/- 0.09*	**3.4** *+/- 4.6%*
30°C, "A" test	**3.67** *+/-0.16*	**3.67** *+/-0.18*	**0.1** *+/- 4.8%*
30°C, "C" test	**2.66** *+/-0.12*	**2.63***+/-0.13*	**-1.3** *+/- 4.9%*

7 Conclusions

A test rig was constructed in the Heat Pump Laboratory at the University of Maryland to investigate the performance and oil retention characteristics of a CO_2 heat pump water heater. The project was divided into four stages.

In the first stage, full heating tests were performed to investigate the effect of three environmental parameters on the overall COP and average capacity. Rising ambient temperatures boosted the COP and capacity by facilitating a higher evaporating temperature and pressure. This had the dual effect of reducing the pressure ratio, and increasing the mass flow rate. A corresponding reduction in high side pressure, however, caused a decrease in the enthalpy difference across the gas cooler, limiting capacity gains, especially for tests with warmer inlet water. An increasing hot water temperature decreased the COP because the discharge temperature/pressure had to be raised to facilitate this increase. On the right side of the P-h diagram, where the compressor operates, the specific heat of the CO_2 is relatively small, so the increase in gas cooler capacity generally does not compensate enough for the rise in compressor work. At warmer water temperatures, however, it nearly does compensate, and the reduction in COP is very minimal at increasing hot water temperature. The study of the effect of the heating scenario on the performance of the system revealed the true strengths and weaknesses of the CO_2 cycle for water heating. When the inlet water temperature is cool, the gas cooler can reject substantial heat to the cold reservoir of

water, at relatively low pressure ratios. On the cool end of the gas cooler, the specific heat of CO_2 is especially high. Under these operating conditions, the temperature profile of the CO_2 and the water match well with each other, and the gas cooler is fully utilized. For tank reheating after standby losses, however, the gas cooling capacity is much reduced. On the P-h diagram of CO_2, the 40°C isotherm makes a sharp bend to the right in the supercritical region as the pressure falls from 11 to 8 MPa. This means that the gas cooling pressure must be kept very high to achieve reasonable performance if the cold water reservoir is above 40°C. Under these conditions, the water in the gas cooler has a much higher heat capacity than the CO_2, a large temperature difference is created on the hot side of the gas cooler, and that is where the bulk of the heat transfer takes place. For standby loss reheating, the COP is about 30-40% lower than for heating at corresponding ambient and hot water temperatures for initial tank heating.

In the second stage of the project, the CO_2 cycle was modeled in EES to investigate the performance potential at some untested conditions and to simulate the use of larger heat exchangers and a more efficient compression process. The model revealed that for cold water heating, the best performance payback comes from increasing the size or effectiveness of the gas cooler, since the gas cooler is typically working “all out” at these conditions. For heating warmer water, the best performance payback comes from either increasing the size of the evaporator, or limiting the heat loss from the compressor.

The third stage of the project featured an investigation of the oil retention characteristics of a heat pump water heater, using a microchannel gas cooler and a fin-and-tube evaporator. In this system, about half of the oil was retained in the evaporator, one quarter was retained in the gas cooler, and the remaining quarter was retained in the suction and liquid lines. The total oil retention ranged from 25 grams for low oil mass fractions and high flow rates to 180 grams for high oil mass fraction and low flow rates. Under low oil mass fraction conditions, the increase in pressure drop in the heat exchangers was generally in the range of 5-15%, but could increase to 30-60% with high oil mass fractions. Oil is expected to cause a COP reduction on the order of 2-4.5% in CO_2 HPWHs, depending on the OMF. Unlike the oil retention mass and pressure drop penalty factor, this relationship, does not appear to be strongly dependent on OMF.

In the final stage of the project, the performance enhancement potential of two alternative system configurations was investigated. In the first configuration, an internal heat exchanger was used in a two-stage compression cycle. Under these conditions, the system realized an increase in COP (up to 7.5%) during tests in which the baseline cycle had a low approach temperature on the cold side of the gas cooler (generally speaking, low-ambient, warm inlet water tests). The second cycle configuration used a suction line heat exchanger to subcool the CO_2 at the outlet of the gas cooler and provide additional superheat to the inlet of the gas cooler. This cycle allowed the pressure ratio to be reduced at nearly constant gas cooling capacity, increasing the COP by up to 7%. Since the tests were performed at constant charge,

optimized at 10°C ambient, and since there was no charge management device, the higher ambient temperature tests were performed at undercharged conditions. The COP, therefore, could not be improved over the baseline cycle under these conditions, because the high side pressure had to be maintained near its previous level in order to provide acceptable capacity.

The SLHX cycle testing underscored the need for a charge management device in a CO_2 HPWH – a need that was recognized during the baseline testing. During baseline testing, at low ambient temperatures, and high inlet water temperatures, the discharge pressure approached 13 MPa. It had to be maintained at this level in order to keep the evaporating pressure low enough to fully vaporize refrigerant in the evaporator. This discharge pressure was well above the optimum pressure for the cycle at those conditions, and more importantly, approached levels that were dangerous for some of the system's tubing. A HPWH with an evaporator installed outdoors would have to face ambient temperatures well below 10°C in most climates. To maintain safe operation and optimum performance under these conditions, two charge management approaches are recommended. First, the volume of the high pressure side of the system should be designed so that it is nearly equal to the volume of the low pressure side of the system. In this test facility, the high-pressure side of the system contained much less volume than the low-pressure side. Decreasing the pressure in the evaporator often involved disproportionate increases in the gas cooling pressure. The second recommendation is to install an accumulator at the outlet of the evaporator. In the accumulator, liquid CO_2 could be stored at low ambient temperatures, where the

optimum charge of the cycle is lower. At high ambient temperatures, some of this liquid CO_2 could be evaporated to effectively provide more charge to the system. It would also enable performance optimization by allowing the superheat to be safely lowered to nearly zero.

Overall, the CO_2 cycle seems uniquely suited for the task of heating water. As mentioned, its biggest drawback is its performance reduction for heating warm water. This means that CO_2 HPWHs are not well suited, for example, for use in hybrid systems that involve solar preheating of the water. CO_2 HPWHs seems to have enormous energy savings potential if the cooling provided by the evaporator can be harnessed during the summer months, and rejected to the environment during the colder months.

8 References

[1] Lorentzen G., 1995, The use of natural refrigerants: A complete solution to the CFC/HCFC replacement. International Journal of Refrigeration 18(3): 190-197.

[2] Hwang, Y, 1997, Comprehensive Investigation of Carbon Dioxide Refrigeration Cycle, Ph.D Dissertation, University of Maryland, College Park, MD.

[3] Hwang Y., Radermacher R. 1998, Theoretical Evaluation of Carbon Dioxide Refrigeration Cycle, International Journal of HVAC&R Research, 4(3): 245-263.

[4] Neksa P., Rekstad H., Zakeri G.R., Schiefloe P.A. 1998, CO_2-heat pump water heater: characteristics, system design and experimental results, International Journal of Refrigeration, 21 (3): 171-178.

[5] Hwang Y., Radermacher R.1998, Experimental Evaluation of CO_2 Water Heater, Proceedings of the IIR-Gustav Lorentzen Conference, Oslo, Norway: 321-328

[6] Rieberer R., Gassler M., Halozan H. 2000, Control of CO_2 heat pumps, Proceedings of the 4th IIR-Gustav Lorentzen conference on natural working fluids at Purdue, West Lafayette, IN: 75–82.

[7] Meyer J., Raubenheimer J.A., Kruger E. 2000 , The Influence of Return Loop Stratification in a Vertical Hot Water Storage Tank Connected to a Heat Pump Water Heater, Heat Transfer Engineering, 21 (2): 67-73.

[8] Hubacher B., Groll E. 2002, Measurement of Performance of Carbon Dioxide Compressors, The Air-Conditioning and Refrigeration Technology Institute, Final report, West Lafayette, IN, ARTI-21CR/611-10070-01

[9] J.P. Lee, 2002, Experimental and Theoretical Investigation of Oil Retention in a Carbon Dioxide Air Conditioning System, Ph.D Dissertation, University of Maryland, College Park, MD.

[10] Chaichana C., Aye L., Charters W. 2003, Natural Working Fluids for Solar-Boosted Heat Pumps, International Journal of Refrigeration, 26 (6): 637-643.

[11] Yoon S.H., Kim J.H., Hwang Y.W., Kim M.S., Min K., Kim Y., 2003, Heat transfer and pressure drop characteristics during the in-tube cooling process of carbon dioxide in the supercritical region, International Journal of Refrigeration, 26(6): 857-864.

[12] Youbi-Idrissi M., Bonjour J.,Terrier M., 2003, Solubility of CO_2 in a Synthetic Oil, Proceedings of International Congress of Refrigeration 2003, ICR0300

[13] L. Cremaschi, Y. Hwang, R. Radermacher, 2005, Experimental investigation of oil retention in air conditioning systems, International Journal of Refrigeration, 28(7): 1018-1028.

[14] L. Cremaschi, 2004, Experimental and Theoretical Investigation of Oil Retention in Vapor Compression Systems, Ph.D Dissertation,University of Maryland, College Park, MD

[15] Cecchinato L., Corradi M., Fornasieri E., Zamboni L. 2005, Carbon dioxide as refrigerant for tap water heat pumps: A comparison with the traditional solution, International Journal of Refrigeration, 28(8): 1250-1288.

[16] Cho H., Ryu C., Kim Y., Kim H.Y., 2005, Effects of refrigerant charge amount on the performance of a transcritical CO_2 heat pump, International Journal of Refrigeration, 28(8): 1266-1273.

[17] Code of Federal Regulations, Chapter 2; Department of Energy, 10 CFR Ch.2, part 430, subpart B, Appendix E, Uniform test method for measuring the energy consumption of water heaters.

[18] Kim S., Kim Y.J., Lee G., Kim M.S. 2005, The performance of a transcritical CO_2 cycle with an internal heat exchanger for hot water heating, International Journal of Refrigeration, 28(7): 1064–1072.

[19] Stene J. 2005, Residential CO_2 Heat Pump for Combined Space Heating and Hot Water Heating, International Journal of Refrigeration, 28(8): 1259-1265.

[20] Rigola J., Raush G., Perez-Segarra C.D., Olivia A., 2005, numerical simulation and experimental validation of vapor compression refrigeration systems - Special emphasis on CO_2 transcritical cycles, International Journal of Refrigeration, 28(8): 1225-1237.

[21] Japanese Heat-Pump Water Heater Market Growing, Appliance Magazine, September 2005, p.20.

[22] ANSI/ASHRAE standard 118.2-2006, Method of Testing for Rating Residential Water Heaters, Atlanta, GA

[23] Hashimoto K., 2006, Technology and market development of CO_2 heat pump water heaters (ECO Cute) in Japan, IEA Heat Pump Centre Newsletter, 24(3): 12-16.

[24] C.H. Son, S.J. Park, 2006, An experimental study on heat transfer and pressure drop characteristics of carbon dioxide during gas cooling process in horizontal tube, International Journal of Refrigeration, 29(4): 539-546.

[25] Yang M., Guo X.M. 2007, Experimental Investigation on the dynamic performance of an exhaust-air heat pump water heater, Proceedings of International Congress on Refrigeration, Beijing, China. ICR07-E2-689

[26] Zogg R., Roth K., Radermacher R. 2007 CO_2 Heat Pump Water Heaters, ASHRAE Journal, 47(3): 52-54.

[27] Laipradit P., Tiansuwan J., Kiatsiriroat T., Aye L., 2007, Theoretical performance analysis of heat pump water heaters using carbon dioxide as a refrigerant, International Journal of Energy Research, 32: 356-366

[28] Anderson T.N., Morrison G.L., 2007, Effect of load pattern on solar boosted heat pump water heater performance, Solar Energy, 81: 1386-1395.

[29] Yokozeki A., 2007, Solubility correlation and phase behaviors of carbon dioxide and lubricant oil mixtures, Applied Energy, 84: 159-17.

[30] Dang C., Iino K., Fukuoka K., Hihara E., 2007, Effect of lubricating oil on cooling heat transfer of supercritical carbon dioxide, International Journal of Refrigeration, 30(4): 724-731.

[31] HVAC Systems and Equipment, 2008 ASHRAE Handbook, I-P Edition, Atlanta, GA